Doctoral Thesis

[1]

Development and Performance of a Velocity Control System for Modern Combustion-Powered Scooters

Jannis Kreß

Doctoral Thesis

Development and Performance of a Velocity Control System for Modern Combustion-Powered Scooters

Supervisors:
Prof. Dr. Arturo Morgado-Estévez (UCA)
Prof. Dr. Hektor Hebert (Fra UAS)

by
Jannis Kreß
Hauptstraße 318
65760, Eschborn
Germany
jannis.kress@fb2.fra-uas.de

University of Cadiz
8212 Manufacturing, Materials and Environmental Engineering

Statutory Declaration in Lieu of an Oath

I hereby declare in lieu of an oath that I have written this thesis independently and only with the aid of the resources indicated. All passages in this thesis that are taken in wording or meaning from other works or texts have been identified by complete references and citations to the respective authors of the sources. Literal quotations are also indicated in the text by enclosing the relevant passages in quotation marks. I certify that I have never submitted this thesis in this or a similar form to an examination authority.

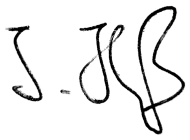

Eschborn, March 13, 2024

Abstract

This doctoral thesis covers the development of a velocity-controlled Throttle-by-Wire-System for modern four-stroke 50 cc scooters (Euro 5). Further, the system performance, fuel-saving effect and exhaust optimization was investigated. The European Parliament has adopted major CO_2 emission reductions by 2030. But modern combustion-powered scooters are inefficiently restricted and emit unnecessary amounts of CO_2. Replacing the original restriction method with the velocity-controlled Throttle-by-Wire-System, the engine's operating point is being improved significantly. Controlling the throttle valve opening prevents an inefficient ignition timing shift. The Throttle-by-Wire-System consists of an anisotropic magnetoresistance throttle position sensor and a position controlled stepper motor-driven throttle valve actuator. The sensor unit comes with a measurement deviation of less than 0.16% whereas the actuator unit can approach throttle valve positions with a deviation of less than 0.37%. The actuators settling time does not exceed 0.13 seconds in the case of stable, step-loss free and noiseless operation. A redundant wheel speed sensor measures the vehicle velocity using the Hall effect with a precision of 0.04 km/h. The entire system is managed by a central ECU, executing the actual velocity control, fail-safe functions, power supply and handling inputs/outputs. For velocity control, an adaptive PI-controller has been simulated, virtually tuned and implemented, limiting the top speed regulated by legal constraints (45 km/h). By implementing a human-machine interface, including a virtual dashboard, the system is capable of interfacing with the rider. For sensor evaluation, Hardware-in-the-Loop test benches have been developed. During test drives, a specially developed measurement box logs vehicle orientation, system/control variables and engine parameters. A *Peugeot Kisbee 50 4T* (Euro 5) severed as test vehicle. The system has been evaluated regarding performance and fuel efficiency both through simulation and road testing. Fuel savings of 13.6% in real-world test scenarios were achieved while maintaining vehicle performance. Finally, the system behavior, the combustion process and the exhaust gas composition were investigated. The original and the optimized restriction were subjected to various load points on a roller dynamometer at top speed. The resistance parameters required, were previously determined in a coast down test. When driving on level ground, a difference of 50% in the throttle opening leads to a 17% improvement in fuel economy. By measuring the engine parameters, the optimum ignition timing could be proven with increasing internal cylinder pressure. Further, 17% reduction in exhaust gas flow was demonstrated. CO emissions decreased by a factor of 8.4, CO_2 by 1.17 and HC by 2.1 while NO_x increased by a factor of 3. Overall, the exhaust emissions at top speed have been significantly improved with regard to the existing emission standards. By comparing the CO_2 equivalents of the test vehicle with a modern electric scooter, a CO_2 saving of 21% could be estimated over the life cycle favoring the combustion engine.

Contents

List of Figures

List of Tables

List of Equations

List of Abbreviations

ADC	Analog to Digital Converter
AMR	Anisotrop Magnetoresistance
CAN	Controller Area Network
CC	Cruise Control
CVT	Continuous Variable Transmission
DMA	Direct Memory Access
EC	Engine Controller
ECU	Electronic Control Unit
EFM	Exhaust Flow Meter
ET	Electronic Throttle
GMR	Gaint Magnetoresistance
HiL	Hardware-in-the-Loop
HMI	Human-Machine Interface
IC	Integrated Circuit
IMU	Inertial Measurement Unit
I/O	Input/Output
ITM	Ignition Timing Manipulation
LCD	Liquid Chrystal Display
MAF	Moving Average Filter
MB	Measurement Box
MCU	Microcontroller Unit
MECU	Main ECU
OR	Original Restriction
PCB	Printed Circuit Board
RTC	Real-Time Clock
TbWS	Throttle-by-Wire-System
TDC	Top Dead Center
TPS	Throttle Position Sensor
TSS	Transmission Speed Sensor

TVA	Throttle Valve Actuator
UART	Universal Asynchronous Receiver Transmitter
VC	Velocity Control
WSS	Wheel Speed Sensor

1 Introduction

The demands on individual transportation are increasing while traffic densities in urban areas are becoming steadily higher. According to the climate targets of the European Climate Change Act, at least 55% of greenhouse gases are to be saved by 2030 compared to 1990 levels [2]. Considering the average distance traveled per inhabitant in the EU, the values vary between 5 and 20 km a day. Depending on the country of origin, 57% to 81% of this daily distance is covered by car. Most often, the distance traveled by two-wheelers corresponds to less than 1% [3]. However, for urban mobility, scooters are an excellent alternative. The potential for saving fuel and thus minimizing CO_2 emissions is enormous and can make a significant contribution to EU climate targets. Environmentally harmful two-stroke engines are banned and the Euro 5 standard also applies to 50 cc scooters [4]. Comparing modern four-stroke combustion and electrically powered scooters of *Peugeot*, *Piaggio* and *Vespa*, an average price for electric models of almost 160% can be noticed. These price differences are generally seen for electric vehicles [5]. The difference in average range is even more striking, as the combustion engine exceeds that of the electric drive by a factor of 6. Especially when used in cities, users require longer ranges because frequent recharging is often difficult.

Modern Euro 5 scooters could serve as an eco-friendly alternative to cars, reasoned by better fuel-economy and thus a minimized CO_2 footprint. To fulfill Euro 5 requirements, modern combustion-powered scooters are equipped with gasoline injection and a catalytic converter [6, 7]. To ensure optimal operation of the catalyst, the air/fuel mixture (λ) must be approx. 1 [8]. Legal requirements state that 50 cc scooters cannot exceed a max. speed of 45 km/h [9]. In the past, speed limitation was often realized through mechanical restrictors, manipulating the transmission ratio or mixture/exhaust flow [10]. Nowadays engine controllers are mostly shifting the ignition timing to limit the engine's performance. Reducing the injection quantity would lead to an unfavorable stoichiometric ratio ($\lambda > 1$) [8, 11] and thus negatively affect the functioning of the catalyst [12, 13]. The Original Restriction (OR) will be bypassed and replaced by a velocity-dependent control of the throttle valve position (air supply). For this purpose, the throttle position needs to be sensed and the throttle valve must be manipulated by an actuator. As a consequence, instead of the ignition timing, the airflow is regulated by means of the throttle valve position. A reduction of the fuel injection volume and exhaust gas emissions is to be expected. The Velocity Control (VC) could contribute substantially to reaching EU climate targets. According to the current state of knowledge, this is the first approach of a VC application on a modern four-stroke 50 cc (Euro 5) scooter as an alternative restriction. The VC system investigated here is intended to optimize fuel economy, improve driving performance and reduce exhaust gas emissions.

2 State of the Art

In order to frame this research, its focal points are placed in a scientific context. A thorough understanding of the combustion process, exhaust gas generation and aftertreatment of four-stroke engines is essential to comprehend the chain of effects of the developed system. Limiting the scooter's top speed, resulting restriction effects directly or indirectly influence the combustion quality. For this reason, restriction methods are being examined in the context of performance, fuel-economy and current exhaust gas regulations. To substantiate the development of a low-cost Throttle-by-Wire-System (TbWS), researched Throttle Position Sensors (TPSs) and Throttle Valve Actuators (TVAs) are explicitly presented. Finally, existing TbWS on two-wheelers and VC algorithms in general are presented.

2.1 Background on Internal Combustion

Internal combustion engines generate mechanic work through the chemical conversion of fuels [14]. In nowadays scooters, mostly four-stroke gasoline engines are used. A mixture of air and gasoline is compressed, ignited and the expansion is used to accelerate the piston. Combustion is influenced by many factors. The mechanical design of the engine is not considered below, as VC focuses on the engine's control. Ignition timing and injection quantity are relevant, as these are influenced by manipulating the throttle valve opening and restriction. The ignition timing determines the start of the combustion process. Ideally, the mixture is ignited shortly before the Top Dead Center (TDC) is reached. Thus, the max. cylinder pressure is achieved shortly after passing the TDC [15]. For complete and low-emission combustion, the fuel-air mixture (λ) is essential. An optimum stoichiometric ratio is given when λ equals 1, corresponding to a ratio of 14.7 parts air to 1 part gasoline [16]. The composition of pollutants depends considerably on the mixture supplied [17].

Four-stroke gasoline engines burn fuels consisting of multiple short-chain hydrocarbons, also called CHO compounds. A perfect and complete combustion would convert CHO to carbon dioxide (CO_2) and water (H_2O) through oxidation. During the combustion process several reaction stages are passed through, temporarily producing hydrogen (H), H_2, oxygen (O), O_2, hydroxide (OH), carbon monoxide (CO), CO_2 and H_2O. Only at high temperatures CO and H_2 are initially formed before CO oxidizes to CO_2 and H_2 to H_2O [18]. In terms of emissions, on the one hand unburned components such as CO and hydrocarbons (HC) on the other nitrogen oxides (NO_x) are critical constituents. The gases are produced as follows:

- CO_2: A complete combustion of carbon converts a max. amount of CO_2 (if $\lambda = 1$).
- CO: It is formed as an intermediate stage of carbon dioxide formation and in incomplete combustion under oxygen deficiency.

- HC: Unburned hydrocarbons are formed by the attachment of unreacted molecules to the cylinder wall, especially in the absence of oxygen.
- NO_x: It is formed during combustion by nitrogen and oxygen. A surplus of air and high combustion temperatures lead to high emission.

Consequently, Figure 2.1 shows the relation between λ and the raw exhaust gas composition of CO, NO_x and HC. Further, when the Euro 2 standard was introduced, the emission reduction of 50 cc scooters was investigated for different drive types. In particular, four-stroke engines with direct injection and catalytic converter were found to be promising. CO and HC emissions were significantly lower compared to carburetor-fueled engines or two-stroke engines [19]. To convert pollutants in a Euro 5-compliant manner, regulated three-way catalytic converters are usually used with four-stroke engines and fuel injection. CO and HC oxide to CO_2 and H_2O, while reduction converts NO_x to nitrogen (N) and CO_2 [20]. The resulting conversion rates are better than 85% as long as $\lambda = 1$ [21]. Accordingly, pollutants cannot be completely converted and the formation of the raw gases depends on the oxygen concentration of the mixture. Figure 2.2 shows the catalyst's conversion rate as a function of λ. It is noticed that the operating range is now significantly smaller and precise control is required to ensure effective conversion of the pollutants.

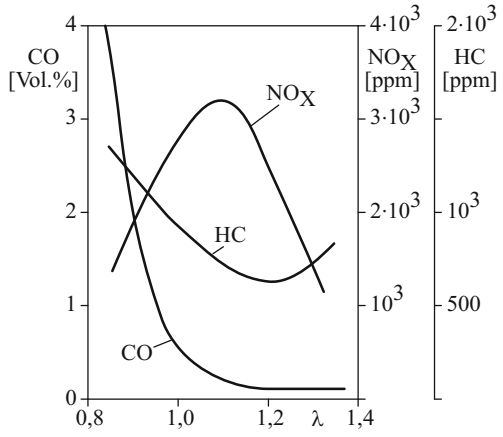

Figure 2.1 – Raw gas emissions [17]

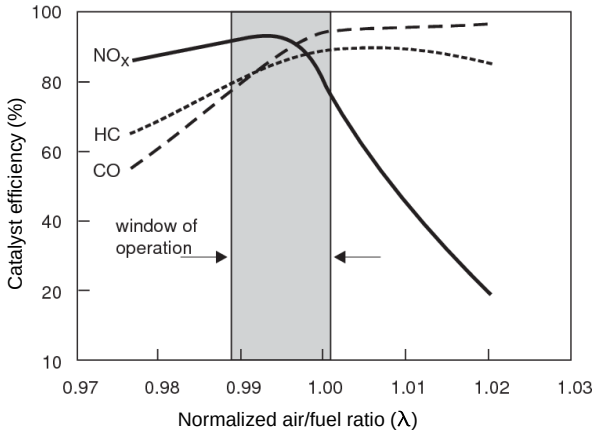

Figure 2.2 – Catalytic conversion rate [16]

2.2 Background on Restrictions

Restrictors are used for limiting the engine performance by decreasing top speed or power output. Some reduce power across the entire velocity range, others for higher velocities only. Initially, restrictions were implemented purely mechanically. Modern methods do not solely reduce the engine power. Instead, they lower the vehicle's top speed by use of electronics. The following methods provide an outline of the various restriction principles:

- **Throttle stop:** By the use of a sheet metal, the throttle grip cannot be operated to its maximum. The engine is supplied with less mixture and develops less power.

- **Orifice in the intake/exhaust:** By decreasing the diameter of the intake/exhaust, the engine does not get enough mixture or the exhaust gas is dammed up and the piston must overcome this pressure when expelling the exhaust gases [10].
- **Ignition interruption:** When the velocity exceeds a threshold of 45 km/h, the ignition is interrupted and the velocity is limited.
- **Continuous Variable Transmission (CVT) limitation:** A distance plate limits the ratio of the CVT. The velocity is then limited by the max. speed of the engine.
- **Mixture leaning:** When the vehicle's top speed is reached, the fuel injected is reduced while remaining the throttle fully opened ($\lambda > 1$) resulting in less engine power [22].
- **Ignition Timing Manipulation (ITM):** When the vehicle's top speed is reached, the performance of the engine can be reduced by retarding the ignition timing [15].

The disadvantages of restrictors result from performance losses and increased fuel economy. Design changes that manipulate the flow behavior lead to power losses. Restrictors that aim to reduce top speed often lead to slower acceleration and deviating top speeds under heavy loads or on inclines. Restricting the CVT's variator retains the original power, but increases the engine speed, fuel consumption, noise and mechanical wear. These mechanical limitations are rarely used anymore due to significant performance losses and high powertrain stresses. Ignition interruption would lead to strong vibrations in single-cylinder four-stroke engines and were used primarily on two-stroke engines. Since modern scooters are equipped with a three-way catalytic converter, the restriction must not have any influence on the oxygen concentration in the exhaust gas, as otherwise the degree of conversion will be affected. For this reason, restricting by leaning is not further applied, even if it leads to good fuel economy. To comply with the Euro 3 standard, four-stroke engines with fuel injection and three-way catalytic converters were certainly used. By operating in the lean range ($\lambda > 1$), more recent emissions standards (e.g. Euro 5) can no longer be met due to high NO_x emissions [22]. To enable the effective use of catalysts and still achieve max. engine performance, the ITM represents the state of the art. The ignition timing is dependent on engine speed and varies between 6° to 40° before the TDC. For restriction, the timing is delayed and causes an inefficient engine operation. Consequently, combustion takes place during the downward movement of the piston (expansion) [23]. Figure 2.3 shows optimum timing left and retarded timing right. The compression curve shown, corresponds to that of the test vehicle's engine.

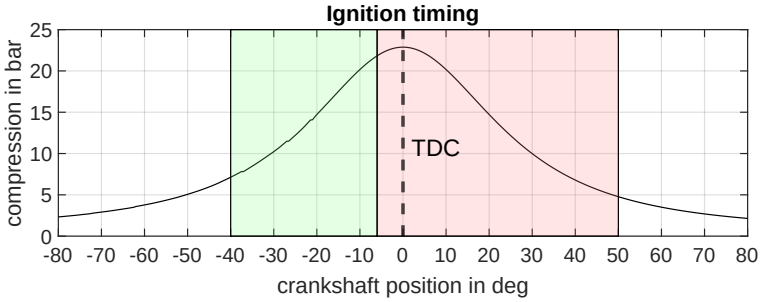

Figure 2.3 – Ignition timing

2.3 Background on Throttle-by-Wire-Systems

In the automotive sector, TbWSs have been state of the art since the late 1980s [24]. To enable assistance and safety systems, the intervention into longitudinal vehicle dynamics, mechanical connections are being replaced by electronic signals. A TPS measures the throttle grip/pedal position and provides a digital value to the Engine Controller (EC). The throttle valve is controlled by an actuator using the control signal provided by the EC [25]. It took years until the benefits of TbWSs outweighed the technical challenges for the use in motorcycles. The need for additional systems with extra weight and space requirements was evident. With the arrival of advanced driver assistance systems, the advantages of TbWSs became obvious. TbWSs have been researched and integrated industrially to motorcycles [26, 27, 28]. A TbWS has also been applied successfully to small-volume engines, coming with the minimum number of low-cost components, combined in the throttle body. The system is based on a throttle servo, throttle position sensor, throttle demand and engine speed sensor. To limit and adapt the engine speed in various load situations, the speed can be adjusted by an integral electronic control and resonant frequencies can be avoided. Besides the performance limitation, the system is capable of managing speed and load reductions during overheating. For cold starts, the idle speed can be adjusted on the outside temperature [29]. The developed TbWS will be placed in the engine compartment to simplify vehicle integration and minimizing the electronic effort by using the original throttle cable. In this way, the TbWS could also be retrofitted with little effort. The approach is novel within this specific powertrain type and vehicle class.

2.3.1 Throttle Position Sensors

The TPS transfers the physical rider input to an electronic signal while monitoring for plausibility. Figure 2.4 is giving a black box approach for TPSs, showing inputs and outputs. The TPS needs power supply and converts the rotary/translatory physical input from the throttle grip. External influences like vibrations, electro-magnetic and magnetic fields must also be considered. The unit outputs a digital throttle position via vehicle bus for further processing.

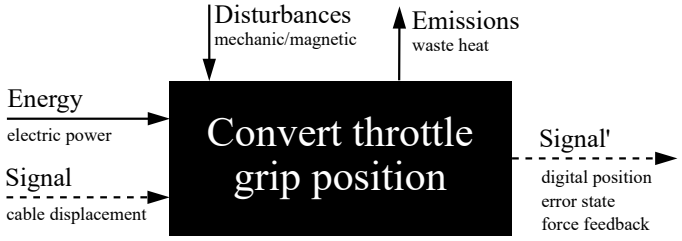

Figure 2.4 – TPS black box schematic

Positions can generally be measured with relative and absolute sensors. Relative sensors are not considered due to their comparatively high error rate. With an absolute measurement, the sensor directly provides the angular position depending on its current location. The current state of the art is described by resistive, inductive and magneto-static sensor principles. Slip potentiometers are the cheapest and simplest method, but tent to long-term errors due to their contact-based design [30]. Inductive sensors measure angles contactless by induction changes within the coils. A redundant layout is difficult to design due to the larger and more

complex setup. Since inductive sensors are based on alternating current effects, evaluation by a microcontroller is only possible with complex measurement circuitry [31]. For measuring the strength or orientation of magnetic DC fields, magneto-static sensors are used. Most commonly applied are galvano-magnetic effects like Hall, Gaussian and magneto-resistive effects. Anisotrop Magnetoresistance (AMR) and Gaint Magnetoresistance (GMR) allow standstill detection and distinction of rotation direction [32]. In contrast to inductive sensors, they can be miniaturized better and manufactured at low cost. The Hall effect is the best known magneto-static effect, but the sensor's characteristic is related to temperature fluctuations and aging. To avoid saturation and under-run, the magnetic field strength must be within a defined range. AMR and GMR sensors measure absolute angular positions within a 180° (GMR: 360°) range by a varying resistance related to the orientation of a magnetic field. Sensor elements are set up in a Wheatstone arrangement, giving a sinusoidal output signal [33]. Placing two AMR-elements in 45° angular offset, a position can be calculated by applying the *arctan* function. In contrast to the GMR sensor, the AMR effect can also handle strong magnetic fields while operating in saturation. Therefore, the AMR sensor can be operated independently of magnetic intensity fluctuations. Temperature related non-linearity of max. 3% must be taken into account during measurement [34]. Due to modern manufacturing processes, AMR sensors can be manufactured redundantly on tiny chips.

2.3.2 Throttle Valve Actuators

In modern systems, to control the throttle valve opening, a TVA is used. Typically, a DC motor with a multi-stage transmission provides the required torque. For setting a desired position, a position control algorithm uses the feedback of an absolute angular position sensor. In the event of failure (fail-safe mode), a torsion spring moves the valve back to its initial state (limp-home position). Additionally, a motor driver is required to interface the set position and to supply the motor with electrical energy. Figure 2.5 is giving the basic schematic of a TVA.

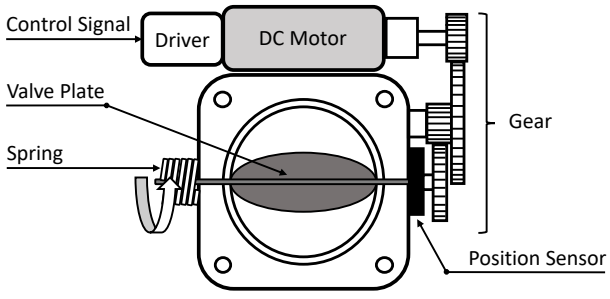

Figure 2.5 – TVA schematic

Previous research was often based on a combination of DC motor, planetary or geared transmission, torsion spring and angular potentiometers for position measurement [26, 35, 36]. In addition to the hardware setup, the research effort is mostly focused on the position control algorithm. Even though TVAs may appear trivial in terms of their design, mechanical and electrical non-linearity can lead to complicated control behavior [37]. Controlling TVAs, the upcoming throttle valve friction and in the case of an integrated spring, the corresponding torque must be overcome. For that reason, a common approach is a model-based control

strategy, designed on the specific spring and friction characteristics. Setting the position is mostly realized through friction compensated PID-controllers, manipulating the motor's supply voltage through a PWM signal [26, 35, 38]. Alternatives such as neural network based self-learning control [39] and adaptive sliding mode controllers have been applied successfully [40, 41, 42]. Further, linear parameter varying controllers [43] or strategies such as minimal controller synthesis [44] could also lead to high control performance. In context of automotive TVAs, a single, comparatively large throttle valve is attached independently from the number of cylinders. In motorcycles, the number of throttle valves corresponds to the number of cylinders. Complex mechanics are required, resulting in proportionally more friction effects. In case of the TbWS investigated, one throttle valve for single-cylinder engines is used.

2.3.3 Velocity Control

VC requires the precise measurement of the vehicle velocity as a reference variable. Wheel Speed Sensors (WSSs) are used since decades for wheel speed determination in automotive industry [45]. Firstly, the sensors were based on a passive steel pulse generator within the wheel hub that delivered an induced voltage, where the amplitude was directly related to the wheel speed [46]. However, the position and adaption remained, but the sensor element had been replaced with a multipole magnet pulse generator and a magnetostatic sensor. Measurement data is actively processed inside the sensor and sent digitally to the Electronic Control Unit (ECU). The wheel speed signal is digitally modulated in the form of current changes to the two-pole power line [47].

VC systems are state of the art in four-wheeled motor vehicles. Conventional static Cruise Control (CC) and adaptive CC are based on regulating the vehicle velocity. To maintain the set velocity, access is granted to the throttle control as well as brake intervention [48]. In this way, rapid changes to the setpoint or strong downhill forces can be compensated for. To control the throttle valve and brake actuator, acceleration requests are often transferred to summed wheel torques. This parameter is similar to the accelerator pedal position and can be interpreted by both subsystems. Therefore, the actual total wheel torque is needed as a reference variable [49]. Two-wheelers rarely have CC. In addition, the engine brake is sufficient for negative acceleration due to the low vehicle mass and brake intervention is not necessary. For this reason, the following controls relate exclusively to the throttle valve position. The velocity is usually regulated by a model-based acceleration control. Here, acceleration limits are derived from the real driver profile in order to generate a system behavior that is comfortable for the passengers [49, 50, 51]. Velocity control systems that directly transfer the control difference into a throttle valve position have also been used. Both model-based PI controllers [50] and non-model-based PID controllers [52] have been applied successfully. To compensate for the non-linear behavior of the controlled system, the controller's gains are often adjusted depending on the vehicle velocity [48, 50, 51].

Adjustable CC is not used as standard on scooters. The legally stipulated top speed (45 km/h) requires a limitation that could be described as limiting/static VC at a single operating point. *Peugeot* and *Scion-Sprays Ltd.* have developed an electronic velocity-

controlled throttle control for 50 cc two-stroke scooters, improving fuel economy and idle-stability. Therefore, the mechanical restriction in the CVT is removed, leading to fuel savings of 22% caused by the lowered engine speed. Additionally, the system allows controlling the idle engine speed after the start-up. The system is based on a carburetor-driven two-stroke scooter with a power of 4.2 kW and a twin variator pulley CVT [53]. Due to their design, two-stroke engines emit many times more HC (hydrocarbons) and NO_x (nitrogen oxides) emissions than four-stroke engines [54]. Due to emissions, the system is not compliant with the Euro 5 standard. In addition, the excessive engine power of the powertrain used leads to low mean cylinder pressures at top speed and consequently to less optimized operating points. Nowadays, originally optimal-designed CVTs are used. Modern air-cooled four-strokes have a power output of max. 2.5 kW due to the significantly lower power density. The potential within power surplus and transmission thus no longer exists. The fuel consumption of modern non-optimized drives is considerably lower than that of an optimized two-stroke [19]. CO_2 emissions are directly related to fuel consumption. To achieve climate targets, they must also be taken into account along with the exhaust emission standards. Consequently, a velocity-controlled TbWS on a 50 cc scooter with a four-stroke engine, gasoline injection and a regulated three-way catalytic converter would promise the best possible eco-friendliness and economic efficiency.

3 Hypotheses and Objectives

There is no doubt that the energy transition is one of the key challenges of the 21st century. The focus is increasingly shifting to the sustainability of individuals and therefore also of their individual mobility. The potential of scooters in terms of climate protection was outlined initially. In a high-tech age, however, the restriction methods used are in conflict with environmental protection and the technical capabilities. Modern 50 cc scooter powertrains offer a good basis for efficient and clean operation thanks to regulated exhaust gas aftertreatment. Nevertheless, manual adjustment of the throttle valve position prevents the full potential from being exploited. Hypotheses (H) and objectives (O) are listed below, starting with the research question.

Does the development and application of a velocity-controlled TbWS in a modern combustion-powered 50 cc scooter (Euro 5) lead to significant ecological, economical and driving dynamical improvements?

H1: The velocity-dependent control of the throttle valve position allows ITM to be bypassed and the top speed to be limited.
O1: To bypass the OR by ITM, the EC must be manipulated by a speed sensor emulation. Otherwise, two restrictions will be superimposed. An actuator must be developed to control the throttle valve and a sensor to detect the throttle command. In order to control the throttle valve depending on the velocity, the vehicle velocity must be precisely measured over the entire dynamic range using WSSs. By the implementation of a VC algorithm, the throttle valve position is controlled and the top speed is limited at the same time.

H2: In accordance with the optimum stoichiometric control, the reduced air supply leads to an optimized fuel economy.
O2: During operation with OR, the ignition timing is retarded at top speed. This operating point is predominantly reached on scooters due to the low top speed and is prevented by the developed VC. The injection quantity is regulated automatically by the EC. Based on the sensed oxygen concentration in the exhaust gas, the gasoline will be injected according to $\lambda = 1$. The regulation of the air volume supplied is higher-level and independent. As the amount of fuel injected is proportional to the amount of air drawn in, a limited air mass flow will result in fuel savings. By examining the implemented system on the roller dynamometer and in road tests, the savings are to be investigated.

H3: Regulating the air supply and bypassing ITM enables optimized combustion and significantly improves exhaust emissions.
O3: By reaching the optimum ignition timing, the mixture is expected to burn more efficiently and the internal cylinder pressure should increase. Faster combustion raises the temperature, which influences the exhaust gas composition. CO and HC reductions are to be expected, while NO_x emissions could increase. As a consequence of reduced injection quantities, analogous reductions in CO_2 values will be achieved. System validation is to be carried out by means of a load point-dependent investigation of the system variables, engine parameters and exhaust emissions on a roller dynamometer.

H4: The VC implementation improves the vehicle's driving characteristics.
O4: The integration of precise WSSs enables more accurate speed detection and control. While the OR only controls the top speed in a fluctuating manner and noticeable overshooting is observed, significant improvements can be expected in both steady-state accuracy and overshooting behavior. To evaluate both restriction methods, onboard measurements of the system variables are to be compared in various road scenarios.

4 System Design

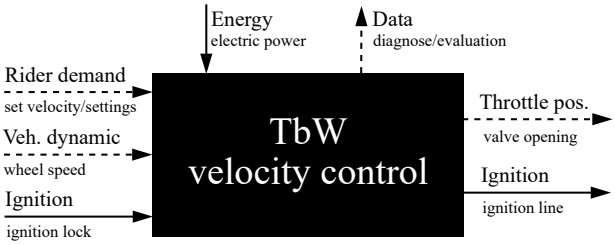

Figure 4.1 – VC black box schematic

The TbWS-based VC uses the set velocity (throttle grip position) specified by the rider as the command variable/input. A WSS measures the vehicle's dynamics (velocity), used as control reference variable. Driving mode and settings serve as additional rider input. The desired vehicle velocity is manipulated through an electronically set throttle valve position (output). For safety reasons, the system is capable of interrupting the engine's ignition line. Lastly, the system requires power supply, outputs diagnose data and rider-intended system information for evaluation purposes. Figure 4.1 shows a general black box schematic. Several bus-connected subsystems are required to implement VC and efficient restriction. The sensing of the rider's demand (throttle grip position) and the vehicle velocity must be achieved. To be able to influence the scooter's longitudinal driving dynamics, the throttle valve position must be controlled electronically. In parallel, emulation of the EC is essential to prevent ITM. The remaining drivetrain, consisting of the engine, gearbox and rear wheel, retains its original condition. A central Main ECU (MECU) processes input variables, performs VC, provides necessary data on the bus and ensures safe vehicle operation. Furthermore, the ECU serves as power box, providing electric energy to all subsystems. The overall system shall be designed in such way, as to allow switching between restrictions by ignition timing and throttle valve manipulation. By means of a virtual dashboard, system quantities and an eco-score are to be displayed to the rider. For evaluation, this Human-Machine Interface (HMI) will be used to switch between restrictions and to start recordings. These are to be recorded by a measurement box accessing the vehicle bus. Now that the foundation has been laid for assistance systems, a CC function is to be implemented. This section presents the architecture developed, including the sensors and systems needed. Figure 4.2 gives the system layout which has been outlined.

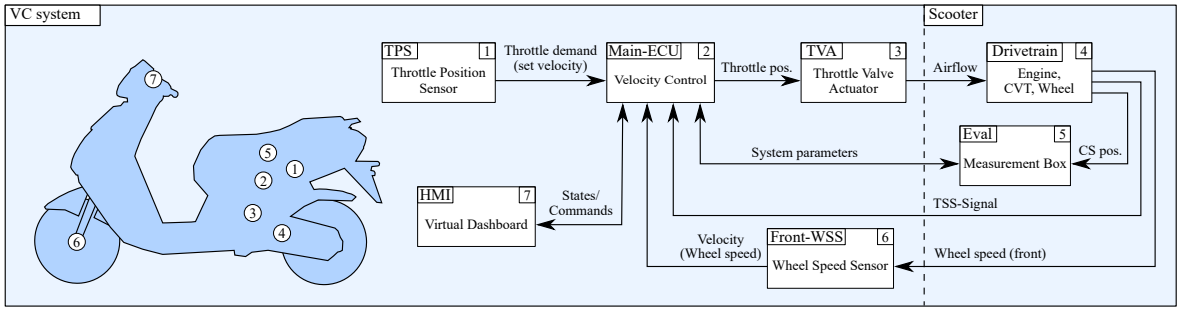

Figure 4.2 – VC system layout

5 Development of a Throttle-by-Wire-System

Since a TbWS is subdivided into the previously introduced components (TPS & TVA), subsequent development steps are described accordingly. The overall requirements include the criteria of low component and manufacturing costs, based on the small vehicle class. Moreover, a steady-state error and overshoot of max. 1% of the throttle travel with a max. settling time of 200 ms is assumed. Requirements are shown in Table 5.1. In addition to dynamic performance, fail-safe requirements are fundamental in automotive industries, such as a redundant and contactless TPS. On top, failure detection of both components and the resulting handling of error conditions need to be managed [55].

	TPS	TVA	**TbWS**
Bus rate (Hz)	50	50	**50**
Error (%)	0.5	0.5	**1.0**
Settling time (ms)	50	150	**200**
Overshoot (%)	0	1	**1**
Displacement (deg)	180	69	**180/69 (I/O)**
Temperature (°C)	-40/125	-40/125	**-40/125**

Table 5.1 – TbWS requirements

5.1 Throttle Position Sensor

Basically, the sub-tasks can be grouped into mechanics, electronics and software. Electronic aspects are the provision of electrical power, redundant detection of the throttle grip position and the consecutive pre-amplification. Then, both measured values are digitized. Before conversion, the now digital values need to be normalized with the previously measured calibration values by software. Results are checked for plausibility and sent to the Controller Area Network (CAN) bus. From mechanical point of view, foreign matter must be retained by a housing and components must be shielded. In addition, the throttle cable must be guided and limited through end stops, while a counterforce must be built up as driver feedback.

5.1.1 System Architecture

In order to implement the above-mentioned sub-functions, the following architecture results for the TPS. Figure 5.1 shows the merging into one assembly of housing and Printed Circuit Board (PCB), covering the introduced levels. After considering the sensor characteristics, the decision was made of a cost-effective AMR sensor Integrated Circuit (IC) (*TLE5109A16D E1210*) from *Infineon Technologies AG* [56]. Placing the TPS directly within the engine compartment, represents a harsh operating environment. This requires a robust sensor which is not susceptible to electromagnetic interference fields and operates properly even under

highly dynamic loads. The original 69° rotation angle can be optimally changed to the 180° by adjusting the cable pulley. Due to position measurement under magnetic saturation, strong magnetic fields can be applied minimizing the susceptibility to interference. By its design, the measurement principle is contactless and the IC is equipped with redundant electrically isolated AMR measuring bridges. The measurement signals are internally amplified and output as analog voltages. Here, the output signal can optionally be tapped differentially. These are being processed by a compact *STM32G431KB* Microcontroller Unit (MCU) which features two symmetrical digital conversions, one differentially. To perform trigonometric calculation more efficient, the processor has the option of hardware-acceleration by the CORDIC. Scaling, conversion and plausibility checks are done by software before CAN message creation. Finally, a CAN transceivcer is executing the CAN communication including the from the MCU provided TPS message.

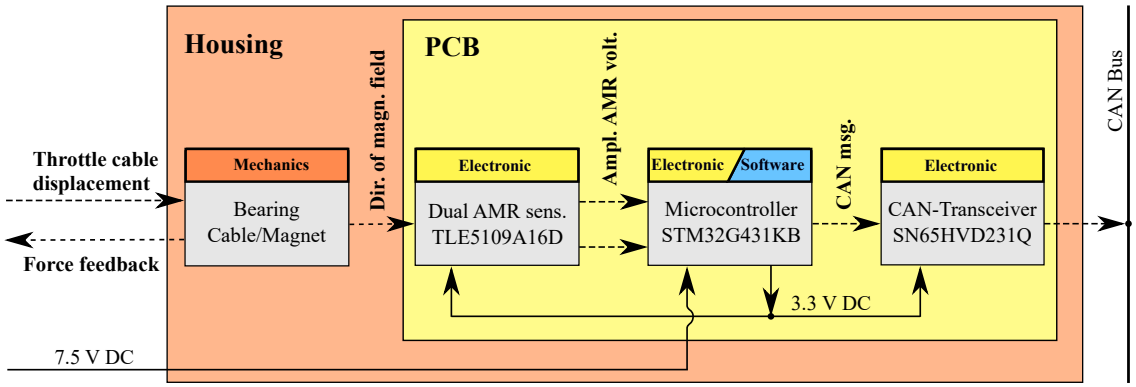

Figure 5.1 – TPS architecture

5.1.2 Mechanical Implementation

To measure the angular position of an axis, a permanent magnet needs to be placed centered above the AMR-IC at the end of shaft. The throttle cable is picked up by a pulley. Its circumference has to be designed in such a way that the cable travel makes optimum use of the sensor measuring range. Manufacturing tolerances (3%), positional inaccuracies within the chip/on the board (5%), and error bands for error detection (5%) were considered [56]. Consequently, 148° can be effectively used of the measurement range (180°). Figure 5.2 illustrates the shaft arrangement. Good guidance of the shaft is achieved with a floating/fixed bearing arrangement. To generate the required throttle feedback, the bearing features a

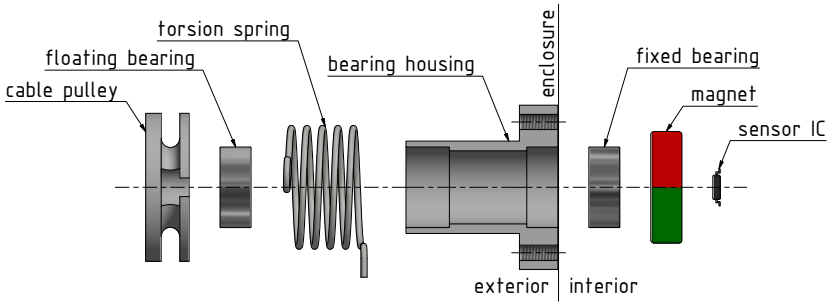

Figure 5.2 – TPS mechanics

torsion spring, which applies the torque for a restoring force. Besides handling the mechanical input, a housing is to be designed. External environmental influences must be prevented from the TPS while the PCB and the bearing unit must be integrated.

5.1.3 Electronic Implementation

The PCB ensures a secure electrical connection of all electronic components, enabling space-saving arrangement. The assembled PCB is mounted in the sensor housing and represents the electronic system level. Amplified sine/cosine signals are provided by the AMR-IC in redundant way. One measuring bridge is to be read out differentially in order to minimize noise due to electromagnetic interference. In addition, due to better EMC low-pass filtering, support capacitors are connected to the signal outputs. The MCU provides sufficient Analog to Digital Converter (ADC) channels for differential conversion of a single measuring bridge. By non-differential conversion of the second one, a reference for plausibility check is generated.

5.1.4 Software Implementation

For secure and immediate engine control, the throttle position is to be detected with a sampling rate of min. 50 Hz. Two ADCs digitize the measured values, which are directly transferred to the memory by the Direct Memory Access (DMA) controller. Thereby, the max. angular velocity of the pulley must be taken into account, which has been determined experimentally to $\omega_{\max} = 9\frac{^\circ}{\mathrm{ms}}$. In order to meet the accuracy requirement of 1%, the occurring differences in the conversion time, resulting from the sequential conversion, must be respected. The longest possible conversion time is represented in (5.1).

$$t_{conv,max} = \frac{Angle_{max}}{100 \cdot \omega_{max}} = \frac{148^\circ}{100 \cdot 9\frac{^\circ}{ms}} = 164\mu s \tag{5.1}$$

Transferring $t_{conv,max}$ into CPU cycles, Equation (5.2) is used.

$$t_{conv(52MHz),max} = 164\mu s \cdot 52\frac{cycles}{\mu s} = 8528 cycles \tag{5.2}$$

It is necessary to balance sampling time and over-sampling (multiple averaged measurements by hardware). A sampling time of 640.5 c with eight-fold oversampling was determined experimentally. The precise ADC time can be determined with (5.3) [57].

$$\begin{aligned} t_{conv} &= t_s[cycles] + resolution[bits] + 0.5 \\ t_{conv} &= (640.5 + 12 + 0.5) \cdot 8 = 5224 cycles \end{aligned} \tag{5.3}$$

The cycles required are less than for $t_{conv(52MHz),max}$ and the precision requirements can be fulfilled. To be energetically efficient, the ADCs are triggered by timer based interrupts and storage is processor-independent via the MCUs DMA. After ADC conversion, calibration calculations are applied to convert the measurements to normalized values within range. The AMR output signals can be described by (5.4a) and (5.4b).

$$sin_{AMR} = Y = A_Y \cdot sin(2 \cdot \alpha) + O_Y \tag{5.4a}$$
$$cos_{AMR} = X = A_X \cdot sin(2 \cdot \alpha) + O_X \tag{5.4b}$$

The function *atan2* calculates the angle of rotation α from the ratio of both output signals. They must be transformed to the same value range of [-1,1] by absolute displacement and scaling of the measured values given in (5.5) (likewise for X).

$$Y_1 = Y - O_Y \;\; ; \;\; Y_2 = \frac{Y_1}{A_Y} \tag{5.5}$$

Now, the angle of rotation can be calculated from both normalized values: $\alpha = atan2(X2, Y2)$. To solve the trigonometric function, a Taylor series is used to approximate the result in a computationally intensive way. This is remedied by the MCUs CORDIC coprocessor, which approximates trigonometric functions at hardware level in less processor cycles. To avoid amplitude shifts and offsets, an end-of-line calibration can be performed, which requires the complete measuring range to be scanned. Offset (O) and amplitude maxima (A) can be calculated from the recorded values by means of (5.6).

$$A = \frac{Max - Min}{2} \;\; ; \;\; O = \frac{Max + Min}{2} \tag{5.6}$$

Before the throttle position is transmitted, the redundantly acquired measured values must be checked for plausibility. The range of values and the signal's magnitude can be verified as properties of the individual signals. Redundantly acquired measurements are checked by signal or angle comparison. With equations (5.7a)/(5.7b) the by the manufacturer specified value range of the AMR sensors can be verified with regard to its minimum/maximum.

$$Min_{diff} = O_{diff,min} - A_{diff,max} - V_{Noise}$$
$$Min_{diff} = -200mV - 2.6V - 5mV = -2.805V \tag{5.7a}$$
$$Max_{diff} = O_{diff,max} + A_{diff,max} + V_{Noise}$$
$$Max_{diff} = 200mV + 2.6V + 5mV = 2.805V \tag{5.7b}$$

To detect erroneous measured values, the magnitude check can also be beneficial. For this purpose, the phase shift of a quarter period (orthogonality) is exploited by plotting the sine over the cosine function. The resulting location vector traverses a unit circle with the radius (r) for changes of the rotation angle (φ). Based on the max. permissible angular error (1.48°) an upper limit of $\Delta r = 2.5\%$ results. Finally, the values are compared with the reference of the second AMR sensor with regard to the concrete value and the resulting angular offset. Again, the angular error must not exceed 1.48° and the deviation must be less than $\Delta SIN_{max} = 0.26$ (tolerance 5%). These analyses allow to detect short circuits, cable breaks, defects of the measuring bridges and electromagnetic interference. After plausibility checks, a CAN message can be created featuring the digitized throttle position, message counter and error status of the sensor unit. For a precise position transmission, a 10 bit resolution has been chosen, resulting in a percentage quantity with one decimal place precision.

5.2 Throttle Valve Actuator

Developing the TVA also requires decomposition into electronics, software and hardware level. Electronic aspects are the conversion and amplification of the stepper motor control signal, the contactless measurement of the valve position and the belonging preamplification/digitization. The measured position needs to be checked for plausibility by software and will serve as control feedback. A position control must set the requested throttle valve position, received by the bus. For fail-safe reasons, the actuator's operation needs to be monitored regarding stability, precision and failure. To guarantee smooth/energy-efficient operation and good engine idle speed behavior, an online calibration and energy saving mode has to be implemented. From the mechanic point of view, foreign matter must be retained by a housing and components must be protected. The powertrain must be designed consisting of a motor, a proper transmission and the position sensor adaption, taking into account error-security. All parameters considered below are also summarized in Table A.1 of the appendix to improve clarity.

5.2.1 System Architecture

Based on the given sub-functions, the following architecture can be derived, consisting of a circuit board and a housing like shown in Figure 5.3.

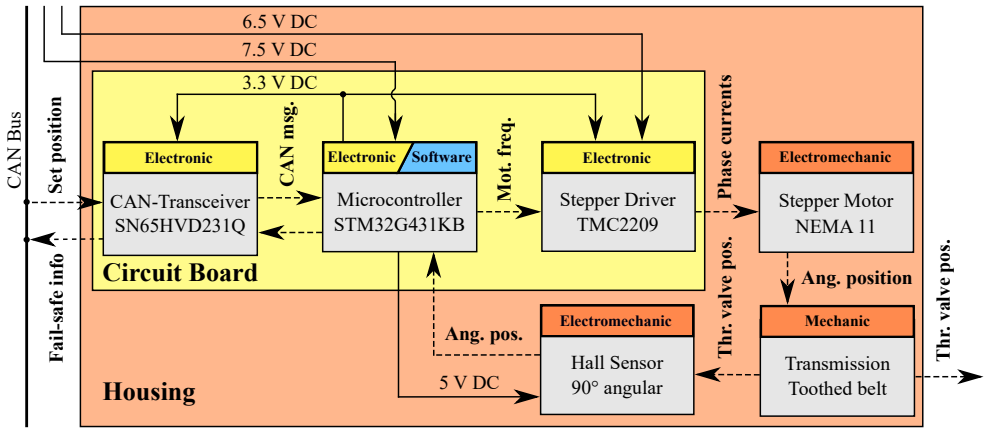

Figure 5.3 – TVA architecture

The TVA is supplied with two separately fused DC voltages to guarantee operation even in case of a collapsed TVA powertrain. Output is the controlled throttle valve position. The electric motor selected is a *NEMA 11* (*HS20-0674S*) two-phase bipolar stepper motor [58]. In contrast to DC motor application, the use of a stepper motor means that friction effects can be neglected, as long as the torque provided is sufficient at the max. speed required. Thus, the need for a model-based controller is obsolete. Closed-loop position control allows readjustment in the event of step loss. To control stepper motors, the integration of a driver is mandatory. Therefore, a *TMC2209* from *TRINAMIC* had been utilized, offering high phase current supply and enabling precise motor control through micro-stepping [59]. In comparison to most TVAs, the one developed is coming without any torsion spring for fail-safe reasons. Typically, the spring is resetting the TVA to idle position and keeps the engine running to drive all safety critical auxiliary units. In case of scooters/small motorcycles, there are no such systems. All safety critical systems are driven manually, why fail-safe states can be realized

by interrupting the ignition and simplifying the TVAs design that way. The torque provided by the motor is translated by a toothed belt transmission. Both output shaft ends are used to adapt the position sensor as well as the throttle valve. For position measurement, the decision was made for a non-contacting Hall effect single-turn position sensor (*6127V1A90L.25FS*) from *TT Electronics* [60]. With a min. resolution of 0.022° and a max. linearity deviation of ± 0.25%, the sensor meets the accuracy requirements of ± 1%. Coming with a range of travel over 90°, this results in a max. measurement deviation of ± 0.247° (1% = 0.7°). The remaining 21° range is used as an upper and lower error band of 10.5° each. It far exceeds the service life requirement of 500 000 (scooter service life) with 10 million cycles. Sensor read out, signal processing, motor and throttle valve position control are implemented on a similar *STM32G431KB*. Fail-safe functions, calibration and CAN communication are handled by the MCU and a CAN transceiver.

5.2.2 Mechanical Implementation

In order to reach responsive system reactions, the max. original valve angle of 69° needs to be traveled in less than 200 ms to prevent lagging throttle behavior. This results in a max. speed of 345°/s. Caused by the high inertial characteristics of fan-cooled small-volume engines, the performance required is significantly lower than that of sports motorcycles. Stepper motors have torque losses with increasing speed, which is why the torque required for the highest operating point is a major criterion. To determine the characteristics with the chosen driver, a load series test was performed, showing a stable max. torque of 12 Ncm up to a speed of 360°/s. The requirement of 5 Ncm was derived from measurements carried out by *Scion-Sprays Ltd* and *Peugeot Scooter, France* [53]. Beside providing the needed performance, the torque must be transferred to the throttle valve shaft while enabling the positioning of the Hall sensor. For fail-safe reasons, the sensor should be mounted directly on the shaft to avoid measuring random position values in the event of a gearbox or motor failure. In case of a broken belt, the TVA is still capable to distinguish between faulty or proper operation. Therefore, an adaption plate was designed, connecting the shaft with the sensor by the belonging toothed belt pulley. With regard to the transmission, the decision was made of a slip-less toothed belt due to the low gear backlash and low maintenance. A 1.5-fold transmission ratio was selected, improving position accuracy. The resulting slight drop in max. torque can be accepted thanks to the motor's torque surplus. Figure 5.4 shows the mechanical TVA setup.

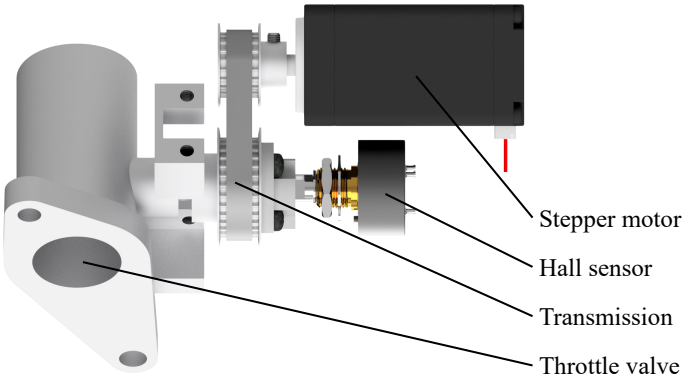

Figure 5.4 – TVA mechanics

5.2.3 Electronic Implementation

The circuit board, shown in Figure 5.3, ensures a secure electrical connection of the CAN transceiver, MCU and stepper driver. 6.5 V and 7.5 V supply voltages are provided by a central power supply, whereby the 6.5 V line is individually fused for driving the motor. 3.3 V supply for the CAN transceiver as well as the stepper drivers processing electronics are provided stabilized by the MCU itself. The assembled circuit board is mounted at the throttle valve body and represents the electronic system level. An analog position signal is delivered by the externally placed Hall sensor, which is to be digitized by the MCUs ADC. A 256-fold oversampling was figured out for best noise reduction. Stepper motors characteristics depend on the driver used. The chosen driver realizes an extremely smooth and yet powerful motor run through automatic micro-stepping (up to 256). Thus, the step-like rotation becomes harmonic and slow position changes can be realized noiseless.

5.2.4 Software Implementation

The TPS request needs to be received and processed every 20 ms (50 Hz). For creating the final throttle valve set position, the received 10 bit quantity is transferred to an opening relation with one decimal place precision (0.0% $\hat{=}$ idle state). At the same rate, the current throttle position, message counter and error status are sent to the bus for diagnostic purposes. Beside knowing the set position, it is most important to measure the current valve position to implement a closed-loop control algorithm. Therefore, the digitized and averaged position value is also being transferred into a relative quantity (%) with a precision of one decimal place every millisecond. Afterwards, the position is again smoothed by applying a Moving Average Filter (MAF) to compensate lowest powertrain vibrations. Now all variables required for position control are known and the 1 kHz clocked PI-control algorithm can be set up like shown in Figure 5.5.

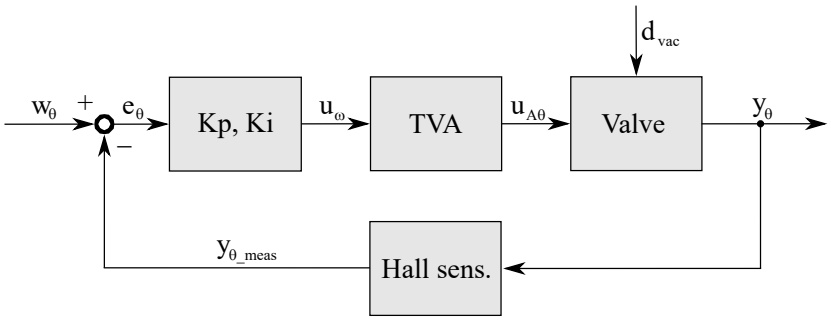

Figure 5.5 – TVA control loop

If stepper motors are operated without micro-stepping, their angular increments of 1.8° are the best possible control resolution and a P-controller is sufficient. The required position would always be achieved position controlled, assuming that the motor was sufficiently dimensioned. Step loss-free operation is the prerequisite. Here, the up to 256-fold micro-stepping results in a harmonic, almost step-free motor rotation. To compensate small, longer lasting deviations, an I-controller was implemented. The controller's parameter set was determined iteratively according to the requirements presented ($K_P = 0.11$, $K_I = 0.001$, $Speed_{max} = 360°/s$). The required valve position (w_θ) serves as input variable. After building

the control deviation (e_θ) by summing w_θ and the inverted Hall sensor feedback (y_{θ_meas}), the PI-controller outputs the manipulated variable u_ω in form of an angular velocity/step frequency. Next, the TVA adjusts the throttle valve by the actuator manipulated variable $u_{A\theta}$, which can be disturbed by the engine speed-dependent intake pressure (d_{vac}). Nevertheless, d_{vac} is too weak to falsify the set position, since the motor torque is sufficient. The resulting valve position y_θ is measured by the Hall sensor and fed back. Beside the step frequency, the drivers enabling/disabling and direction of rotation must be preset by the MCU.

In terms of fault tolerance, the TVA must clearly be classified as safety-critical. In the event of malfunction or defect, the longitudinal dynamics of the vehicle can be strongly influenced. Although the performance of scooters is still low that manually over-braking is possible, this is not to be expected. To detect failures like a broken transmission belt (1), stepper motor (2), motor driver (3), position sensor (4) or the MCU (5), a fail-safe algorithm is to be developed. In case (1), (2) and (3) the TPS set position will clearly differ from the Hall sensor acquired position. Therefore, the error is determined with two MAFs (w_θ & y_{θ_meas}). If the error exceeds a predefined threshold of 5%, the error state is declared by the overflow of a fail-safe timer. In the event of a faulty/defect sensor (4), the predefined angular range can be monitored to detect mechanical issues like overshoots/undershoots or even a total failure by comparing the signal line to the supply voltage/GND. Even if one MCU fails (5), the system must be able to induce a safe state. If the TPS MCU fails, the error will be detected by the TVA due to the faulty message counter. Then, the actuator refuses commands and moves back to idle position. In the event of self-detected TVA errors, the TPS is addressed by sending an error report, interrupting the ignition by means of a safety contactor. In case of total failure of the TVA MCU (5), the same effect occurs by detecting an outdated message counter.

Stepper motors can consume the phase short-circuit current in energized standstill. For this reason, an energy-saving mode has been implemented that tolerates the smallest deviations while taking the control deviation into account. If the deviation is less than 0.15% within a predefined time period, the motor is no longer energized by disabling the driver. That way, the current consumption and the generated waste heat can be significantly reduced, enabling a passive cooling strategy. In addition, a small permanent deviation of the set TVA position can occur due to minimal temperature-related drifts of the Hall sensor. These minimal deviations do not have any remarkable effect on partial or full-load behavior, but the engine's idle speed is already affected by 0.5% deviations. To avoid this, a calibration function has been implemented which calibrates the actuator within 0.5 s when the system is switched on. This process is repeated in larger time intervals. As soon as the vehicle does not receive a throttle command, the re-calibration is executed. For this purpose, a three-point controller was specially tuned, which determines the correct initial position depending on the measured unstable position when the lower throttle valve end stop is reached.

5.3 Temperature Resistance

When selecting the components, explicit attention was paid to temperature resistance in accordance with ISO 16750-4 (Road vehicles - climate loads). Hall sensor, AMR sensor, stepper motor driver, MCUs and manufactured housing parts meet the temperature requirements (-40 to 125°C). According to the manufacturer, the stepper motor is suitable for temperatures down to -10°C and may need to be replaced. Temperature-dependent friction variations are neglected due to the drive's significant torque reserves. Shifting of the end stops due to material expansion is compensated by the automated TVA calibration. The temperature influence on the position measurements can be neglected, as the AMR sensor internally compensates fluctuations and the measurement error of the Hall sensor can be max. 0.07% (Δ 165°C). Table 5.2 shows the temperature limits of the TbWS components.

Component	Min. T	Max. T	Note
Requirement	-40°C	85°C	Interior
(ISO 16750-4)	-40°C	125°C	Engine compartment
AMR sensor	-40°C	125°C	Internal T compens.
Hall sensor	-40°C	125°C	Max. error: 0.07 %
Motor driver	-50°C	150°C	/
Stepper	-10°C	130°C	Insulation resilience
MCUs	-40°C	125°C	/
Carbon Fiber FDM Nylon	<-40°C	140°C	Housings

Table 5.2 – TbWS temperature limits

6 Development of Velocity Control

The TbWS provides the basis for actuating the throttle valve independently of the set throttle grip position. Up to this point, the TbWS has no benefit, as the throttle valve position would equal the throttle grip position. The potential of the powertrain is only unleashed by the velocity-controlled throttle valve opening while disabling ITM. As explained in Chapter 4, further subsystems are required to implement the VC/alternative restriction. A redundant WSS needs to be developed and adapted to reliably detect the vehicle velocity. The higher-level MECU will act as the system master and, among other things, perform the VC. The VC algorithm is to be designed, simulated and tuned. As an HMI, a virtual dashboard will enable communication between the scooter and rider. All subsystems are power supplied and networked by CAN, meaning an appropriate wiring architecture is required [61].

6.1 Wheel Speed Sensor

The scooter's velocity is required as a control variable for VC. Since 50 cc scooters are not legally obligated to be equipped with an anti-lock braking system, they do not have WSSs [62]. In the test vehicle, the rear wheel speed is only measured with a passive inductive Transmission Speed Sensor (TSS) on the clutch bell for restriction purposes. Due to its design, it is not suitable for measuring low speeds. To keep the system costs low, the speed should only be measured on one wheel. The integration of two sensors on one axis enables plausibility checks of the measurements. A resolution of 0.1 km/h is required for adequate VC. Therefore, a redundant WSS must be developed, which enables the precise sensing of the wheel speed. The sub-tasks can be grouped into mechanics, electronics and software. On a mechanical level, the encoder disk and sensors must be adapted to the wheel. Electronic requirements include the power supply for the sensors, the generation of a measurement voltage and the digitization of the signals. The sensor pulses must be converted into a vehicle velocity, processed and checked for plausibility using software [63].

6.1.1 System Architecture

Two automotive Hall effect WSSs independently measure the motion of a 48-step encoder disc by determining the width of successive pulses. The decision was made for WSSs of the type *Bosch 0265004254*. This sensor is installed by numerous motorcycle manufacturers and is easy to integrate due to its small design. A magnetic excitation field of the sensor stimulates the encoder disk, while a probe simultaneously measures the generated Hall voltage. The WSS modulates the encoder step frequency by applying step-like current changes to the two supply lines. By using a measuring resistor, a measuring voltage can be generated and tapped for each sensor. For effective processing, both signals are digitized using a two-channel

comparator (*LM393*). Thus, external interrupts can be used for pulse width measurement by the MECU (*STM32G431KB*). The resulting high-resolution vehicle velocity is used in the MECU for precise VC. It is also provided to other subsystems via CAN message, using a CAN transceiver. The module is supplied with 12 V for the WSSs and 7.5 V for the MECU. The operating voltage of 3.3 V for the comparator and CAN transceiver is provided internally by the MECU. Figure 6.1 shows the WSS architecture.

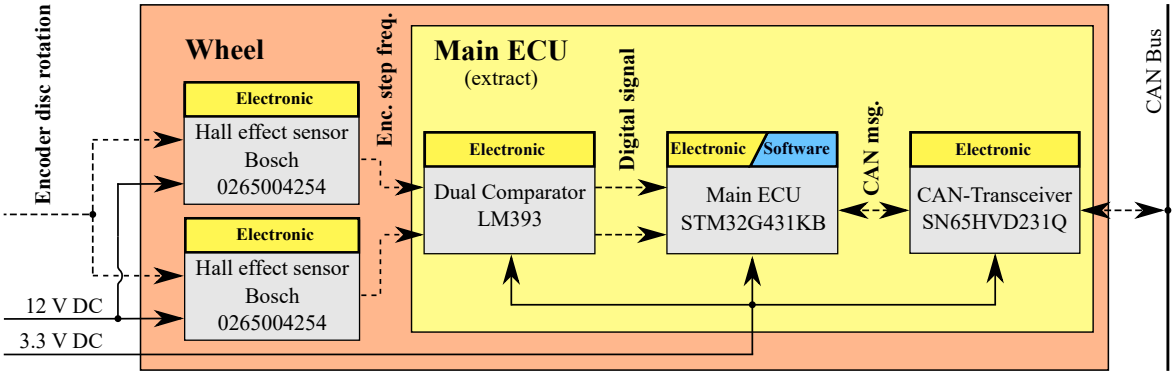

Figure 6.1 – WSS architecture

6.1.2 Mechanical Implementation

The assembly is to be integrated, whereby a constant distance (<0.5 mm) between sensors and the encoder disc is to be ensured. Preferably, the controlled rear wheel speed is sensed to intervene in case of wheel slip. Adaptations were developed in several iterations. Unlike chain-driven motorcycles, there is no decoupling between the driven wheel and the engine/gearbox. Vibrations from strong low to high frequencies are directly transferred to the WSS resulting in extreme measurement inaccuracies. Some engine speeds trigger resonance oscillations, leading to amplitudes of the encoder disk in the millimeter range. Decoupling, damping, mechanical changes on the encoder disc and software filters for signal processing could not achieve sufficient signal quality. For that reason, the WSS is adapted to the front wheel. With a bracket, both sensors are precisely placed, as shown in Figure 6.2.

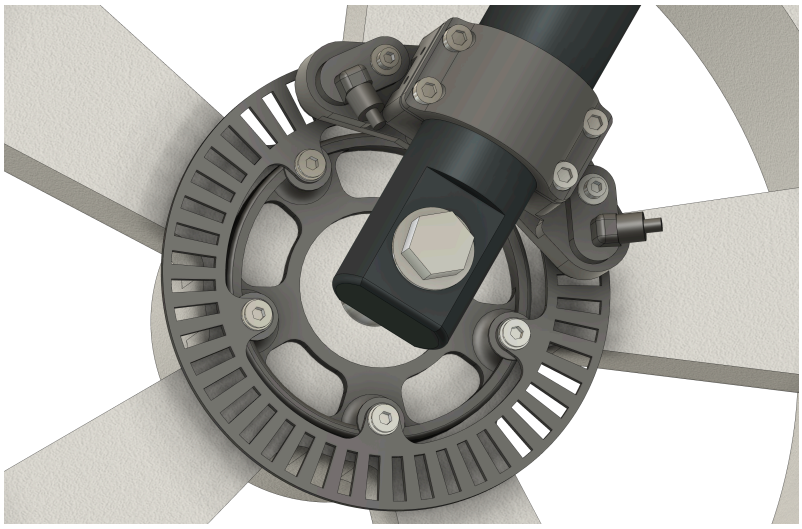

Figure 6.2 – WSS adaption

The encoder disc is screwed onto an adaptation plate, which is centered on the wheel rim using two-component metal adhesive. Both WSSs are inserted into the bracket and fastened with screws. The sensor carrier is attached to the left-hand telescopic fork bar using a form-fitting clamp connection. It can be slid and rotated axially for fine adjustment. The design was developed with the criterion of high rigidity and consequently low susceptibility to vibration. Cables are routed under the scooter cladding in the system's wiring harness to the MECU in the engine compartment (see Fig. 4.2). The design of the MECU, including the comparator and CAN transceiver, is described in Chapter 6.2.

6.1.3 Electronic Implementation

Each WSS modulates the measurement signal in the form of a change in current intensity on the supply cables. The MCU can only tap the signal by measuring or exceeding a threshold voltage. For this purpose, two carbon film resistors generate a measuring voltage, which is processed by a two-channel comparator. The signal can then be processed by the MCU using external interrupts to conserve resources. The TSS already installed is a passive, inductive sensor that provides an analog, oscillating signal that varies strongly in amplitude. For further processing, the voltage of the TSS signal (± 30 V) must be limited to a rectified and digitized voltage that can be processed by the MCU (3.3 V). A voltage divider reduces the signal voltage before it is digitized by an optocoupler.

6.1.4 Software Implementation

Two approaches are conceivable for calculating the wheel speed/vehicle velocity. On the one hand, incoming pulses could be counted within a defined period of time. However, the measurement accuracy would depend on the number of encoder steps and the selected time span. On the other hand, the time period between two successive positive edges can be measured to determine the speed. Here, the resolution only depends on the timer's clock frequency, which is why faster and more accurate measurements are possible. Consequently, the evaluation is carried out by a 32 bit timer measuring the pulse width. A sampling rate of 1 MHz results in a min. resolution of 0.02 km/h at 50 km/h (0.0002 km/h at 5 km/h). As the MCU used is only equipped with a 32 bit timer, a 16 bit timer is selected for the reference measurement of the second WSS. As the raw data from the WSSs does not lead to a satisfying measurement quality, the data is processed in two stages.

- Stage 1: The measured pulse length (T_{WSS}) is transferred into a velocity (v_{wss}) and stored in an array to achieve smoothing by applying a MAF with the size s_A. For the determination, the wheel circumference (D_{wheel}) and the resolution of the encoder disc (n_{steps}) are required. If the timer counter is exceeded at 0.44 km/h, timeout values are saved, which are interpreted as 0 km/h. Equation (6.1) transfers the pulse widths into a velocity.

$$v_{wss} = \frac{d_{step}}{t_{step}} = \frac{D_{wheel}}{n_{steps}} \cdot \frac{s_A}{\sum_0^{s_A} T_{wss}} \tag{6.1}$$

At low vehicle velocities, large arrays would lead to longer dead times of the measured variable resulting in unstable control behavior. By implementing a velocity-adaptive MAF, dead times are kept low and almost constant (e.g.: 5 km/h $\widehat{=}$ 80 ms, 50 km/h $\widehat{=}$ 100 ms). An array with 4 fields (v_{A4}) and second with 48 fields (v_{A48}) are filled simultaneously. Equation 6.2 shows the velocity-dependent weighting of both MAFs, resulting in an adaptively filtered final vehicle velocity.

$$v_{scooter}[n] = v_{A4}[n] \cdot \left(1 - \left(\frac{v_{wss}[n-1]}{v_{max}}\right)\right) + v_{A48}[n] \cdot \left(\frac{v_{wss}[n-1]}{v_{max}}\right) \tag{6.2}$$

- Stage 2: The raw data of the WSS is theoretically solely limited in the min. velocity by the timer overflow. However, measurements often generate erroneous pulse lengths that are transferred to four-digit velocity ranges. Despite the MAF, these individual measurements result in extreme velocity jumps due to their magnitude. Firstly, sensed velocities above 70 km/h are not stored in the array but are discarded. Secondly, measured values are compared with an error band, which is based on the previously filtered velocity. Outlying measurements are overwritten with the previous filtered velocity before they are included in the MAF algorithm.

Both arrays are filled at the frequency of the incoming sensor pulses. At top speed, this corresponds to a frequency of 460 Hz. As the VC/data provision on the CAN bus is required at a rate of 50 Hz, the velocity is calculated at the same rate for runtime optimization. The data processing described here is carried out analogously for both WSS. The measured wheel speeds are compared for plausibility checks and error detection. If deviations exceed 2 km/h, an error status is set. The original TSS is processed using the same algorithm as the two WSSs. Due to the passive operating principle of the TSS, no pulse lengths can be measured for slow speeds. At speeds faster than 6 km/h, the signal reaches the threshold of the electronics. The measured velocity is of low quality, but is used to detect rear wheel lock-up or spinning. If the rear wheel is locked, no system intervention is possible, as the scooter is not equipped with an anti-lock braking system. If the front wheel locks, the accelerator command is interrupted, as otherwise additional acceleration would hinder braking.

6.2 Main ECU

Chapter 4 gives an overview about all subsystems required, including the MECU. In addition to a stable and secure power supply, a system master is needed to safeguard the overall system in the event of a fault. An interface between the scooter and the system is required, which covers the general power supply, TSS signal, ignition cable, oxygen sensor and the original EC. At software level, the VC needs to be implemented, adjusting the vehicle's velocity to the rider's demand. Moreover, the selection of operating modes, setting user parameters or operating the CC must be implemented in interaction with the HMI. The MECU is integrated in the engine compartment and should not affect the function of the helmet compartment as much as possible. Due to the proximity to the engine, increased operating temperatures can occur, which is why the module is actively cooled. Like all subsystems, the unit is designed to be modular by means of quick connectors.

6.2.1 System Architecture

The MECU is intended to act as a higher-level system master and the decision was once again made for a *STM32G431KB* MCU, as it is equipped with sufficient Input/Output (I/O) peripherals, computing resources, ADCs and timers [57]. On the input side, the battery voltage, oxygen sensor signal and wheel speed signals (WSS & TSS) are connected. Further, the TPS measured throttle value, the rider command from the HMI and subsystem states are received via CAN. On the output side, stabilized/fused power lines, the emulated TSS signal and CAN connection must be provided. CAN communication includes, for example, the TVA throttle valve position, HMI system states and safety information from all subsystems. At the hardware level, the MECU must convert three individual supply voltages by using DC/DC step-down converters (*LM2596S*). Measurement electronics of the WSSs/TSS (*LM393* comparators) must be provided and the emulated speed signal is to be amplified by use of a MOSFET. To empower the failsafe functions, a relay must be capable of interrupting the ignition line. Figure 6.3 shows the MECU's system architecture. On power box level, power supply, fuse protection and active cooling are managed. On ECU level, the MECU itself represents the central hub where all signal inputs and outputs originate.

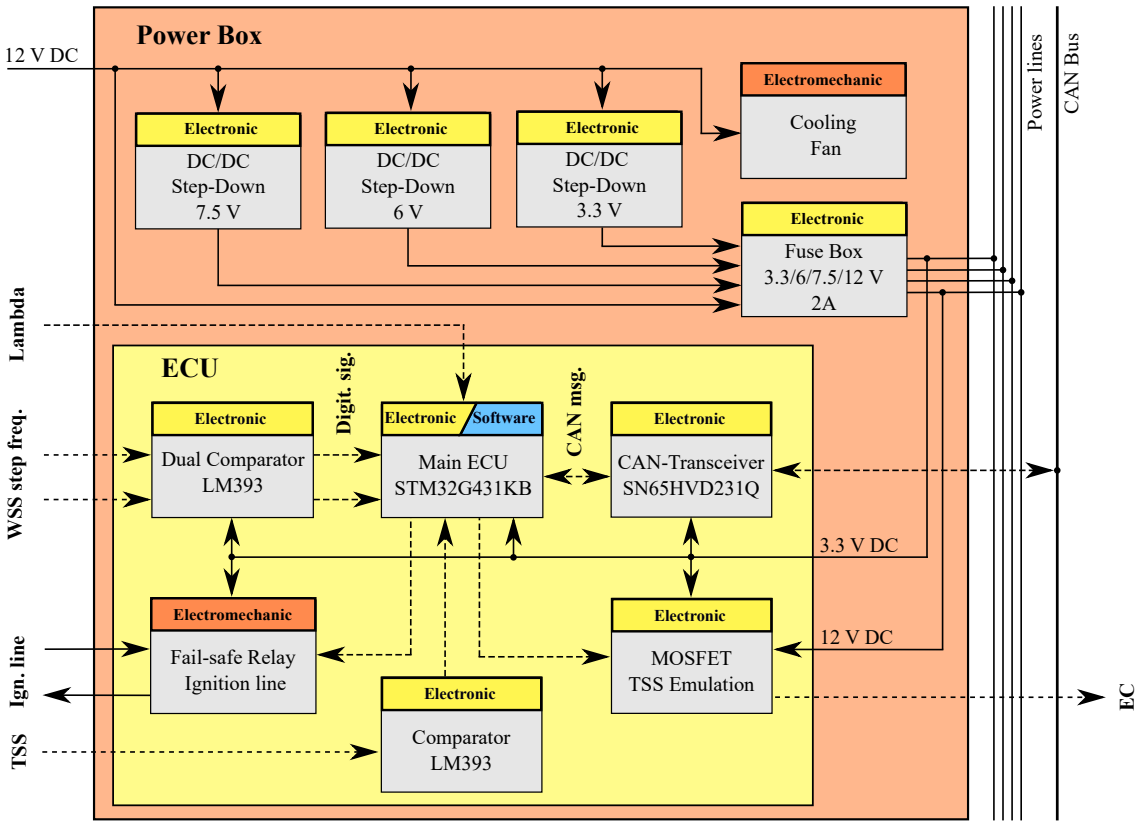

Figure 6.3 – MECU architecture

6.2.2 Subfunctions

To fulfill the tasks introduced, the MECU can be divided into the subfunctions wheel speed processing, power box, sensor emulation and fail-safe. As the processing of the wheel speed has already been addressed extensively in Chapter 6.1, it will not be considered further.

Power box: The MECU provides individually fused voltages to all subsystems. Especially the TVA stepper motor is to be supplied with an independent power line to prevent system errors in case of motor/mechanical damage. Three 12 V DC/DC step-down converters provide stabilized voltages of 3.3 V (MECU internal), 6 V (TVA stepper motor) and 7.5 V (common system voltage). In addition, the 12 V battery voltage is also provided. A wiring harness originates from the MECU that connects all subsystems, consisting of 6 wires: GND, VCC_{step}, VCC_{sys}, VCC_{bat}, CAN_H and CAN_L.

Sensor emulation: For bypassing the OR, the original EC needs to be emulated with a synthetic TSS signal. Therefore, a signal is to be emulated and amplified, depending on the current velocity ($v_{scooter}$). The output frequency is two times lower than the by the original TSS provided oscillating signal. That way, the EC is not interfering the optimal ignition timing. For proper stimulation, the emulated signal has to be within the original speed-dependent voltage range ($\pm 30\ V$). The emulated signal is generated by switching the 12 V battery voltage by a MOSFET, overcoming the ECs threshold. Equation (6.3) is used to calculate the emulating frequency (f_{emul}) for the pulse width modulated timer, based on the second-stage transmission ratio ($i_{gear} = 13$) and the number of poles ($n_{pole} = 4$) attached to the clutch bell. For a velocity of max. 50 km/h, a frequency of 3.64 kHz results. To facilitate the comparison between the OR and VC system, a switch can be used to select between transferring the emulated or original TSS signal to the EC.

$$f_{emul}(v_{scooter}) = v_{scooter} \cdot \frac{2 \cdot i_{gear} \cdot n_{pole}}{D_{wheel}} \tag{6.3}$$

Fail-safe: Every system interfering with vehicle dynamics, is to be classified as safety critical. The system manipulates longitudinal dynamics by throttle intervention. Depending on the error detected, the MECU must react by predefined fail-safe states to ensure safe vehicle operation. Table 6.1 shows the error cases identified as possible. The fail-safe states are classified into four classes (C). Class 1 describes warnings that require re-calibration but do not danger safe operation. Class 2 can affect the operation by malfunction of the CC, which is why it is disabled. Class 3 can lead to total scooter misbehavior by loss of acceleration control. In this case, the TVA is not accepting throttle requests. Class 4 represents the worst case. The MECU can no longer control the powertrain and a contactor interrupts the ignition line to shut down the engine. A relay is to be integrated, controlling the ignition line. All error cases include monitoring of CAN communication, using safety features and life detection.

ID	C	Error	Type	Action
1	1	TPS calib. req.	Warning	HMI notification
2	1	TVA calib. req.	Warning	HMI notification
3	2	HMI CAN error	Error	Disable cruise contr.
4	3	WSS inaccuracy	Error	Reset TVA & set vel.
5	3	TPS error det.	Error	Reset TVA & set vel.
6	4	TVA error det.	Error	Engine shut down

Table 6.1 – List of fail-safe states

6.3 Velocity Control Algorithm

Conventional vehicles require a throttle command by the rider that relates to the required power needed. The rider controls the desired vehicle velocity. The VC approach describes a continuous control of the velocity. Instead of a required engine power, the throttle grip position represents a set velocity. Basically, the system performs a continuously varying CC algorithm. For this, a controller is designed, as shown in Figure 6.4. The TPS set velocity (w_θ) serves as input reference variable. After determining the control deviation (e_θ) by using the WSS measurement as control variable feedback (y_{θ_meas}), the PI-controller outputs the manipulated variable u_ω in form of a throttle valve opening. Next, the TVA controls the airflow ($u_{A\theta}$) within the air intake. Then, the powertrain reacts to the system's throttle demand and generates a propulsion force in relation to the throttle valve opening. Windy conditions, heavy load or street gradients can result in a disturbing/varying resistance force (F_{resist}). The vehicle velocity y_θ is measured by the WSS and fed back. CC can be realized by simply maintaining the current velocity setpoint.

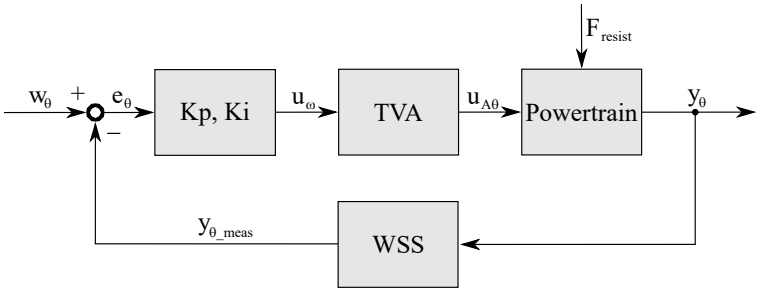

Figure 6.4 – VC control loop

6.3.1 Modeling and Simulation

For adequate controller design, the system is simulated. Considering translatory ($F_{I_{trans}}$) and rotational ($F_{I_{rot}}$) mass inertia, air (F_{Air}) and rolling (F_{Roll}) resistance, the equilibrium of forces is described in (6.4). The sum of all resistance forces equals the driving force (F_{Drive}).

$$F_{Drive} = F_{I_{trans}} + F_{I_{rot}} + F_{Air} + F_{Roll} \tag{6.4}$$

Translatory mass inertia directly counteracts the acceleration of the scooter. The counterforce results from the inertia of the total mass and the applied acceleration, as in (6.5).

$$F_{I_{trans}}(x) = (m_{sc} + m_r) \cdot \ddot{x} \tag{6.5}$$

Rotational mass inertia counteracts the rotary acceleration of the scooter's wheels. The movement of the wheels is composed of a translatory and rotatory component. Due to the vehicle mass contained in (6.5), the translational part is taken into account. Rotatory mass inertias also result as forces opposing the direction of travel. The rotational acceleration occurs tangentially (r) due to the road adhesion. Front and rear counterforces result from the rotary inertia of each wheel (J_f, J_r), mass and the applied acceleration, as in (6.6). The rotatory wheel inertias were experimentally determined to 0.327 Nms^2 (J_f) and 1.3228 Nms^2

(J_r). The comparatively high rotational inertia at the rear wheel is due to the permanently connected second gear stage, including the clutch bell.

$$F_{I_{rot}}(x) = \frac{(J_f + J_r)}{r^2} \cdot \ddot{x} \tag{6.6}$$

Air resistance is velocity-dependent in square relation. The resulting counterforce, given in (6.7), is mainly influenced by the frontal area (A) of the scooter including the rider and the drag coefficient (c_w). In order to determine the frontal area, the scooter and rider (1.8 m, protective clothing) were photographed next to reference markers. To reduce perspective measurement errors, the camera was positioned at a medium height and at the greatest possible distance. By determining the pixel ratio between background and object, the area was approximated to 0.78 m^2. The drag coefficient was measured at 0.64 by coast down tests.

$$F_{Air}(x) = \frac{A \cdot \rho \cdot c_w}{2} \cdot \dot{x}^2 \tag{6.7}$$

Rolling resistance depends on the weight (m) and the resistance coefficient (c_r), described in (6.8) as a constant force. The coefficient was measured at 0.015 by coast down tests.

$$F_{Roll} = c_r \cdot (m_{sc} + m_r) \cdot g \tag{6.8}$$

Substituting all the partial forces introduced into Equation (6.4), a non-linear differential equation of second-order results for F_{Drive} in (6.9) depending on the vehicle position.

$$\begin{aligned} F_{Drive}(x) = (m_{sc} + m_r) \cdot \ddot{x} + \frac{(J_f + J_r)}{r^2} \cdot \ddot{x} \\ + \frac{A \cdot \rho \cdot c_w}{2} \cdot \dot{x}^2 + c_r \cdot (m_{sc} + m_r) \cdot g \end{aligned} \tag{6.9}$$

F_{drive} depends on the operating point of the engine and gearbox. To determine the power characteristics, performance measurements were taken on a roller dynamometer at various operating points, shown in Figure 6.5. With the clutch engagement, the power increases up to 15 km/h. The power declines with growing velocity due to the poor CVT efficiency and the speed-dependent power drop of the engine. Caused by the test setup, F_{Roll} is part of the measured power and has to be compensated proportionally in case of partial load conditions.

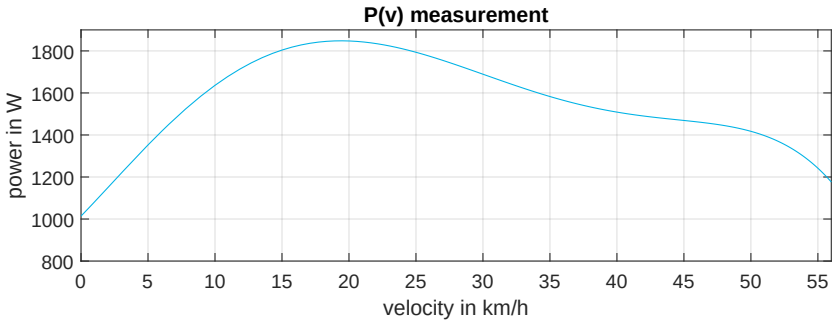

Figure 6.5 – Engine characteristics

A polynomial ($P(v)_{poly}$) is derived from the data set. For a full throttle acceleration, the driving force can be determined by Equation (6.10).

$$F_{Drive}(\dot{x}) = \frac{P(v)_{poly}}{\dot{x}} \tag{6.10}$$

Table 6.2 lists all known or measured variables that are required for the simulation.

	Property	Symbol	Value
1	Frontal area	A	0.78 m^2
2	Wheel radius	r	0.226 m
3	Inertia front wheel	J_f	0.327 Nms^2
4	Inertia rear wheel	J_r	1.3228 Nms^2
5	Mass scooter	m_{sc}	99 kg
6	Mass rider	m_r	80 kg
7	Air resistance coeff.	c_w	0.64
8	Rolling resis. coeff.	c_r	0.015
9	Air density	ρ	1.225 kg/m^3

Table 6.2 – List of simulation related properties

Figure 6.6 illustrates the conversion of the differential Equation (6.9) into a block diagram. Since an acceleration under full load is simulated, the rolling resistance is not considered.

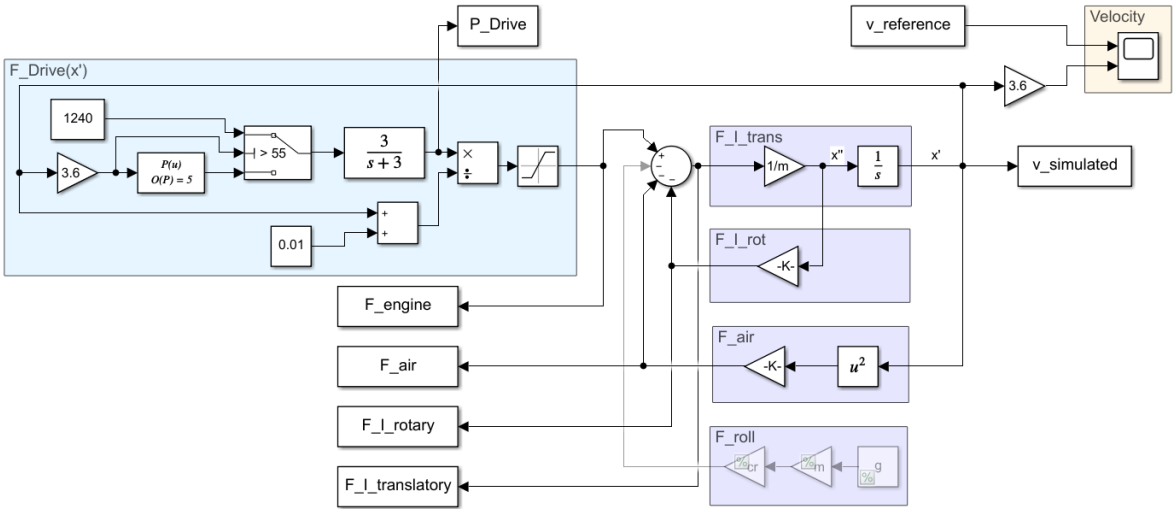

Figure 6.6 – Simulink block diagram

To check on model plausibility, the simulated step response was compared to a reference measurement, shown in Figure 6.7. The final velocities and the acceleration behavior match. The max. deviation is ±1 km/h and the validity of the simulation is sufficient. In addition, the simulated forces are shown as further simulation output.

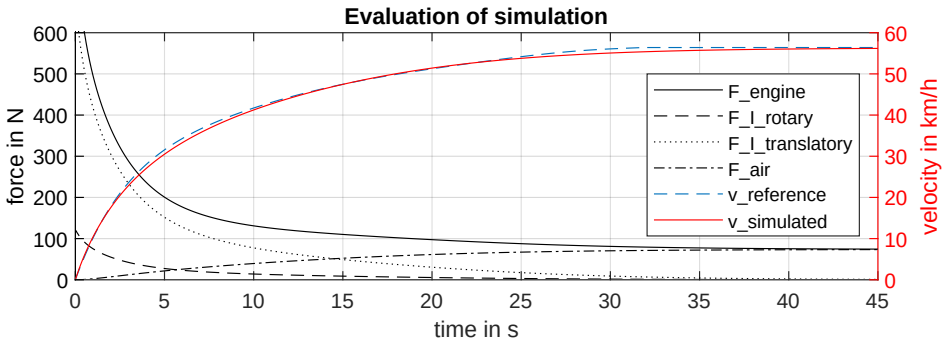

Figure 6.7 – Evaluation of simulation

6.3.2 Control Algorithm

By applying the VC, the throttle grip position equals a set velocity. Controlling the scooter's velocity constitutes a non-linear system. With increasing velocity, the air resistance rises in square relation. Typically, control algorithms for non-linear systems are optimized for a certain operating point by linearization. Here, an adaptive PI-controller is proposed to change its characteristics velocity-dependent. This strategy achieves a balance between high controllability and control accuracy over the whole velocity range. In theory, a P-controller could already lead to adequate control behavior. If the gain is too high, not only the overshoot behavior but also signal disturbances of the velocity feedback would negatively affect the performance. Through adding an I-controller, the set velocity can be reached by smaller P-gains, stabilizing the controller and decreasing the susceptibility to disturbances. The controller's parametrization needs to adapt continuously to the scooter's operating point. Proportional (K_P) and integral (K_I) gain adapts to the current scooter velocity (v_{sc}) given in (6.11) and (6.12). For both, the max./min. gain is to be determined. A constant 3.0 km/h offset (Os) of the linear I gain curve prevents instability at very low velocities.

$$K_P = \frac{v_{sc}}{v_{max}} \cdot (K_{P_{max}} - K_{P_{min}}) + K_{P_{min}} \tag{6.11}$$

$$K_I = \frac{v_{sc} - Os}{v_{max}} \cdot (K_{I_{max}} - K_{I_{min}}) + K_{I_{min}} \tag{6.12}$$

Caused by the continuously changing set velocity and the varying steps within the throttle command, the I-controller can not perform precisely. Depending on the operating point, there are different settling times for different velocities and, as a result, varying integral values/overshoots. By implementing a set velocity-dependent threshold (T_I), the enabling time of the I-controller can be predefined related to the rising control deviation (dev) and set velocity (v_{set}). T_I is described by Equation (6.13).

$$T_I = \frac{v_{set}}{v_{max}} \cdot (K_{T_{max}} - K_{T_{min}}) + K_{T_{min}} \tag{6.13}$$

If the control deviation overcomes the threshold in its current operating point, the integrator is reset and disabled by (6.14). The I-controller is only enabled in a certain error band in order to adjust the system as precisely as possible. This error band is centered around the setpoint and changes its size relative to the setpoint. This allows the control behavior to be kept consistent, regardless of the operating point and abrupt throttle commands. Additionally, the integrator is limited to prevent an integration wind-up when the actuator is saturated.

$$(dev > T_I) \quad I_{enbl} = 0 \quad ; \quad (dev \leq T_I) \quad I_{enbl} = 1 \tag{6.14}$$

The throttle valve position (Pos_{thr}) is given by Equation (6.15).

$$Pos_{thr} = K_P(v_{sc}) \cdot dev + K_I(v_{sc}) \cdot I_{enbl}(T_I) \cdot \int dev \tag{6.15}$$

Based on the longitudinal scooter model, a closed-loop simulation was set up for tuning the controller. A max. overshoot of 0.3 km/h (barely noticeable) and robust control behavior,

under consideration of sensor disturbances, were required. In addition to a fast settling time, driveability was taken into account. At high gains, the powertrain reacts too sensitively to small throttle deflections, despite constantly stable control behavior. Therefore, a parameter set was chosen that combines the highest possible performance with enabling smooth accelerations. Using simulation, it was determined which parameter set was best with regard to control performance. This was then optimized for driveability in a road test. Figure 6.8 shows the closed-loop block diagram. The algorithm is being executed with a cycle time of 20 ms.

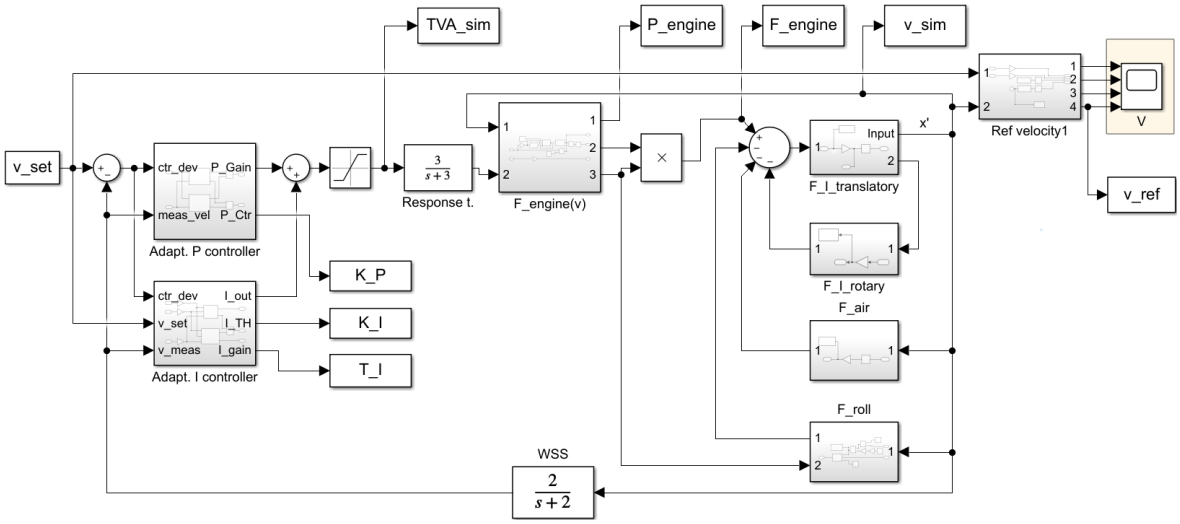

Figure 6.8 – Simulink closed-loop block diagram

Figure 6.9 shows the implementation of the I-controller, including the velocity-dependent gain (K_I) and the set velocity-dependent threshold (T_I). The P-controller is similar, except the adaptive threshold. Table 6.3 shows the determined parameters.

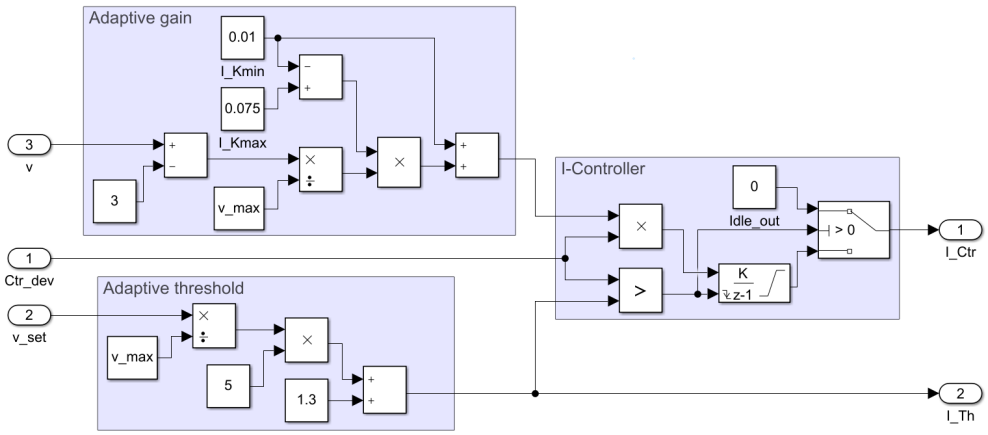

Figure 6.9 – Simulink I-controller

	P	I_{sim}	I	$T_{I,sim}$	T_I
K_{min}	2.1	0.02	0.01	1.44	1.3
K_{max}	16	0.07	0.075	6.84	6.3
Os	/	3.0	3.0	3.0	3.0
$Limit$ (%)	-100/100	0/100	0/100	0/100	0/100

Table 6.3 – List of controller parameters

6.4 Human Machine Interface

50 cc scooters are usually equipped with cost-effective analog speedometers. Most often, they solely display rudimentary information like velocity, mileage, fuel level and states for turn signal, high beam and engine failure. The more features a vehicle is offering to the rider, the more requirements are set on the HMI to enable intuitive operation. With implementing the VC, coming with a new throttle behavior, different driving modes, CC implementation and further functions related to the system evaluation, an analog speedometer is not sufficient anymore. Virtual dashboards are uncommon in this vehicle class, but offer plenty of opportunities for adequate visualization and interaction. The purpose of the HMI includes the visualization of vehicle and system information as well as various functionalities:

1. **Previous features:** Information displayed by the original speedometer such as indicators for turn signals, high beam, malfunction, fuel level and mileage is visualized.
2. **Set/scooter velocity:** Based on the VC strategy, the velocity demand given by the rider is displayed in addition to the scooter's velocity to improve driveability.
3. **Throttle valve opening:** The throttle valve opening is displayed to demonstrate the function of the VC by the deviation to the throttle grip position.
4. **Rider input:** Beside providing information to the rider, the HMI interfaces inputs from the rider by use of a physical operating unit placed at the scooter's handlebar.
5. **CC interface:** For enabling/disabling the CC and setting the desired velocity, an interface is implemented achieving intuitive and safe operation.
6. **Eco-score:** To encourage eco-friendly driving, an eco-score is built up with fuel savings achieved by the developed VC.
7. **Measurement Box (MB) control:** The MB developed for recording measurement data must be operated safely. Recordings can be started and stopped via the HMI while driving. The current recording status of the MB is displayed.
8. **Evaluation information:** Measured quantities like engine speed, exhaust oxygen concentration and fuel consumption are displayed in addition to a resettable trip.
9. **Developer view:** A development mode enables the visualization of all system and control variables as a real-time graph view.
10. **Driving mode:** By use of the HMI, the developer can switch between the OR (TSS signal) and enabled VC system (emulated TSS signal) for evaluation purposes.
11. **Fail-safe states:** In case of a detected TbWS, VC or CAN malfunction, fail-safe states are displayed on screen.
12. **Menu:** Switching operation and driving modes is enabled by a menu that can be entered while the scooter is at a standstill. Settings like the system time can be edited.

6.4.1 System Architecture

The virtual dashboard consists of a 4.3" Liquid Chrystal Display (LCD) combined with a *STM32H7B3* MCU [64]. To adjust the LCD light intensity by night, a photodiode is sensing the ambient light close to the screen. Most system information that are to be displayed are received by the internal CAN transceiver. The opening duty cycle of the engine's injector is measured by tapping the injector voltage with an optocoupler. Rider inputs could be realized using the integrated touch screen, resulting in an openly accessible and unprotected display. Also, system commands should be given safely while riding without the need to release the handlebars. A micro-joystick is integrated into the throttle armature, enabling safe operation and LCD protection against splash water and damage by a plexiglass cover. Vehicle data that was displayed from the original analog speedometer (turn signals, head beam state, engine malfunction and fuel level) are interfaced by the ECUs ADC. In addition, both brake light switches were tapped in order to sense the brake actuation as an abort condition for the CC. The HMI unit is supplied with a 12 V DC voltage reasoned by the comparably high max. power consumption of 500 mA (5 V). To relief the MECU's power box, an onboard step-down converter is providing the HMI supply voltage of 5 V. Internal 3.3 V power supply is given by the ECU. Most visualized system data is real-time data. Mileage and odometer, in contrast, must be saved when the system is switched off and called up when it is switched on. To avoid memory conflicts with the internal ECU flash memory, an external data logger receives both parameters via a Universal Asynchronous Receiver Transmitter (UART) connection and supplies them during system startup. Therefore, an *OpenLog* module from *SparkFun* is used, storing its data cyclically on a microSD card [65]. CC related commands, control of the MB, driving modes and the injector duty cycle are transmitted via CAN. Figure 6.10 shows the described HMI architecture including I/O, HMI and belonging peripherals.

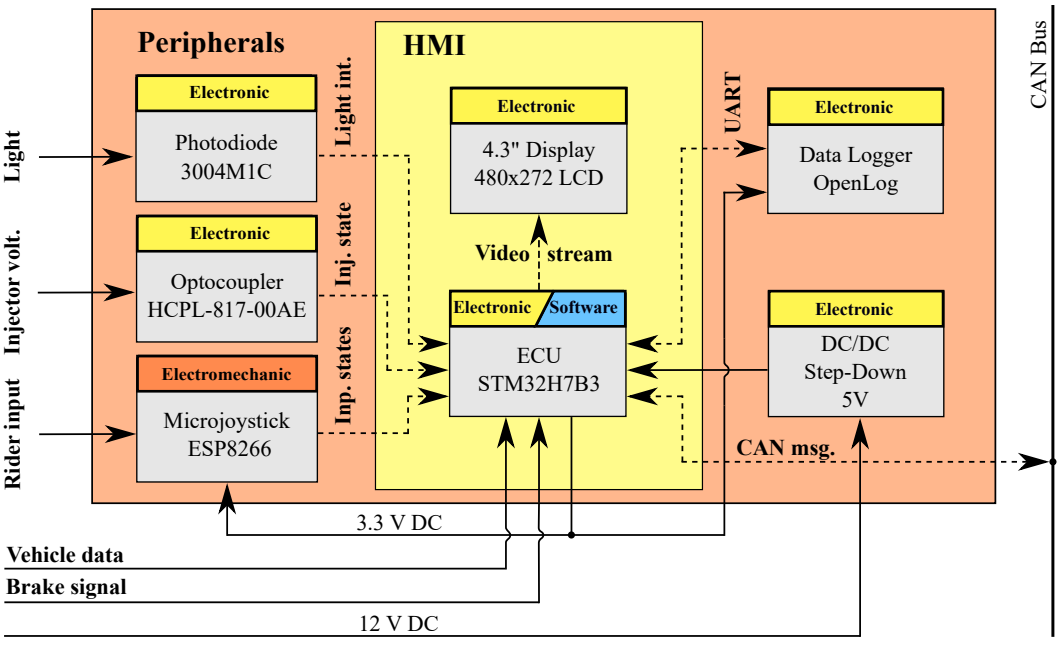

Figure 6.10 – HMI architecture

6.4.2 Mechanical Implementation

The virtual dashboard replaces the analog speedometer. Here, the design of the cockpit is to be retained by keeping the same cockpit mask. The HMI module consists of the LCD, the ECU and peripherals as shown in Figure 6.10. The LCD and ECU form a single unit thanks to screw connections. Peripherals are later plugged to the ECU by a circuit board and thus complete the module by connectors. A carrier mounts the assembly, framing the display, fixing the photodiode and adapting the module to the vehicle's handlebar. To protect the HMI against environmental influences, a plexiglass is inserted between the carrier and the mask. By applying an anti-reflective film, reflection effects are reduced and readability is enhanced. Figure 6.11 shows the mechanical setup of the HMI (left) and micro-joystick (right).

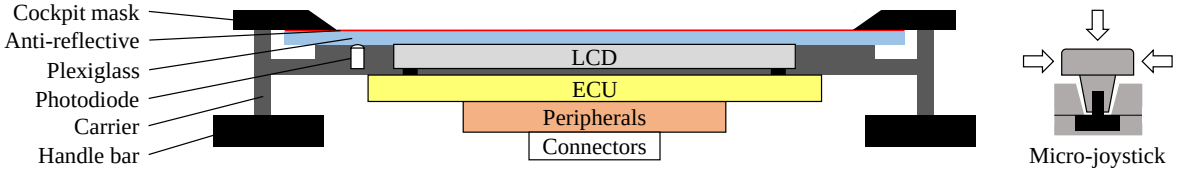

Figure 6.11 – HMI mechanical setup

The development of the micro-joystick also requires mechanical solutions. Sensing is performed by the electromechanical *ESP8266* five-direction button element (black). The commands UP, DOWN, LEFT, RIGHT and CENTER are required for menu navigation and operation. A plastic knob is designed to improve the joystick's handling. Further, the degree of freedom in tilt and push direction needs to be limited to prevent damage to the button element. This also creates haptic feedback through solid end stops. For this purpose a plastic housing is designed, guiding the knob and limiting its movement by a conical opening. The micro-joystick assembly is installed at the right handlebar to ensure intuitive operation with the thumb while accelerating.

6.4.3 Electronic Implementation

To meet electrical needs, a circuit board was designed which can be plugged onto the back of the ECU. The board contains the DC/DC step-down converter, the optocoupler for interpreting the injection valve and several voltage dividers. Fuel level and light signals, originally displayed by the speedometer, are coming with a voltage of 12 V. These must be reduced to 3.3 V before analog-digital conversion. Three connectors enable access to the scooter's original wiring harness (speedometer light signals, fuel level, brake switch signal), the VC wiring (CAN, 12 V power supply) and connection of the micro-joystick. Data logger and micro-joystick are supplied with a stabilized 3.3 V voltage of the ECU. In contrast to the TPS's, TVA's and MECU's MCUs, the *STM32H7B3* provides an onboard CAN transceiver.

6.4.4 Software Implementation

Appropriate software modules must be developed to implement the functions mentioned in Chapter 6.4. The HMI data processing can generally be grouped in externally transferred and internally processed. External data is received through CAN and visualized. Internal data is

to be measured, processed and visualized as driving information. Further, the VC evaluation and comfort features must be executed before feedback data is transmitted via CAN.

- **Inputs:** As shown in Figure 6.10, several inputs are processed by the HMI. Caused by non-compliance with digital switching thresholds of the MCU, two ADCs achieve sensing of all six inputs by multiplexing. One ADC indicates steady state signals of engine malfunction, turn signals and variable fuel level. A second ADC detects steady-state signals of high beam, braking switches and variable ambient light. The micro-joystick is operated at 3.3 V, thus being interfaced through five external interrupt inputs. In addition to inputs from direct peripherals, the HMI communicates with other ECUs such as MECU, TVA and MB via CAN. Vehicle velocity, set velocity, set throttle position, lambda value, CC status and fail-safe states are provided by the MECU. The current throttle valve position is received directly from the TVA. System time and engine speed are received from the MB.

- **Driving information:** Analog speedometers display the mileage through a mechanical counter. Based on the current vehicle velocity, trip and mileage can be updated by summing the distance traveled per second. The fuel level is strongly damped for continuous displaying and initiated with the first measured values when the HMI is switched on. With every detected injector valve opening, the opening time is measured and summed up. The duty cycle (100% $\widehat{=}$ permanently open) can therefore be calculated every second. Based on duty cycle and fuel flow, the current fuel consumption (l/100 km) can be determined. An absolute trip-related consumption (l) can be indicated by integration. Based on the absolute trip-related consumption, a distance-related average consumption can then be calculated (l/100 km). At standstill, the current fuel consumption is displayed in l/h. Engine speed and lambda value are received via CAN.

- **Features:** The driving mode can be set through the HMI by switching between OR and VC. In dependence on the mode selected, visualization and MECU settings are adapted. Modes can be changed by entering the system menu. Recordings of the MB are started/stopped remotely via the HMI and the recording status is displayed. This function is enabled by activating a recording mode. Recordings are now started/stopped by pressing the micro-joystick. A visualized eco-score highlights the savings achieved by VC. As soon as the VC's operating point is reached, leading to optimized emissions and fuel consumption, a variable (%) is incremented or decremented. The growth is proportional to the throttle valve difference between OR (100%) and VC (load dependent). Description of the CC function is given in Chapter 6.5.

- **Outputs:** The HMI communicates bidirectionally via CAN. The sent message contains the CC parameterization and activation, commands for remote control of the MB and the selected driving mode. In addition to the signal flow, the visual representation on the LCD is also to be interpreted as an output. The design of the visualization follows subsequently.

6.4.5 Visualization

Once all inputs have been pre-processed, they are to be displayed graphically. The focus here is on readability, functionality and system understanding. Graphical user interfaces are created using *STM*'s own *TouchGFX* tool. Figure 6.12 shows the standard view including all activated features and symbols such as recording mode, activated CC and fail-safe states.

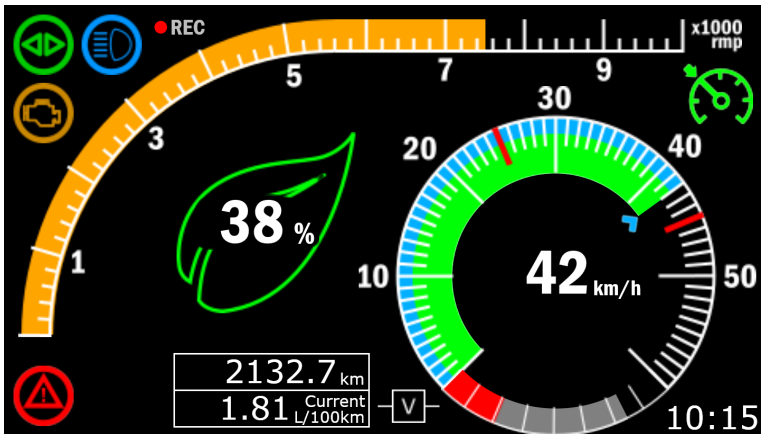

Figure 6.12 – Virtual dashboard - Rider view

Indicating light signals and the **recording symbol** are displayed on the top left-hand corner of the virtual dashboard. The recording symbol appears after enabling the recording mode in the main menu and turns red after starting a recording. In the upper area, the **rev counter** is displayed as a yellow bar. A **warning signal** in the lower left-hand corner is showing the VC fail-safe state (see Table 6.1). With a gray permanent status, error class 1 and 2 are indicated. A permanently illuminated red symbol indicates a class 3 error. Flashing red represents the highest error of class 4. In the center left, the **throttle valve opening** is shown as a percentage value, which is surrounded by the **eco-score**. It is shown by a green leaf that slowly increases and decreases in proportion to the fuel savings made while driving. The speedometer is visualized on the right. An outer blue arc shows the **set velocity**, while a second inner green arc represents the **vehicle velocity**. In addition, the measured velocity is shown in the center as a digital value. VC accelerations can be easily understood and estimated based on the dual velocity speedometer. The **CC interface** is integrated within the same visualization. With CC enabling, the CC symbol appears in the upper right-hand corner turning green when activated. An arrow marks the set CC velocity turning blue when activated. In the lower left-center area, the info box is visualized, providing mileage and **Evaluation information**. Rider inputs at the micro-joystick allow step-wise selection between trip, lambda value, average and current fuel consumption. **Driving modes** are displayed on the right-hand side (V: VC; Bypass symbol: OR). The lower section of the speedometer is used to display the **fuel level** and **system time** is shown at the bottom right-hand edge. Changes to the settings, modes and features of the HMI can be found in the menu presented in Figure A.1 in the appendix. Figure 6.13 shows the developer view, which offers real-time evaluation of the system and control variables. Individual variables can be enabled or disabled by selecting through the micro-joystick. The signals displayed were generated randomly and do not originate from real measurement runs.

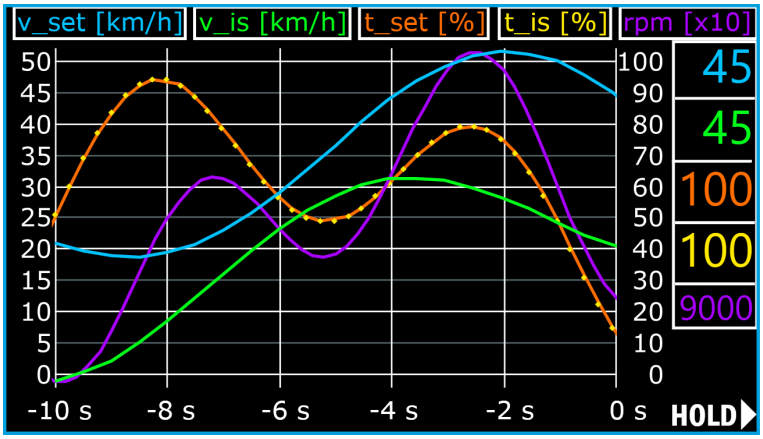

Figure 6.13 – Virtual dashboard - Developer view

6.5 Cruise Control

The implementation of CC in a scooter would usually involve major modifications. Precise sensing of the vehicle velocity and automatic throttle actuation that is independent of the throttle grip position are prerequisites. However, the function of the VC is similar to CC that constantly adjusts to the throttle position. Sensors (WSS, TPS), actuator (TVA) and a rider interface (HMI) are already integrated. The development is therefore limited solely to the software modification of the existing VC. CC merely describes a new operating mode. A suitable rider interface has been created with the HMI, offering adjustments and enabling. CC can only be executed in VC mode for velocities above 10 km/h. Otherwise, the HMI does not react to CC requests. In VC mode, the set velocity can be adjusted after enabling CC and is performed by the MECU. After the CC request of the HMI has been confirmed by the MECU, the set velocity is adopted as setpoint for VC. The MECU acknowledges the activation and the HMI's CC symbol/velocity arrow changes color. During control, the set velocity can be adjusted in 2.5 km/h increments by moving the micro-joystick up and down. The function can be deactivated at any time. In addition, the HMI senses the activation of both brake levers, which leads to an immediate cancellation of the CC when activated. The function improves driving comfort over longer distances and also enables reproducible test-driving for system evaluation.

6.6 Overall System Architecture

The system architecture is based on the system layout described in Chapter 4 and illustrated in Figure 4.2. This chapter deals with the wiring, connections and communication of all subsystems covering power supply, data exchange and CAN communication.

6.6.1 Wiring

The wiring mainly consists of the inserted wiring harness. It primarily contains six end-to-end lines for supply voltages, ground and CAN signals. In addition, the ignition line, including the respective feedback line, is routed to the MECU. The wiring harness runs through the scooter bundled and protected by a cable guard. Some subsystems require additional connection from

sensors and signals already installed in the vehicle. In case of the MECU, the emulated TSS signal interfaces with the original EC. Figure 6.14 shows the overall VC-related wiring that has been added within the scooter from back (left) to front (right). The wiring diagram gives information about signal lines, used connectors at the MCUs, the vehicle I/O interface and the main power switch. *Superseal* connections enable fast, robust and secure plug connections in the scooter. These connect the subsystems with the integrated wiring harness. Depending on the connection of each unit, these have four to six poles. Different plug and clamp connections are used to connect additional signal lines from the scooter. In addition to the main wiring harness, the wiring diagram gives information about the power supply design. Turning the ignition key (IGN_LOCK) supplies the scooter with power. A second manual toggle switch (BYPASS_SWITCH) enables the complete electrical disconnection of all added VC components. It should be noted that the scooter can no longer be ridden without activated TbWS due to the removed manual throttle actuation. Without the bypass being activated, the ignition line serves as supply line and is tapped by the MECU before the fail-safe relay. In case of malfunctions, the MECU stays online even if the scooter's power line is interrupted. In this way, the system does not require a separate main switch, but is switched on and off by operating the ignition lock. To prevent interference with sensitive signal lines, CAN and TSS signal lines are shielded. To improve the clarity of the diagram, the original EC is not shown. An additional toggle switch enables signal routing of the TSS between the MECU and EC. This allows the signal flow to be routed when switching the driving mode (OR/VC).

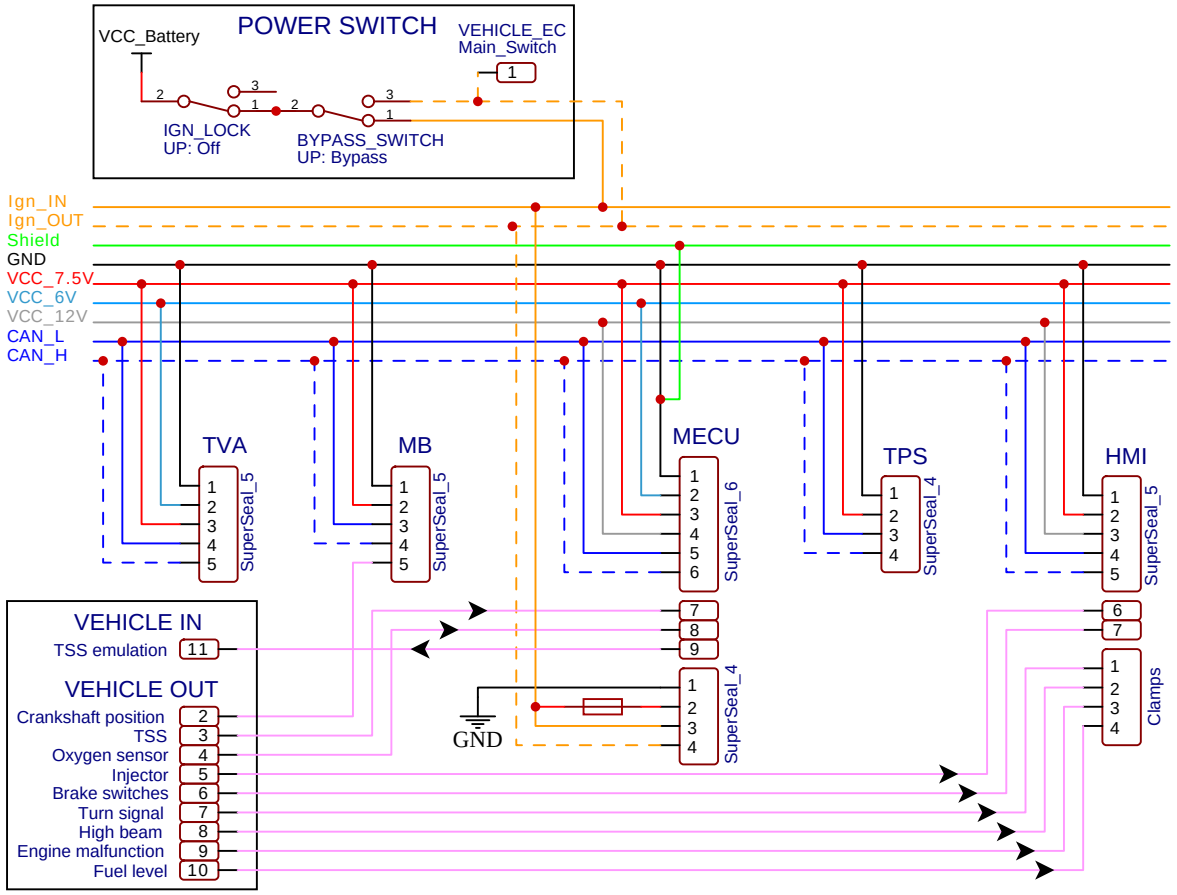

Figure 6.14 – Wiring diagram

6.6.2 Controller Area Network

The vehicle integration of the CAN bus and the hardware implementation in the respective subsystems have already been outlined. A CAN bus requires message management. Each message must be defined by its identifier (ID), data length code (DLC) in bytes, cycle time (CT) in ms and the contained signals. Every signal is related to certain bits (Position) of the data field. Typically, this information is contained in the so-called CAN database, which is known to every network participant for data decoding. In addition, each signal is provided with a description and a unit. Table 6.4 lists all subsystems and the respective transmitted CAN messages on the left-hand side. A receiver matrix on the right-hand side lists which network participants decode and process the sent message. Safety relevant ECUs transmit messages with a cycle time of 20 ms, while a cycle time of 50 ms is sufficient for MB and HMI. CAN features such as prioritization through arbitration are not used. Due to the low number of messages, the bus is barely loaded and message collisions or resulting latencies do not pose any problems. All ECUs except the MB, which is not classified as safety critical, provide additional data like error handler and message counter. Error handlers enable communication of subsystem errors to the MECU. In case of CAN communication failure, the MECU checks on up-to-dateness by the message counter. To guarantee precise transfer of the TPS position (%) and TVA opening (%), these are transmitted with one decimal place precision.

Transmission							Reception				
ECU	ID	DLC	CT	Position	Signal	Unit	MECU	TPS	TVA	HMI	MB
MECU	0x01	6	20	0-10	Set velocity	km/h	✗	✗	✗	✓	✓
				11-20	Scooter vel.	km/h	✗	✗	✗	✓	✓
				21-30	Set TVA pos.	%/10	✗	✗	✓	✓	✓
				31-32	Error handler	No.	✗	✗	✓	✓	✗
				33-36	Message ctr.	No.	✗	✗	✓	✓	✓
				37	CC enable	Flag	✗	✗	✗	✓	✗
				38-47	Lambda value	No.	✗	✗	✗	✓	✓
TPS	0x02	2	20	0-9	Throttle pos.	%/10	✓	✗	✗	✗	✗
				10	Error handler	No.	✓	✗	✗	✗	✗
				11	Calib. handler	Flag	✓	✗	✗	✗	✗
				12-15	Message ctr.	No.	✓	✗	✗	✗	✗
TVA	0x03	2	20	0-9	Valve position	%/10	✓	✗	✗	✓	✗
				10-11	Error handler	No.	✓	✗	✗	✗	✗
				12-15	Message ctr.	No.	✓	✗	✗	✗	✗
HMI	0x04	2	50	0-1	Driving mod.	No.	✓	✗	✗	✗	✗
				2	Start/Stop log.	Flag	✗	✗	✗	✗	✓
				3-6	Message ctr.	No.	✓	✗	✗	✗	✗
				7	Error handler	Flag	✓	✗	✗	✗	✗
				8-14	CC velocity	km/h	✓	✗	✗	✗	✗
				15	CC enable	Flag	✓	✗	✗	✗	✗
MB	0x05	4	50	0-13	Engine speed	rpm	✓	✗	✗	✓	✗
				14-18	RTC hours	t_h	✗	✗	✗	✓	✗
				19-24	RTC minutes	t_m	✗	✗	✗	✓	✗
				25	Meas. state	Flag	✗	✗	✗	✓	✗

Table 6.4 – List of CAN database

7 Methodology of System Evaluation

The development of system components is not limited exclusively to hardware and software, but also requires methods for evaluation. These can involve conventional dynamometer or road testing to examine finished components. In the automotive sector, test methods have become established that are applied at an early stage of development, preventing costly corrections at the end of a development. For example, Hardware-in-the-Loop (HiL) environments are used to test individual systems in a simulated closed-loop environment during developing/before vehicle integration. Once all subsystems have been integrated, the system in total is tested on a chassis dynamometer and in road tests. As such, statements can be made about system and control performance as well as fuel consumption and exhaust gas composition. Besides externally measured variables like exhaust emissions or powertrain performance, internal system variables are of great relevance, why a MB is to be developed for data recordings.

7.1 Hardware-in-the-Loop Testing

HiL describes a test environment for testing individual or multiple networked hardware components. The hardware under test is set up closed-loop, as inputs and outputs are connected and supplied with synthetic data. The environment can be provided by simulated rest buses based on models. The output data generated by the hardware is fed back into the models, which in turn generate system responses and thus close the control loop. This method allows hardware components to be tested under realistic conditions. Hardware faults, such as communication problems or memory overflows, can be detected and improved at an early stage. The main advantage of HiL test environments is the outstanding reproducibility of test procedures, facilitating the identification of error causes and system tuning. HiL testing has been used for sensor development and validation of the WSS and the TPS.

7.1.1 Wheel Speed Sensor HiL Testing

The development of the WSS is divided into three main areas: Measurement data processing, vehicle integration and tackling disturbances. Various measurement strategies can be tested with regard to function, accuracy and reliability by HiL approach. Its hardware structure is similar to the adaptation on the scooter. The influences of relative sensor/encoder position, adjustment and inaccuracies can be investigated. Scenarios can be carried out in a reproducible, cost-effective and safe manner. With the help of the HiL environment, the assembly of the WSS is subjected to real-world conditions. Scooter, longitudinal dynamics and VC are simulated, while the WSS represents the hardware under test. Two of the three previously defined issues can be elaborated. Interferences can only be taken into account after powertrain integration, as a simulation would be disproportionately complex [63].

Architecture: The HiL setup is divided into a host computer and the ECU-managed (*STM32F446RE*) test bench [66], shown in Figure 7.1. The computer interfaces the test bench, simulates the scooter's longitudinal dynamic and performs the VC based on the WSS velocity feedback. On the test bench side, a stepper motor-driven encoder disk represents the scooter's sensed wheel. Two WSSs are placed at the disk, sensing its motion. The WSS setup matches the architecture described in Chapter 6.1. In addition, an HMI enables operation of the test bench. Supply voltages of 12 and 5 V are provided by a 230 V AC/DC power supply unit and a DC/DC step-down converter. The ECU manages stepper motor control, HMI I/O, WSS read-out and velocity measurement. VC is not implemented on the ECU preventing several bidirectional data swaps during a time-critical simulation cycle. Through *Matlab Simulink*, I/O signals are interfaced via a serial bus between computer and test bench.

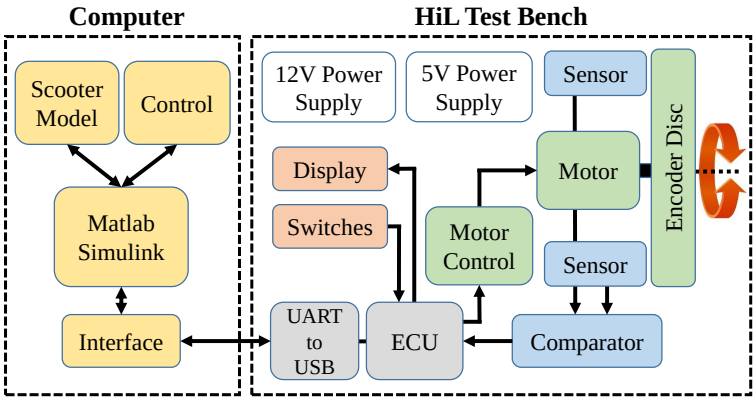

Figure 7.1 – WSS HiL concept

Encoder disc powertrain: To ensure a high level of reproducibility, the encoder disk speed is controlled precisely by the test bench's powertrain. Using a stepper motor, speeds near to 0 1/s can be realized. With rough load changes, the susceptibility to errors increases, resulting in a potentially stationary encoder disk. Due to the low power-to-weight ratio of 50 cc scooters, the vehicle inertia leads to much slower accelerations than the stepper motor is capable to provide. Stepper motors are limited at high speeds by their design. High pulse frequencies increase the inductive resistances, reducing the motor's torque at higher speeds. The required velocity range is set from 0 to 55 km/h to include velocity overshoots. A wheel circumference of 1.42 m is resulting in a max. speed of 10.8 1/s. Speed tests of the stepper motor (*NEMA 11*) proved a max. speed of 12 1/s without step loss. The motor controller (*EasyDriver V4.3*) requires the direction of rotation, enable state, micro-step state and the step frequency from the ECU. Through continuous changes in wheel speed, the stepper pulse generation is realized by an adaptive timer. With velocity changes, the timer's auto-reload register is reset and the current counter value is adapted to avoid timer overflows.

Simulation and measurement: The vehicle velocity is simulated using the model described in Chapter 6.3. After receiving the current velocity at the test bench, a motor control signal is converted by the ECU. The measurement of the redundant wheel speed is conducted according to the software described in Chapter 6.1. The control loop, outlined in Chapter 6.3.2, is closed by transmitting the real measured velocity to the simulated plant/computer.

Operating system and HMI: For user inputs and displaying system states, an HMI has been implemented consisting of switches, push buttons, an LED and LCD. The HiL test bench can be handled by an operating system, consisting of four different user modes. In closed-loop mode, the test bench follows the simulated velocity command and reports the measured velocity value. The open-loop mode solely follows the velocity command. Two test modes allow automated acceleration from stationary to the max. speed and reverse. Otherwise, the operator adjusts the stepper motor speed manually. The measured velocity is continuously transmitted to the host computer.

Assembly: Figure 7.2 shows the assembly of encoder disc (1) and WSSs (2), powertrain, housing, HMI and electronics. The left-hand figure depicts the HiL test bench as a whole. In the center, the opened test bench provides a view into the power supply on the left-hand side, while ECU, motor driver and comparator are positioned on the right-hand side. On the right, the adjustable design of the sensor-encoder unit is illustrated. The sensor unit can be adjusted in axial and radial disk spacing. Furthermore, the encoder disk can be adjusted in the plane of rotation and the tumbling movement.

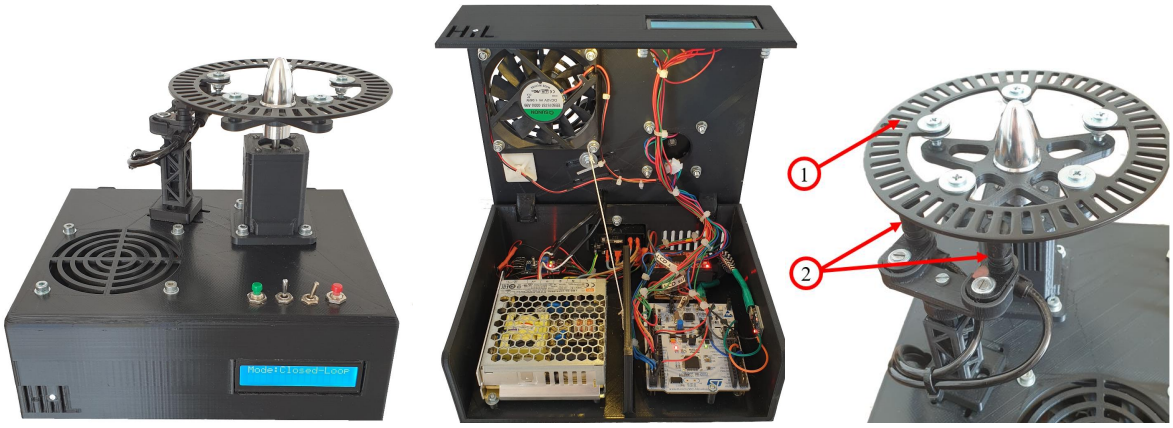

Figure 7.2 – WSS HiL

7.1.2 Throttle Position Sensor HiL Testing

The TPS is subject to high accuracy requirements. Several plausibility checks are performed continuously, as described in Chapter 5.1.4. Safe operation depends on a robust mechanical and software implementation. A HiL test bench is developed to validate the TPS in terms of reliability and measurement accuracy of the data processing. Reliability is evaluated by endurance testing. The TPS is actuated under real-world conditions. Set values are generated randomly and actuation is performed faster than a human driver would be able to. This ensures measurement quality over millions of measurements. Moreover, the total response time of the TbWS can be validated in conjunction with the TVA. The complete chain of throttle grip actuation, TVA actuation and powertrain reaction can be tested. Accuracy of the TPS is described by the linearity deviation. For evaluation, an open-loop scenario was developed, comparing known set positions with the measured throttle positions.

Architecture: To actuate the TPS without requiring another position sensor for plausibility, a stepper motor sets the throttle grip position. An adapted pulley connects the stepper motor directly to the sensor shaft. Using a planetary gearbox improves position accuracy to 0.1% of the desired setpoint. CAN signals are received via an external transceiver. CAN signal processing of the TPS and stepper motor control are performed by an external ECU (*STM32F446RE*). The stepper motor is controlled by an *EasyDriver V4.3* driver. Visualization and data recording of the test bench parameters are done by the host computer via a serial interface. Measurement and data processing are executed like explained in Chapter 5.1.4.

Test scenarios: Position setpoints were generated randomly by the external ECU to provide as many setpoint combinations as possible. The proportional position control was performed by the ECU based on the throttle position measured by the TPS. 90 random throttle grip positions are set in a minute, resulting in 10 800 000 measured value pairs within 60 h of endurance testing. In addition to the setpoint and measured throttle grip position, the up-to-dateness of the messages (message counter) and the transmission rate were also recorded. As no statement can be made about the measuring accuracy through endurance testing, an open-loop test scenario was developed to determine the linearity deviation. The TPS software was adapted in order to output the raw angle values. Using the stepper motor, the sensor shaft can be rotated in steps. With a step width of approx. 0.38° (360°/950 steps), the stepper motor creates a precise reference angle. The angular position of the TPS is examined step by step for the entire measuring range of 69°.

Assembly: Due to the moderate test bench dynamics, the geared drive is screwed directly onto the TPS by means of an adaptation. The ECU, motor driver and power supply are connected using a plug-in board. Figure 7.3 shows the TPS with the drive tower mounted. The TPS remains in its original condition, but torsion spring and throttle cable are removed to allow the motor to rotate freely. To compensate for the gearbox backlash, a rubber band is tensioned to load the gearbox against the direction of rotation.

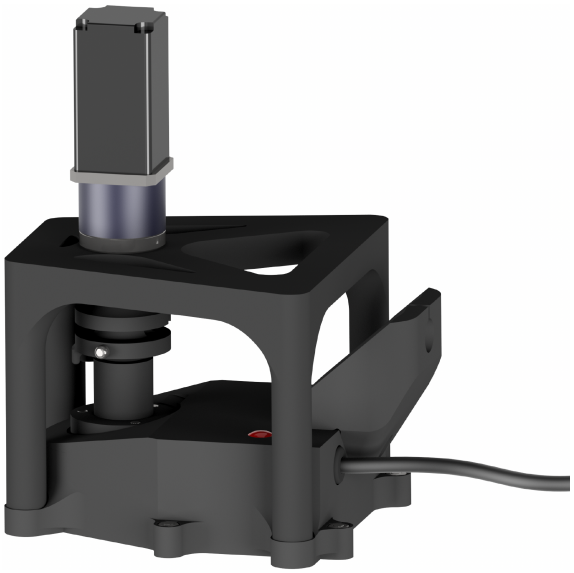

Figure 7.3 – TPS HiL

7.2 Measurement Box

For system integration, VC parametrization and lastly functional verification, system states and dynamic vehicle data must be measured. Therefore, a MB is designed for logging CAN bus data, measuring engine speed, exhaust oxygen concentration and injection cycle. Recordings are stored in real-time on a microSD card, offering data transfer. Setpoint and reference value of the velocity as well as the throttle valve position and oxygen concentration are tapped directly from the vehicle's CAN bus. For the measurement of the current engine speed, the speed signal of the original crankshaft sensor is processed and evaluated. To measure vehicle dynamics, a 6-axis inertial measurement unit is used, fusing sensor values by complementary filters to measure orientation and acceleration. All measured quantities are periodically stored with a time stamp, provided by a Real-Time Clock (RTC). As shown in Figure 4.2, the MB (No. 5) is not part of the VC system. Starting or stopping a recording is done via the HMI. New files are automatically created and adjustments to the recording rate or CAN message selection can be edited quickly. Table 7.1 lists the required quantities to be recorded.

No.	Measured quantity	Method
1	Time	Internal real-time clock
2	Set velocity	CAN read-out
3	Vehicle velocity	CAN read-out
4	Set throttle valve position	CAN read-out
5	Current throttle valve pos.	CAN read-out
6	Injection quantity	CAN read-out
7	Exhaust oxygen concent.	CAN read-out
8	Engine speed	Internal measurement
9	Acceleration in dir. of travel	Accel. sensor/Gyrometer
10	Pitch angle	Accel. sensor/Gyrometer
11	Rolling angle	Accel. sensor/Gyrometer

Table 7.1 – List of recorded quantities

7.2.1 System Architecture

The connections and interfaces of the modules are illustrated in Figure 7.4 as system architecture. A circuit board connects the individual electronic components. The ECU (*STM32G431KB*), which is connected to the surrounding modules via various digital interfaces, is located in the center. The ECU handles the software processing of the measured values and power supply. An integrated voltage regulator provides the supply voltage of 3.3 V for the sub-modules. The Inertial Measurement Unit (IMU) (*MPU6050*) and the battery-powered RTC (*DS3231*) are connected to the ECU via a common I^2C bus. By use of a comparator (*LM393P*) the engine's speed signal from the existing inductive encoder is digitized for frequency measurement by the ECU. Its CAN transceiver serves as interface between ECU and CAN bus. Thus, measured values can be read from or written to the system bus by the ECU. Measured quantities are sent to the data logger (*OpenLog*) for storage on the microSD card via the serial interface. To protect the electronics against external influences, the circuit board and all components are placed in a suitable housing.

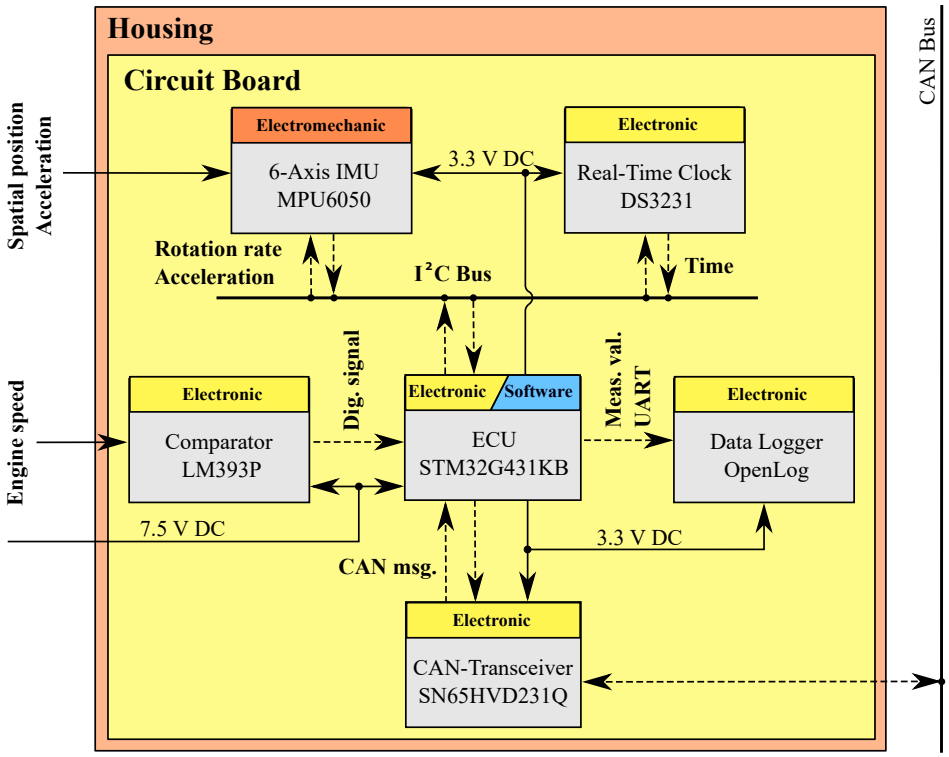

Figure 7.4 – MB architecture

7.2.2 Mechanical Implementation

The housing is not required to be dustproof and waterproof as it is mounted in the helmet compartment. It is designed as a two-part system consisting of an upward-opening housing box and a screw-on cover with a hinge and snap lock. The circuit board is inserted, whereby the cover fixes the circuit board. Cut-outs show the status LED and give access to the microSD card/programming interface. The MB is made from PETG using 3D printing and is screwed into the helmet compartment. As the lid is made of plastic, a snap lock is suitable for tool-free opening and closing. Figure 7.5 illustrates the MB housing and adaption.

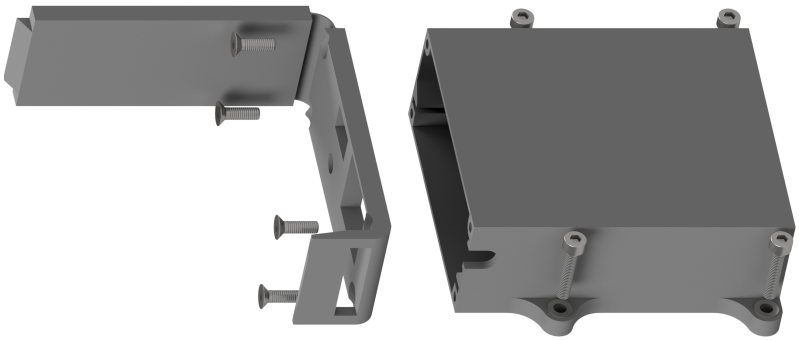

Figure 7.5 – MB mechanics

7.2.3 Electronic Implementation

At the electronic level, a circuit board connects all electronic components of the MB. The individual modules are connected to the ECU via I^2C and UART interfaces. To process the inductive speed sensor, the switching threshold and voltage level are processed with a

comparator, which is adjusted using suitable resistors. The comparator converts the sinusoidal speed signal from the inductive sensor into a square-wave voltage of the same frequency with a signal strength of 3.3 V. As the pulse wheel has 24-1 steps, the engine speed can be calculated by Equation (7.1) based on the signals period time (T).

$$f_{Crankshaft} = \frac{60\frac{s}{min}}{T \cdot 10^{-6} \cdot 24} \tag{7.1}$$

The analysis of the idle speed signal results in a period time of 1400 μs corresponding to an engine speed of 1785 1/min with a peak voltage of 10 V. A measurement at full throttle/max. speed results in a peak voltage of 60 V with a period time of 280 μs and a corresponding engine speed of 8928 1/min. A voltage divider is used to standardize the input voltage, set the comparator switching thresholds and limit the output signal to 3 V. To smooth the output voltage and to avoid signal bouncing, a capacitor is integrated.

7.2.4 Software Implementation

When processing the measured values, the processor is effectively utilized by an interrupt-controlled program flow. Work sequences with low priority can therefore be interrupted by time-critical processes. Data collection includes reading the measured values from the CAN bus, measuring the spatial position and acceleration, calculating the real-time and determining the engine speed. Furthermore, the data is stored and the CAN message of the MB is sent.

CAN access: Setpoints and measurements of velocity and throttle valve position are read from the CAN bus. The controller output, reference, manipulated and controlled variable serve as relevant evaluation data. Both messages are received interrupt-based at a rate of 50 Hz. Time and engine speed are transmitted with a rate of 20 Hz for HMI visualization.

Spatial position and acceleration measurement: To enable comprehensive analysis of the scooter's driving dynamics, pitch and roll angles as well as acceleration along the vehicle's X-axis are to be recorded. The IMU combines an acceleration sensor and a rotation rate sensor. Acceleration is sensed in direction of the three sensor axes. The rotation rate is measured around these three spatial axes. Merging data of both sensor types, the spatial position of the IMU can be determined. Figure 7.6 illustrates the scooter's axes.

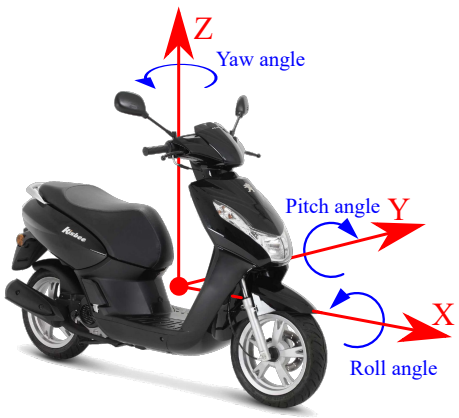

Figure 7.6 – Scooter axes

When calculating the spatial position using the acceleration sensor, gravity serves as a reference. Deflections around the Y and X axes can be transferred to absolute pitch or roll angles. Due to gravity, the acceleration is projected onto the respective sensor axes using trigonometric functions. As the Z-axis is aligned collinear to the acceleration due to gravity, no yaw angle can be measured by the acceleration sensor. In contrast, the calculation of the spatial position is very accurate for stationary behavior. As dynamic accelerations can also act on the sensor in addition to gravity, the calculation from the accelerations results in inaccurate values. For longer lasting accelerations, accurate pitch and roll angles can be determined by Equation 7.2.

$$\theta_{Pitch} = \tan^{-1}\left(\frac{A_{X,OUT}}{\sqrt{A_{Y,OUT}^2 + A_{Z,OUT}^2}}\right) \quad ; \quad \psi_{Roll} = \tan^{-1}\left(\frac{A_{Y,OUT}}{\sqrt{A_{X,OUT}^2 + A_{Z,OUT}^2}}\right) \tag{7.2}$$

The measured values are integrated to convert the rotation rate into a spatial position. Relative to the initial alignment, the spatial position can be calculated around all three spatial axes. Since accelerations do not influence measured rotation rates, this method is particularly suitable for determining the spatial position while driving. Long-term integration can result in measurement errors due to drifting. In order to utilize the advantages of both methods, the measurements are merged using a complementary filter. A low-pass filter cuts off high-frequency errors. Long-term drifts of the rotation rate sensor are removed by a high-pass filter. Both filtered measurements are weighted using a factor K before summing. On the software side, a complementary filter is implemented as described in Equation 7.3.

$$\theta_{fus}[k] = K \cdot (\theta_{fus}[k-1] + (\theta_{Rot} \cdot \Delta t)) + (1-K) \cdot \theta_{Accel} \tag{7.3}$$

The IMU is set to a measuring rate of 1 kHz for high measurement quality. To compensate for influences from engine vibration or uneven road surfaces, the internal digital low-pass filter is activated with a max. cut-off frequency of 5 Hz. As soon as measured values are available, they are read out via the I^2C interface. The readout takes approx. 340 μs at max. data rate (400 kBit/s). Once transmission is complete, the processor receives an interrupt-based notification. The measured values are then scaled and normalized. After separately calculating the spatial angles from the measured accelerations and rotation rates, these are merged using the complementary filter. For all calculations, the offset of the sensor coordinate system to the vehicle coordinate system must then be compensated.

Real-time calculation: In order to assign a time stamp to the recordings, the time must be computed using an RTC. The ECU's RTC is not equipped with a battery and therefore loses time in case of inactivity. Thanks to the integrated battery of the external RTC, the time can also be determined when the VC system is inactive. The time is transmitted via the I^2C interface of the ECU. A transmission at 400 kBit/s takes about 180 μs. To prevent interference with the IMU data transmission, the time is read out at the beginning of each measurement and then calculated by the ECU's internal RTC.

Engine speed determination: Each revolution generates 23 pulses and a pulse gap. The gap represents the crankshaft reference mark and should be recognized by the ECU. The time between two reference marks (period time) is measured and converted into an engine speed. At a max. speed of 10 000 rpm, a pulse interval of 250 μs is created. An input-capture timer is used to accurately measure the time intervals. To recognize the reference mark, the intervals of the last 23 pulses are stored temporarily. If the newly recorded value is approximately twice as long as the average of the last 23 pulses, the reference mark has been detected. The interval between two reference marks is determined by a second timer and used to calculate the final engine speed.

Data recording: The recorded measurements are saved to the microSD card at a repetition rate of 10 Hz. For this purpose, a character string with all measured values is assembled and transmitted to the data logger via UART. The data is then being stored on the microSD card. For optimum synchronization between measurement and time stamp, the internal wake-up timer of the RTC is set to trigger an interrupt every 100 ms. The generated string starts with the current time stamp followed by the individual measured values, which are separated by a comma and appended. In the event of values not being able to be recorded, this is indicated by the last check digit. This check digit represents the up-to-dateness of the individual measured values in binary notation. Depending on the test scenario, the preselection of the recorded measured variables varies, which are stored in a CSV file on the microSD card. The character string can reach a max. length of 67 characters while a transmission rate of 9600 bit/s is recommended, resulting in a transmission time of 56 ms.

7.3 Road Testing

Once the VC system has been integrated into the test vehicle, it is examined in terms of control performance, system behavior and fuel economy. At this stage, safety relevant system components have already been tested regarding safe operation and individual performance. In addition to the simulated evaluation, the road test provides the best possible conditions for system evaluation, taking into account all influences and disturbances. Road testing does not require system changes or the development of supplementary software or hardware, since the MB offers data recording. Several scenarios allow the evaluation of recorded system variables in different driving situations. The scenarios differ depending on the purpose of evaluation. All scenarios must be performed with the same driver, the same protective clothing, a full tank of fuel, the same weather conditions and on the same section of road in order to ensure the highest degree of reproducibility.

7.3.1 Controller Performance

Rating the controller performance is based on two scenarios. Both are performed on the road as well as virtually through computer simulation for validation purposes. In order to test the control algorithm in various operating points, setpoint changes of different size are applied all over the scooter's velocity range. The first scenario covers the step-wise acceleration from standstill to the original top speed of 48.7 km/h. Within 20 s intervals, the set velocity is

increased by 10 km/h steps (0, 10, 20, 30, 40, 48.7 km/h). The second scenario consists of five subscenarios, dealing with bigger set velocity changes from standstill to a desired velocity (0, 10 ; 0, 20; 0, 30; 0, 40; 0, 48.7 km/h). In this way, longer lasting control deviations provoke wind-ups of the adaptive integral controller. The resulting recordings allow evaluation of the implemented integral threshold. Since the rider's unsteady throttle input would prevent reproducible test conditions and stable set velocities, the setpoint is automatically adjusted by a preprogrammed CC sequence. The evaluation is based on the data set of simulated and recorded set velocity, measured velocity and the throttle valve position.

7.3.2 System Behavior

After the control performance has been investigated, the system behavior is evaluated in terms of system reaction to sudden disturbances and drivability. By implementation of the VC, the rider's direct throttle cable was replaced by a system controlling the throttle valve instead. Secure and predictable system behavior are mandatory to establish the rider's confidence in the novel system. Therefore, reproducible measurements of the OR are compared directly to those of the VC. The scooter's velocity, throttle valve position and injection quantity are recorded. Three road scenarios are used to evaluate the VC behavior based on the acceleration performance, sudden gradient changes and steep downhill accelerations. The first scenario compares the acceleration performances from standstill to the top speed of both system states on a level track. The second scenario tests the susceptibility to rough and sudden gradient changes, provoking unstable system reactions. The scooter is driven at top speed until a sudden steep gradient of 8% occurs. Lastly, the overshoot behavior is investigated. The scooter accelerates from standstill to top speed on a 15% downhill slope, followed by a transition to level ground. Recordings of both system states allow the comparison of the original and velocity-controlled restriction regarding overshoot and control accuracy. The evaluation of velocity and throttle valve opening are related to the driving behavior, as the rider is capable of sensing velocity variations and load changes of the powertrain. The evaluation of the injection quantity provides conclusions about the cascading with the mixture control and the resulting fuel consumption.

7.3.3 Fuel Economy

In addition to analyzing the current fuel consumption, the influence of the VC on the average consumption is decisive. Due to the direct correlation between gasoline burned and CO_2 emitted, an improvement in average fuel consumption also describes a reduction of the environmental impact. The measurement is carried out in a road scenario of 50.4 km in length, comprising 61% urban and 39% rural roads. To minimize measurement inaccuracies, the test cycle is repeated three times with both OR and VC, covering around 300 km on the road. As explained in Chapter 7.3, all test conditions are also checked and maintained during the test drives. The volumetric measurement of the fuel is carried out using calibrated measuring cylinders and leading to a measurement error of 0.3%. Measured volumes are referenced to a temperature of 15°C. To verify the test conditions, weather conditions, driving time, mileage, refueled volume and fuel consumption are documented.

7.4 Roller Dynamometer

In addition to the primary effects of VC described in 7.3, the control of the throttle valve also leads to secondary effects. Maintaining the optimum ignition timing in parallel influences the combustion process. Optimized combustion in turn has an influence on the efficiency of the powertrain and consequently on the exhaust gas composition and volume. However, these can significantly influence the degree of conversion of the catalyst. Suitable methods must be considered in order to investigate the interrelationships of the aforementioned chain of effects and to demonstrate improvements. Through precise and reproducible setting of predefined operating points, investigations can be carried out on the engine, the exhaust gas and the internal VC system variables. Therefore, test runs are performed on a roller dynamometer. Parameter determination for dynamometer settings, measurement tools and evaluation strategy are described below [67].

7.4.1 Coast Down Testing

To set suitable dynamometer parameters, rolling and air resistances are determined by a coast down test, to ensure valid test conditions. These were performed in calm wind conditions on a level and straight test track. First, the frontal area of the scooter, including rider (height: 1.8 m) and helmet, was visually determined to be 0.78 m^2. To compensate small differences in gradient, path-time curves of two test runs in opposite directions of travel were averaged. Based on the parameters shown in Table 7.2 and the recorded path-time curves, a general driving resistance polynomial (7.4) is obtained for a *Peugeot Kisbee 50 4T* (Euro 5).

	Property	Symbol	Value
1	Frontal area	A	0.78 m^2
2	Tyre pressure	P	2.3 bar
3	Moment of inertia factor	T_in	1.04
4	Mass scooter	m_{sc}	99 kg
5	Mass rider	m_r	80 kg
6	Air density	ρ	1.232 kg/m^3

Table 7.2 – List of coast down test parameters

$$F(v) = 0.015v^2 + 41.65 \tag{7.4}$$

Equation 7.4 is giving the needed force to overcome the velocity-dependent air resistance and constant rolling resistance at a certain velocity. The determined drag coefficient (c_w) is 0.7 and the rolling resistance coefficient (f_R) is 0.031. To verify the resistances, measurements of the throttle valve positions (TVP) at three reference velocities were taken. Therefore, the CC function of the VC was used. Afterwards the results were compared to throttle valve positions measured on the roller dynamometer. Table 7.3 proves the validity of the parameter set, since the throttle position is proportional to the required driving force.

Velocity	TVP_{Road}	TVP_{Dyno}
25 km/h	16 %	16 %
35 km/h	26 %	27 %
45 km/h	45 %	45 %

Table 7.3 – List of throttle valve positions

7.4.2 Vehicle Sensor Integration

For evaluation, various quantities must be recorded to assess the effects on mixture preparation, engine and finally exhaust gas composition. This was realized by the use of the developed MB and the integration of several sensors.

Measurement box: The developed MB, described in Chapter 7.2, logs TbWS data. In this use case, the command variable (set velocity), the current throttle position (manipulated variable), vehicle velocity (controlled variable) and the engine speed are recorded. To be able to make a statement about the air-fuel mixture, the signal voltage of the lambda sensor is transferred to an oxygen concentration by means of a look-up table. Finally, the cyclic opening time of the injection valve is sensed and stored as a duty cycle.

Encoder: The original crankshaft sensor has a resolution of 24 steps, which makes an exact assignment of the measured engine parameters impossible. For this reason, a high-resolution and speed-resistant encoder must be adapted to the crankshaft. The decision was made for a *Kübler 05.2400.1122.1024* encoder with a resolution of 1024 steps and a max. speed of 12 000 rpm [68]. The motor speed reaches a maximum of 8000 rpm, but the small-volume single cylinder produces plenty of vibrations and therefore requires an adequate bearing/adaptation of the encoder. A torsionally rigid shaft-coupling combination made from a nylon carbon fiber (3D print) is placed on the fan wheel, connecting the encoder to the crankshaft. A dual bearing carrier made from PETG supports on the fan housing and allows alignment in radial and tumbling motion. The assembly is shown in Figure 7.7.

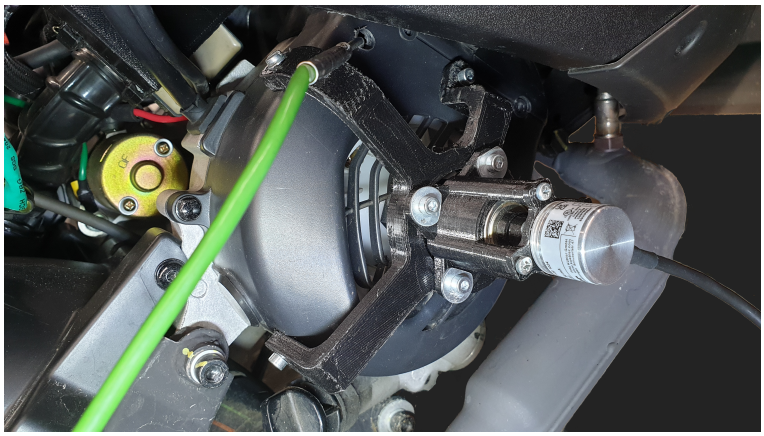

Figure 7.7 – Encoder adaption

Temperature probes: Temperatures at the cylinder and in the exhaust manifold can allow conclusions to be drawn about combustion. Excess energy is converted into thermal energy in the OR range. Thus, the temperature behavior depends on the ignition timing and the resulting combustion process. Two mineral-insulated thermocouples (Type K) are used, which have a temperature resistance of 1200°C [69]. Figure 7.8 shows the placements of both thermocouples. Probe 1 is positioned in a 2 mm deep hole in the cylinder wall and is guided past the fan wheel (left figure). Probe 2 has been welded directly into the exhaust manifold and is thus in the middle of the exhaust gas flow (right figure).

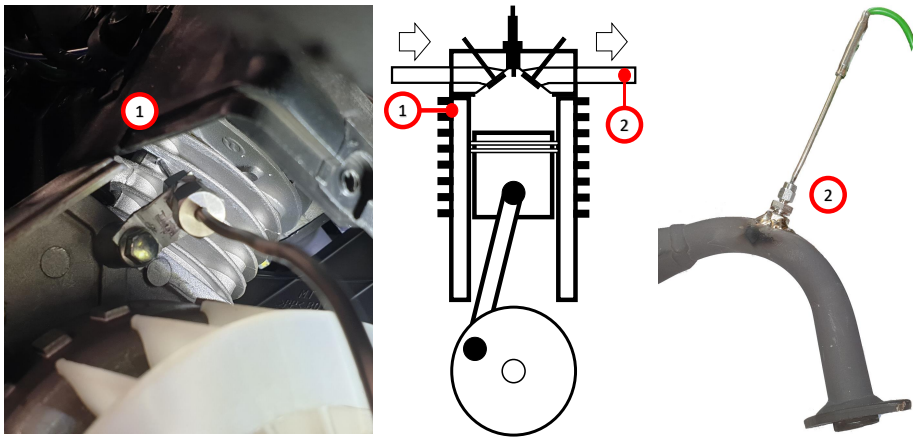

Figure 7.8 – Placement of thermocouples

Indicating spark plug: Statements about the engine's operating cycle can only be made if ignition timing and in-cylinder pressure are measured. The ignition timing is tapped on the high-voltage ignition cable by using a measuring clamp. An indicating spark plug (*AVL ZI22 1_U5D*) fitted with a piezo element is installed to measure the internal pressure [70]. Pressures of up to 200 bar can be measured without modifying the combustion chamber.

7.4.3 Exhaust Gas Measurement

Apart from the actual exhaust gas composition, the mass flow of the entire exhaust gas stream is of interest. For this purpose, so-called Exhaust Flow Meters (EFMs) are used, which can determine the magnitude of the mass flow via a pressure difference. The selected *AVL M.O.V.E* EFM is equipped with a 2.5" exhaust pipe and has a measuring range of approx. 12.5-900 kg/h [71]. The exhaust flow of a 50 cc four-stroke engine is very low despite high engine speeds due to the small displacement. Measurements on motorcycles have already been carried out using this method, but exhaust gases are usually collected for exhaust determination of such small engines. To estimate the scooter's mass flow, a reverse calculation was performed based on the road tested fuel consumption ($Fuel_{con}$ = 1.00 l/h). With OR, the expected exhaust mass flow (m_{exh}) at top speed is determined to 12 kg/h by Equation 7.5. An investigation of measurements showed plausible mass flows at min. 7.9 kg/h. No valid measurements could be made at lower flow rates due to the inherent noise of the EFM.

$$m_{exh} = (Fuel_{con} \cdot \rho_{fuel}) \cdot (1 + 14.7\lambda) \tag{7.5}$$

The exhaust gas composition is determined with the portable emission measuring device *AVL M.O.V.E Gas Pems*. The HC concentration is measured using the flame ionization detector principle. NO_x is detected by a UV analyzer and CO/CO_2 by a non-dispersive infrared gas analyzer [72]. Before measuring, the system was calibrated and warmed up. Zero drifts were compensated periodically with zero gas.

7.4.4 Data Processing

Engine related signals from the encoder, the ignition clamp and the measuring spark plug must be sampled at high rates. At max. engine speed, one crankshaft revolution takes approx. 8 ms. In order to use the full resolution of the crankshaft encoder (1024), the sampling rate would have to be at least 286 kHz according to the sampling theorem. The *Sirius* high speed interface from *ZSE Electronic* achieves a max. sampling rate of 1 MHz [73]. In order to compensate for fluctuating ignition times and mean pressures during measurement, 60 cycles are recorded and standardized afterwards. Data acquisition from the vehicle's internal CAN bus is carried at a sampling rate of 20 Hz. The processes are comparatively slow and static for the measurements to be carried out. The exhaust gas analysis generates standardized measurement data every second, based on a 10 Hz raw data sample rate.

7.4.5 Test Strategy

Restriction by shifting the ignition timing only occurs when the max. permitted speed is reached. The measured top speed of the test vehicle (OR) is 48.7 km/h in factory condition. In the remaining speed range, the driver manually adjusts the throttle valve position to achieve the optimum air supply. However, due to the low max. permitted speed of this vehicle class, it is usually driven at top speed. For this reason, only operating points at 48.7 km/h are examined below. To obtain a load-dependent statement about the effect of the VC compared to the OR, a gradient is simulated using the roller dynamometer. Vehicle parameters and rider weight (80 kg) remain unchanged during all test runs, while the gradient is varied in 1% steps in the range -8% to 0% and in 0.5% steps between 0% and 2%. With a gradient of -8%, the downhill force and the driving force are balanced. Due to the low engine power, the top speed can no longer be reached on gradients exceeding 2%, which also prevents ITM. In order to obtain valid, reproducible and comparable measurements, the specified operating points are approached statically. The measurements are started once the top speed has been reached with the corresponding load (gradients) and the VC has been settled. Figure 7.9 shows the final setup on the roller dynamometer.

Figure 7.9 – Test setup

8 System Evaluation

The evaluation is conducted in a three-stage process. As already introduced in Chapter 7 with regard to the evaluation methodology, individual components as well as the overall integrated system are evaluated. After the functional testing of TbWS/VC associated software and hardware, the system is examined with regard to control performance and system behavior by a combination of simulation and road tests. In order to prove further improvements on sustainability and eco-friendliness, the system influences on engine and exhaust gas composition are analyzed on a roller dynamometer.

8.1 Evaluation of the Throttle-by-Wire-System

The TPS and TVA are evaluated individually before the combination of both are tested in context of a TbWS, including CAN bus communication. Both developed components are described and their performance is evaluated by means of dynamic/static precision and response time by performing dynamic tests. Finally, influences of the engine suction pressure are investigated.

8.1.1 Performance of the Throttle Position Sensor

A PCB was designed to merge all TPS electronic components. Differential signal lines were guided in parallel with same length, to minimize the effect of electro-magnetic interference. To prevent deflection of the magnetic field, passive components such as capacitors and resistors were placed as far away from the sensor-IC as possible. An LED on the circuit board is used to indicate detected errors. Figure 8.1 shows the TPS assembly of the PCB, the housing and the bearing unit including the cable pulley pickup. By using a torsion spring, the original feedback force is encountered to the throttle cable. The unit is connected to a four-pole connector, providing the 7.5 V supply voltage and the CAN bus access. The housing is closed and a circumferential seal protects the installed electronics from environmental influences.

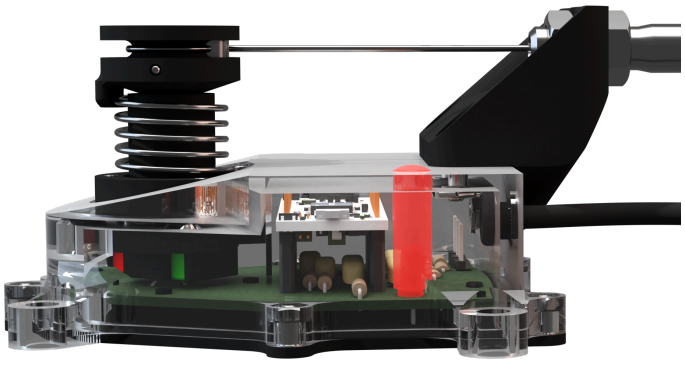

Figure 8.1 – TPS assembly

For evaluating the TPS, a HiL-test environment was set up where the position is varied by use of a stepper motor. Here, the digital throttle position was continuously set to randomly selected values (90 setpoints/min) by position control. The endurance test bench ran for a total of 60 h, where about 324 000 positions were set and 10 800 000 value pairs were processed. No errors occurred during the entire endurance test. By means of the endurance test bench, no statement can be made about the measuring accuracy, why an open-loop test scenario was developed for determining the linearity deviation. A small geared stepper motor rotates the sensor shaft step-wise, while position measurements are output. The angular position of the sensor was analyzed with a step width of approx. 0.38° (360°/950 steps) for the entire measuring range. Figure 8.2 shows the measurement deviation related to the reference position of the stepper motor. Since the deviation varies periodically, caused by tolerances in the stepper's gearbox, this was corrected by applying a moving average filter. A deviation of $\Delta \text{dev}_{max} = 0.155\%$ results.

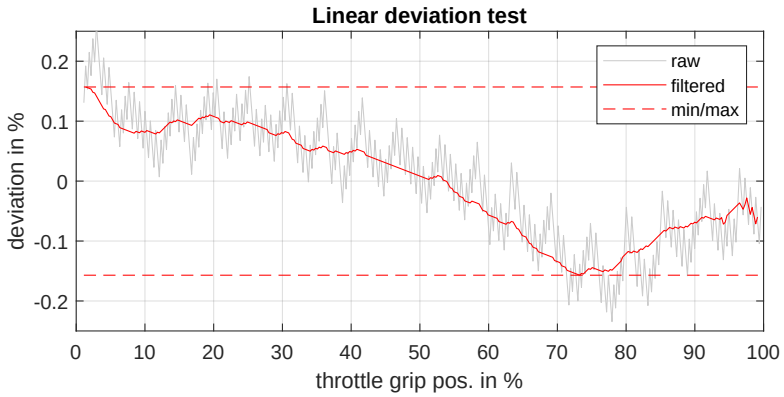

Figure 8.2 – TPS open-loop deviation testing

8.1.2 Performance of the Throttle Valve Actuator

Scooters do not come with a conventional rear swing arm, since the whole powertrain (engine, gearbox, wheel) is mounted movable. If the rear suspension compresses strongly, a large unit mounted on the throttle body would be destroyed. To prevent collisions with the scooters frame, the TVA has been divided into smaller units. An electronic unit was designed, consisting of a circuit board carrying the MCU, stepper driver and CAN transceiver, which is integrated into a housing that fits on the backside of the original EC. The unit is connected through a five-pole connector providing 6.5 V supply for the stepper drivetrain, 7.5 V supply for the MCU and CAN bus access. A circumferential seal protects the electronics from environmental influences. The second unit is carrying the electromechanical and mechanical components like Hall sensor, stepper motor, transmission and adaption plates. Therefore, a three-stage design was developed, whose first stage realizes the adaptation to the throttle valve and the protection of the gearbox. The second is given by a baseplate on which stepper motor, Hall sensor and toothed belt gear are installed. The third component is the housing cover, which enables passive cooling and cable feed-through. Splash water protection is sufficient and no seals are needed due to the robust components. Figure 8.3 shows the electronic (left) and mechanic unit (right). Both are connected with a seven-core cable, enabling sensor supply/readout and motor driving.

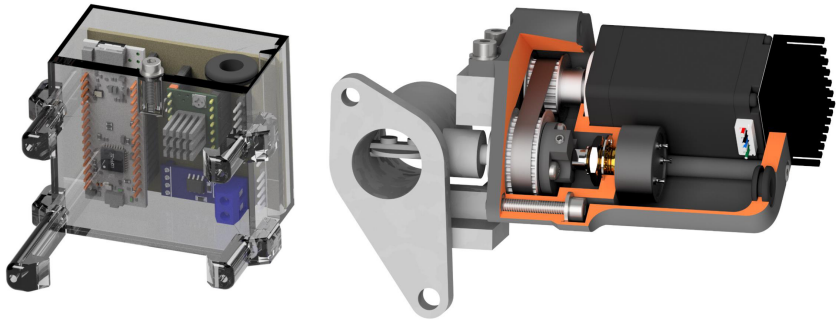

Figure 8.3 – TVA electronic and mechanic unit

The TVA can be evaluated by using its already build in closed-loop control while being installed at the throttle valve. For realistic dead time behavior, the set valve positions were sent via rest bus simulation. In order to make qualitative statements about the control performance, the TVA was excited with a pulse function and a sequence of two ramps. The dynamics of a step response cannot be generated by the rider, but represent a standard approach to control performance evaluation. Figure 8.4 shows the recorded scenarios. The TVA is able to adjust within 130 ms at max. control deviation, including bus communication. An overshoot of less than 0.5% occurs and a stationary deviation of max. 0.1%, excluding Hall sensor error of less than 0.37%, is achieved.

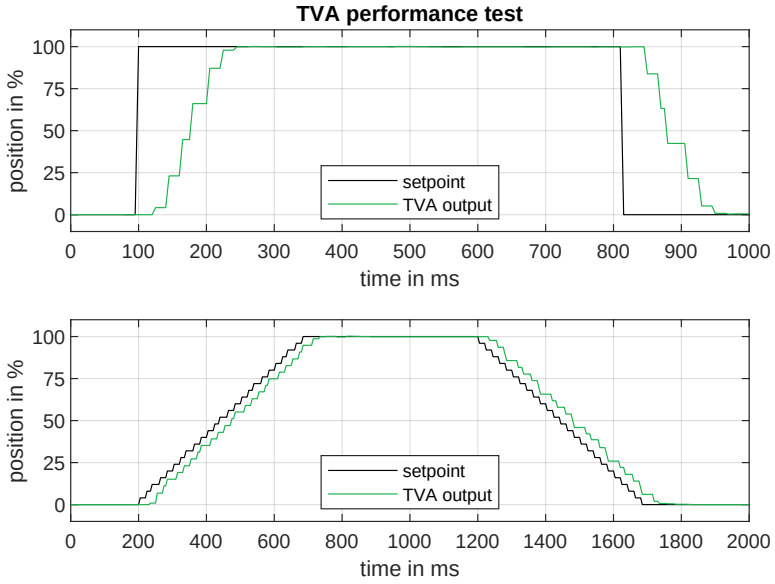

Figure 8.4 – TVA performance evaluation

8.1.3 Performance of the Throttle-by-Wire-System

Finally, the developed TPS and TVA had been integrated into the *Peugeot Kisbee 50 4T (Euro 5)* scooter. In combination, they can operate as TbWS, open up the possibility of throttle manipulation through driving functions. The TPS was placed beside the helmet compartment in such way, that the original throttle cable can be inserted. By mounting the TVA at the engine's air intake manifold and connecting both units with the power supply and the CAN bus, the TbWS is ready to operate.

For testing the whole chain of moved cable pulley up to the actuated throttle valve/resulting engine behavior, the system was tested with a ramp sequence. During the test, the scooter's engine was running for taking into account the suction pressure applied to the throttle valve. This time, the stepper motor is directly turning the TPS cable pulley by means of an ideal straight-line throttle actuation. Figure 8.5 shows the belonging results of applied throttle grip position, TPS-measured throttle grip position, TVA-actuated throttle valve position and additionally the engine speed. The first ramp-based test run performed, proves an excellent measurement of the throttle position, proper CAN communication and precise position control. The ramp used here, corresponds approximately to a rapid full throttle by the rider and subsequent release. After less than 30 ms, the valid result of the TPS was sent via CAN bus. The real time offset is less, but due to the test setup, an offset between motor control and CAN message reception occurs. When reaching the 100% position, a deviation of 1% can be seen by considering the 1% TPS-error band. The recorded values reflect the CAN refreshing rate of 50 Hz. The TVA also follows the required position value within 30 ms, thus the overall dead time is about less than 60 ms. The position accuracy achieved is max. 0.1%, with no overshoot being detected. It can be seen that even when higher engine speeds/various suction pressures are reached, exact position control by the TVA is proven. To evaluate control under high dynamics, the TPS HiL-setup was used to excite the TVA with precise set values. The rear brake was lightly pressed to apply a uniform load to the powertrain. The engine speed exploited the full spectrum of range and dynamics. It can be seen that the accuracy of the TVA is minimally dependent on engine speed. For low and medium speeds, an accuracy of min. 99.9% is achieved. At higher speeds, strong vibrations lead to an accuracy of min. 99.8%. Under consideration of the Hall sensor error (<0.27%) and TPS accuracy (<99.84%), an overall error of max. 0.63% results. An overshoot of 0.25% occurs on average, in the worst case 0.4%. The adjustment is achieved within 70 ms at any time and the TVA is constantly capable of withstanding the torque variations caused by the changing suction pressure. The requirements for precision, overshoot and settling time are exceeded by far.

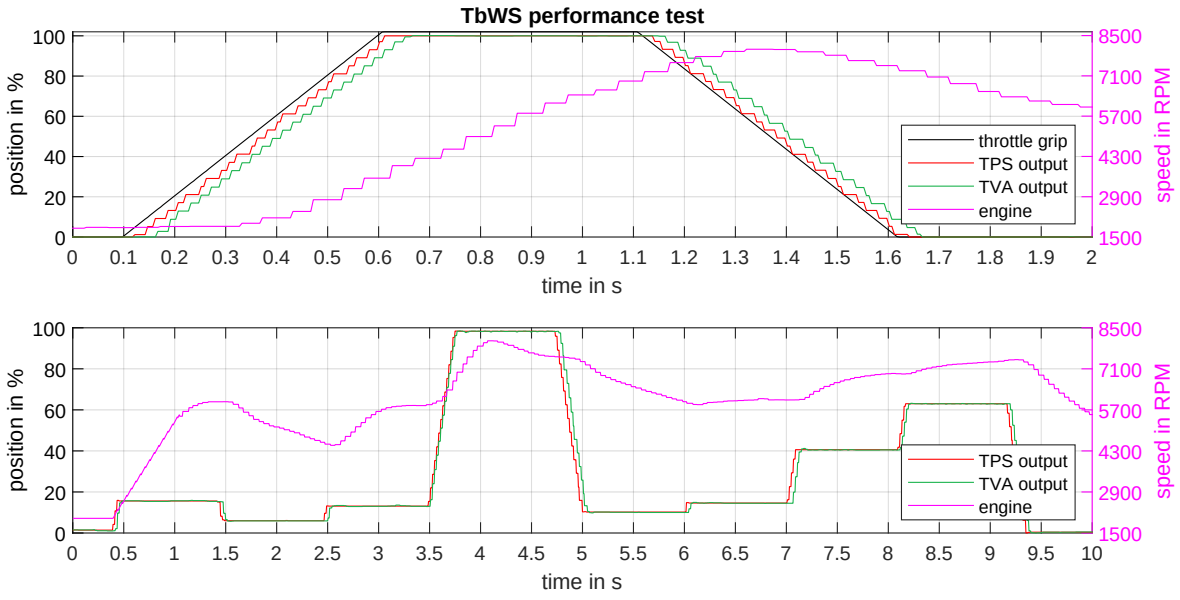

Figure 8.5 – TbWS performance evaluation

Besides the performance, the system also meets low-cost requirements. Component and manufacturing costs for the manufactured prototypes of TPS and TVA amount to approx. 45 € and 95 €, respectively. Also, instead of development boards, the MCU would be soldered directly to the PCB. In combination with further miniaturization of the components, a single-unit design conceivable, eliminating the need for one MCU and reducing costs by about 25%. Experience shows that manufacturing costs in mass production are reduced by up to 90%, due to larger purchase quantities and optimized processes. Consequently, final estimated total costs of min. 15 € per system could be realistic.

8.2 Evaluation of the Velocity Control

Once the sensing of throttle command and throttle valve position have been validated, the last state variable to be evaluated is the scooter velocity. Therefore, the WSS is evaluated with regard to accuracy and dead time behavior. Further, the performance of the control algorithm is crucial for the success of the VC system. By analysis of simulated and recorded scenarios, the controller's performance can be validated in terms of stationary accuracy, overshoot behavior and stability. Since the HMI is not effecting the performance of the VC, it is not considered for evaluation.

8.2.1 Performance of the Wheel Speed Sensor

The measured velocity serves as reference variable for the VC. By use of the WSS HiL test bench described in Chapter 7.1.1, the measurement accuracy can be determined by open-loop testing. The encoder disk is accelerated precisely to target speeds related to velocities between 0 and 50 km/h in 5 km/h increments. For each speed, the measured value is sent back to the host computer and examined for accuracy and measurement error. By differentiating between stationary (offset) and oscillating errors (cyclic), the total error is evaluated. Figure 8.6 shows the measured velocities for each set speed (left) and the measurement error (right).

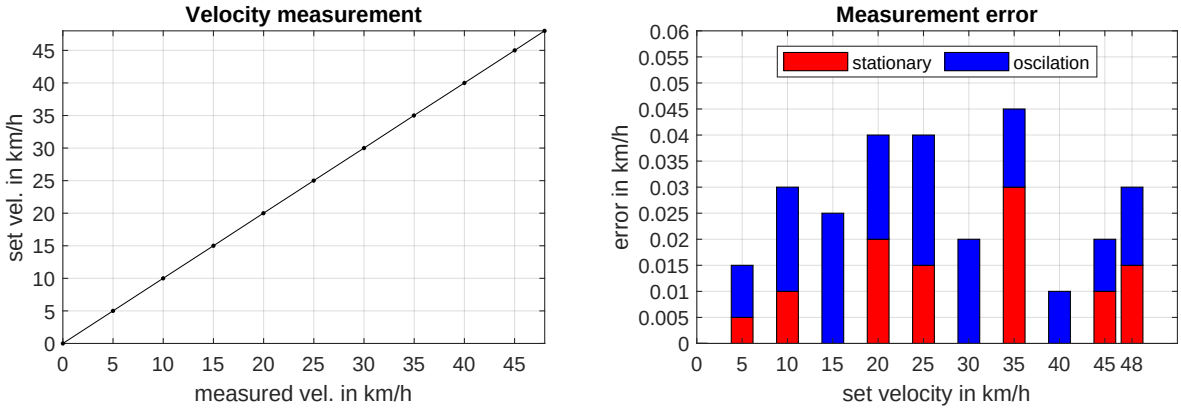

Figure 8.6 – WSS open-loop evaluation

A linear and precise measurement is shown. The total error consists of stationary and oscillating errors. It is proven that the accuracy requirement of 0.1 km/h is fulfilled. At any speed, the WSS's required precision is exceeded by a factor of min. 2. It is observed that cyclically oscillating inaccuracies occur due to the rotation of the encoder disk. Using

larger MAF windows would compensate errors, but would extend the dead time. The low rotational mass inertia of the test bench leads to slight resonance oscillation, resulting in inaccuracies. These are not to be expected on the scooter due to the comparatively massive wheel.

In addition to the static consideration of a dedicated operating point, the sensing of the dynamics is decisive. A closed-loop scenario was simulated for this purpose. The reference variable is measured using the real WSS. In this way, a statement can be made about the dead time behavior. Figure 8.7 shows the test results, including simulated and measured scooter velocity. The scooter accelerates from standstill to 45 km/h. Due to computing cycles and serial communication between the host computer and the test bench, a latency of approx. 100 ms occurs. The analysis of the dead time at two different velocities (1: 1.8 km/h; 2: 42.4 km/h) proves proper functioning of the adaptive MAFs. The WSS dead time of approx. 100 ms remains almost constant due to the constantly velocity-adapted filter size. These measured dead times are consistent with the assumptions previously made in Chapter 6.1.4. When observing the velocity feedback, a slightly unsteady signal behavior is noticed. Using the filter parameters applied to the scooter results in the aforementioned effects. When controlling the stepper motor, small step-like accelerations lead to excitation of the encoder disk. These causes signal fluctuations by oscillation without affecting the evaluation, since the error determination was performed statically.

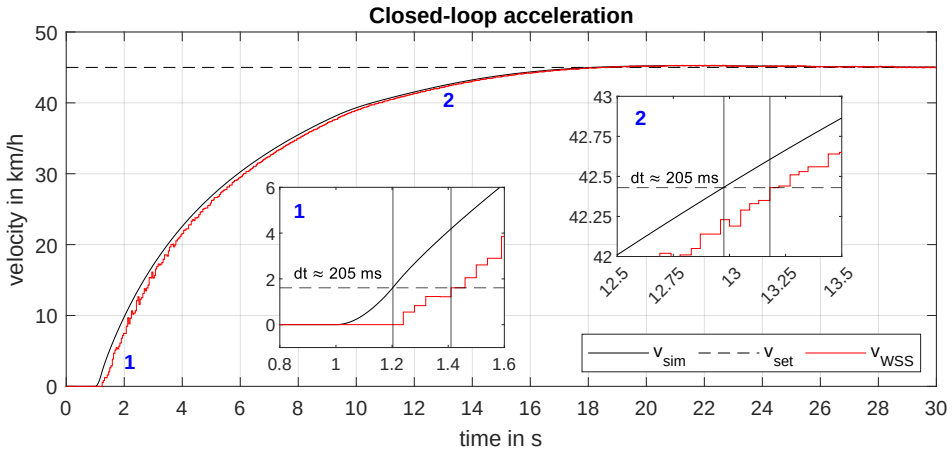

Figure 8.7 – WSS closed-loop evaluation

8.2.2 Controller Performance

To achieve stable, stationary and precise control, an adaptive PI-controller was tuned simulation-based (Table 6.3) under the criteria of max. 0.3 km/h overshoot. A test cycle, consisting of a series of increasing velocity steps (0, 10, 20,... km/h) and sudden accelerations from standstill (0, 10, 0, 20,... km/h), was performed. The set values were provided by the implemented CC in order to achieve optimum reproducibility. That way, the proper function of the adaptive threshold for larger steps in setpoint as well as small variations can be tested. By comparing the set velocity with the simulated/measured velocity and the simulated closed-loop/measured TVA position, the simulation validity and real-world control performance is investigated. Figure 8.8 shows the results (top: incremental, bottom: initial).

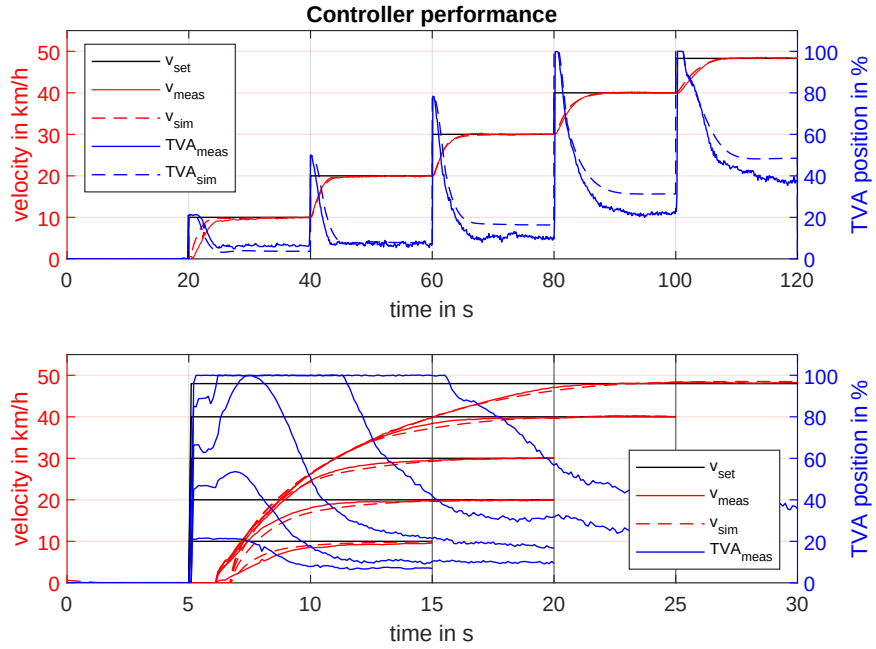

Figure 8.8 – Controller performance

For both scenarios, the controller reached the exact set velocity without any overshoot or instability. Velocities lower than 11 km/h led to unsteady settling due to the centrifugal clutch engagement/slip. For higher velocities, the max. error between simulated and measured dynamics is 1.9% for step-wise increments. Initial accelerations from standstill lead to shifted velocity origins that can be justified by the clutch engagement. The resulting error is max. 2.3%, which proves a plausible controller simulation beyond the engagement process. Deviations in TVA openings are due to the non-linear relationship between throttle opening and engine power output. This was neglected in the simulation, but has no measurable effect on the control behavior. Higher controller gains are feasible but lead to oversensitive responses to throttle changes. Figure 8.8 also demonstrates the proper operation of the CC.

8.2.3 System Behavior

After validation of the control strategy and performance, the effect on vehicle dynamics and engine control is to be examined in real-world scenarios. Three frequently occurring disturbance scenarios were analyzed: max. acceleration (S1), a sudden change from a level

road to an uphill/downhill slope (S2) and an acceleration on a downward slope followed by a transition to a level (S3). The comparison to the OR is shown in Figure 8.9 by measurements of the velocity, throttle valve position and the fuel injected. Differences between scenarios result from small road gradient variations.

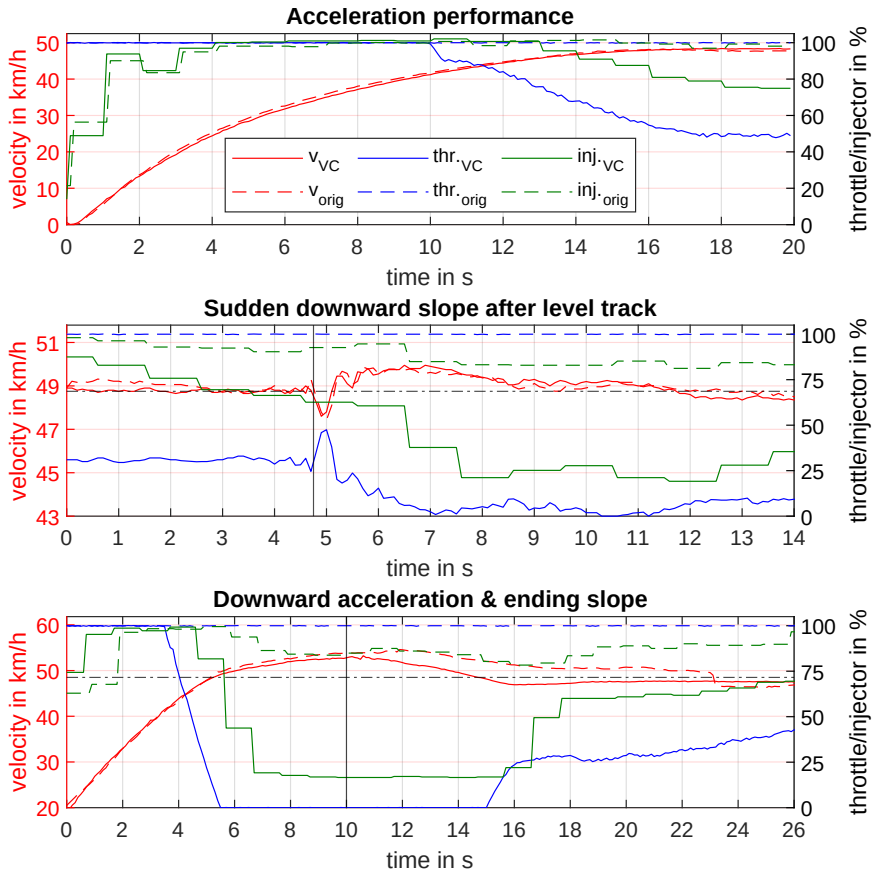

Figure 8.9 – System behavior

Scenario (S1) demonstrates the preservation of driving performance. Acceleration is equally fast with both systems, whereby the OR, contrary to the VC, shows a slight overshoot of 0.3 km/h (VC: 0 km/h) when reaching the speed limit. Significant differences can be found in the throttle valve position and injection quantity. When approaching the speed limit (orig. 48.7 km/h, dash-dotted line), the VC regulates the throttle valve at the corresponding operating point (50%). Consequently, the injection quantity also drops by 25%. Scenario (S2) is initiated at top speed, which is why the VC has already settled to approx. 35% throttle position. At time 4.75 s, an 8% downhill slope suddenly occurs after a small bump. Despite aggressive excitation, the system behavior remains stable and even resembles the response of the control applied by *Peugeot*. In both cases, the overshoot behavior at the entry of the gradient shows max. 1 km/h. The VC closes the throttle valve almost completely, whereas originally it is fully open and three times the fuel is injected. Scenario (S3) shows the max. acceleration on a 15% downhill slope, followed by a transition to level ground. An improved overshoot (1.1 km/h smaller) can be seen with the VC. While the speed limit can no longer be maintained with OR, it can be successfully controlled by the VC. It is shown again that the throttle valve is completely closed and the injection is reduced to idle state. At time 10 s, the gradient ends. The system response is stable, with no discernible fluctuations in velocity.

8.2.4 Fuel Savings

In order to demonstrate the fuel savings/CO_2 reduction under real-world conditions, a 50.4 km long test cycle was driven that depicts 61% urban and 39% rural environments. Three cycles each were driven for the OR and the VC system. Weather conditions, driving time and traffic situation were monitored to create comparable test conditions. The tire pressure was kept constant at the manufacturer's specification of 2.1 bar and the rider (80 kg) was not changed. Consumptions were determined by means of calibrated measuring cylinders. Inaccuracies of max. 2.5 ml occur due to measurement errors, which result in a max. total error of 0.3%. The measured volumes were referenced to a temperature of +15°C. By applying the VC, a saving of 13.6% (1.82 l/100 km) could be demonstrated compared to the OR (2.11 l/100 km). Since the combustion of one liter of gasoline releases 2280 g CO_2, this corresponds to an estimated reduction of approx. 661 g/100 km. Table 8.1 shows the related results.

Mod. /	**Weath.** °C	**Dur.** h	**Mile.** km	**Vol.** ml	**Cons.** $\frac{l}{100km}$	**Aver.** $\frac{l}{100km}$
Orig.	sun,dry,12	1:25	50.4	1060	2.10	
Orig.	sun,dry,16	1:26	50.4	1061	2.10	**2.11**
Orig.	sun,dry,17	1:31	50.4	1065	2.11	
VC	sun,dry,17	1:29	50.4	925	1.83	
VC	sun,dry,12	1:32	50.4	885	1.76	**1.82**
VC	sun,dry,18	1:33	50.4	945	1.87	

Table 8.1 – List of road testing results

This saving can be explained by the optimization of the ignition timing. On the flat, approx. -11.5 degrees before the TDC can be measured with OR. By applying the TbWS, the air supply is controlled instead of the ignition timing. This allows the EC to set the optimum ignition timing and reduce the injection quantity to maintain $\lambda = 1$. Now the ignition timing corresponds to -32 degrees at max. velocity and is thus in the optimum range (compare Fig. 2.3). A significant improvement in exhaust gas composition can also be expected.

8.3 Evaluation through Roller Dynamometer Testing

The results are divided into vehicle CAN data, engine and exhaust gas according to the measurement data acquisition. Contrary to the test strategy described, only gradients down to -5% could be taken into account. The mass flow could not be plausibilized for steeper gradients with activated VC due to its small exhaust gas volume. Despite clustering, all the measurement data shown, relates to the same measurement run and was recorded simultaneously.

8.3.1 Vehicle CAN Bus Data

Figure 8.10 shows the logged vehicle data recorded by the MB. The **Vehicle velocity** of the OR and VC differs in behavior. The VC adjusts the top speed precisely until the engine power is no longer sufficient on gradients overcoming 1.5%. With the OR, the speed fluctuates slightly, with clear deviations on downhill gradients greater than 6% (0.4 km/h) and uphill gradients (up to 1.6 km/h). Further, the **Throttle valve** behavior is demonstrated. Contrary to the original throttle cable actuation (fully open at top speed), the system controls the

throttle valve position load-dependent instead of the ignition timing. A difference of 50% can already be observed on a level road. In addition, the **Engine speed** shows the effects of changing load conditions. Small deviations depend on the differences in vehicle velocity caused by inaccurate OR. In order to make a statement about the fuel-air mixture with regard to the ignition timing shift, the **Oxygen** sensor's measurement data was recorded. The oxygen concentration increases minimally with decreasing road gradient for VC operation. In accordance to the stoichiometric ratio ($\lambda \approx 1$), the **Injector** opening must also be adjusted in proportion to the lowered air supply.

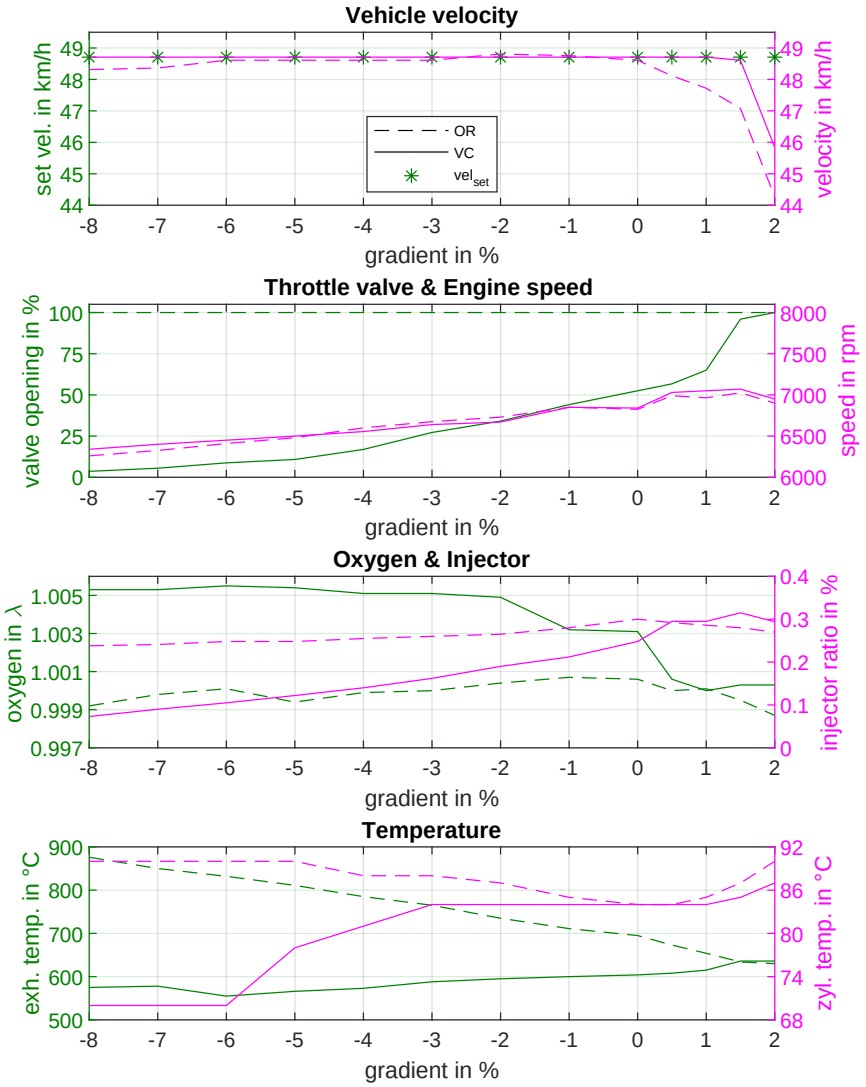

Figure 8.10 – CAN bus data

During activated VC, the injection quantity increases in proportion to the engine load and throttle valve opening. With OR, the injection quantity also increases slightly until a gradient of 0%. When driving uphill, the injection quantity decreases in line with the decreasing velocity, although the powertrain still offers power reserves. On level ground, the VC achieved an improvement of 17%. The **Temperatures** of the VC show a proportional relation to the injection quantity, which in turn, depends on the throttle valve position. The cylinder temperature only differs on steeper gradients and improves by a max. of 22% (Δ20°C). The exhaust gas temperature is reduced by max. 34% (Δ301°C), thus drastically minimizing

the thermal load on the exhaust system, even on level ground. Despite the reduction, the temperature remains within the optimum operating range for three-way catalytic converters. The temperature reduction can be explained by more efficient combustion. Instead of burning excess fuel in the exhaust gas, it is not injected at all. Tests of the engine parameters will confirm this in the following.

8.3.2 Effect on Engine Operation

A measurement of the engine parameters was made for each operating point. As parameters vary slightly with each operating cycle due to the control and combustion processes, a measurement consists of 60 cycles. To illustrate the measurement methodology, an entire series of measurements for a gradient of 0% is shown in Figure 8.11. All other operating points are evaluated summarized.

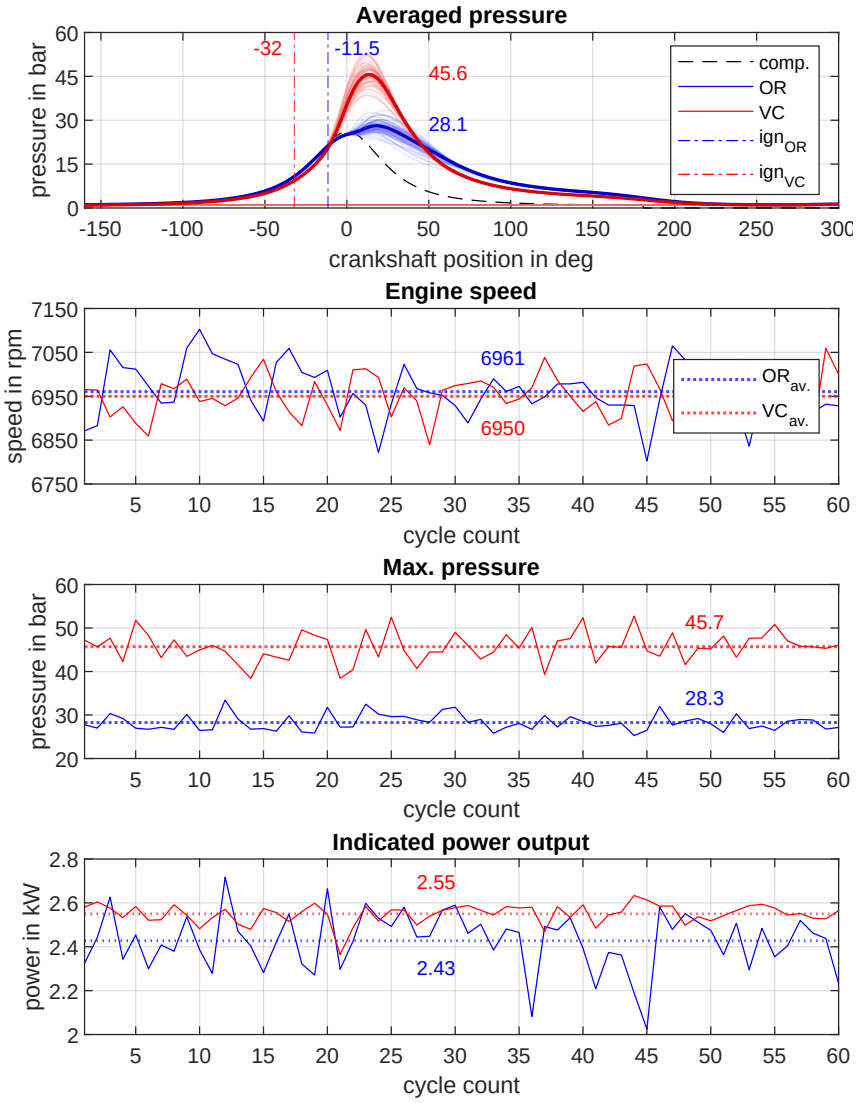

Figure 8.11 – Single engine operating point (0%)

Differences in the indicated cylinder **Pressure** can be seen clearly. Forces acting on the piston, result directly from the cylinder pressure. Accordingly, the amount and duration of the existing pressure is decisive. The max. **Averaged pressure** shows an 63% increase and the peak is slightly brought forward by VC, which can be explained by an optimum ignition timing. Even on a level ground, the ignition timing is shifted forward by 20.5 degrees. The **Engine speed** does not differ noticeably, as the vehicle velocity is the same in both cases (see Fig. 8.10). The **Max. pressure** measured differs minimally from the max. averaged pressure, which can be justified by the averaging. An **Indicated power output** can be calculated by the measured mean pressure and engine speed based on the engine's displacement. Sustained and increased mean pressures result in an improved power output.

Figure 8.12 shows the results of all gradient variations. The pressure curves of the VC are more compressed and higher, while the OR pressure drops slower. Consequently, the combustion process is much faster when VC is enabled. Comparing the pressures only at max. load (2%), the curves are almost identical in magnitude and progression, even if the vehicle velocity comes with a deviation (1.6 km/h). Major differences can be seen in the ignition timings. While the OR shifts the ignition timing towards or slightly after the TDC, the engine controller initiates the mixture ignition up to 29.75 degrees earlier with VC.

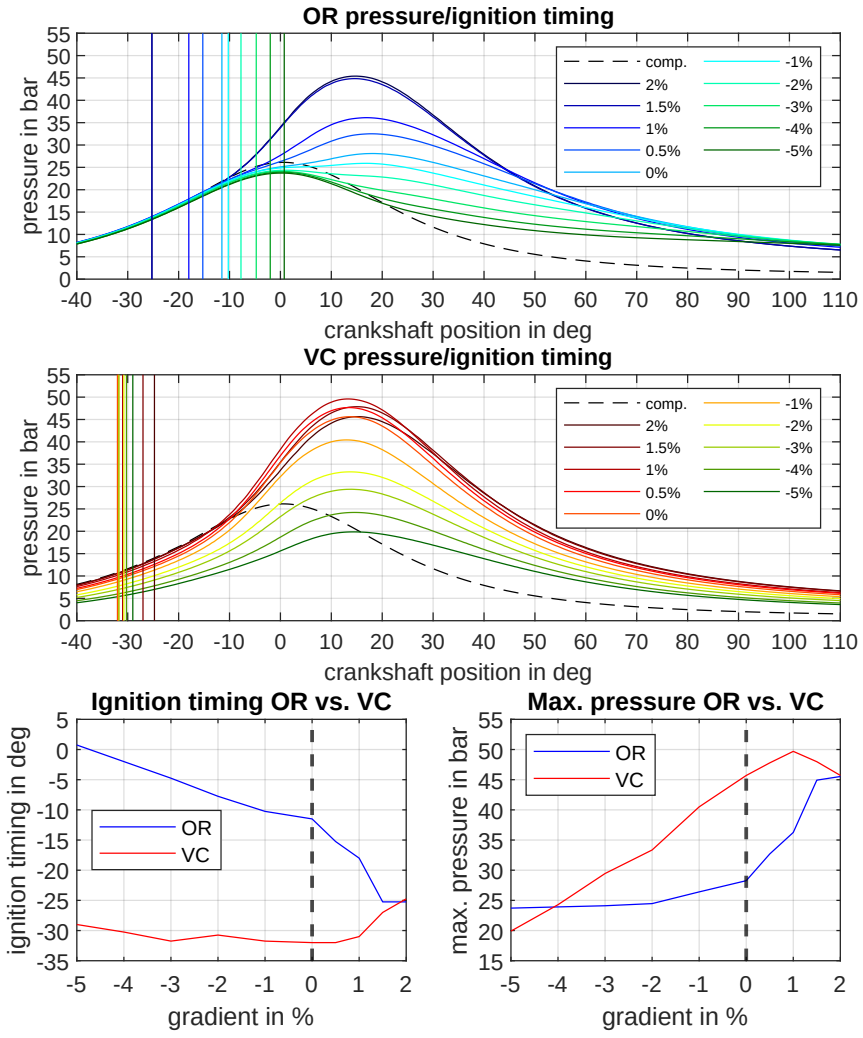

Figure 8.12 – Engine measurement

According to the injection quantity in Figure 8.10, a distinction must be made between the gradient-dependent pressure curves. All pressures of the OR result from the combustion of the max. injected fuel quantity. By shifting the pressure maximum (combustion) to expansion (downward movement of the piston), the energy is converted less effectively. The VC, in contrast, achieves higher pressures using considerably less fuel. The ignition timing and max. pressure graphs illustrate the effect for driving on level ground. The steeper the gradient with OR, the less of the energy provided is required and the more energy is burned in the exhaust. When VC is activated, the ignition timing remains almost constant and is only adapted to the engine speed (see Fig. 8.10). Even on level ground, the timing differs by 20.5 degrees and the mean pressure by 17.4 bar.

8.3.3 Exhaust Optimization

In addition to performance, all the engine parameters described have an influence on the exhaust composition. Figure 8.13 shows the results of the exhaust gas measurement.

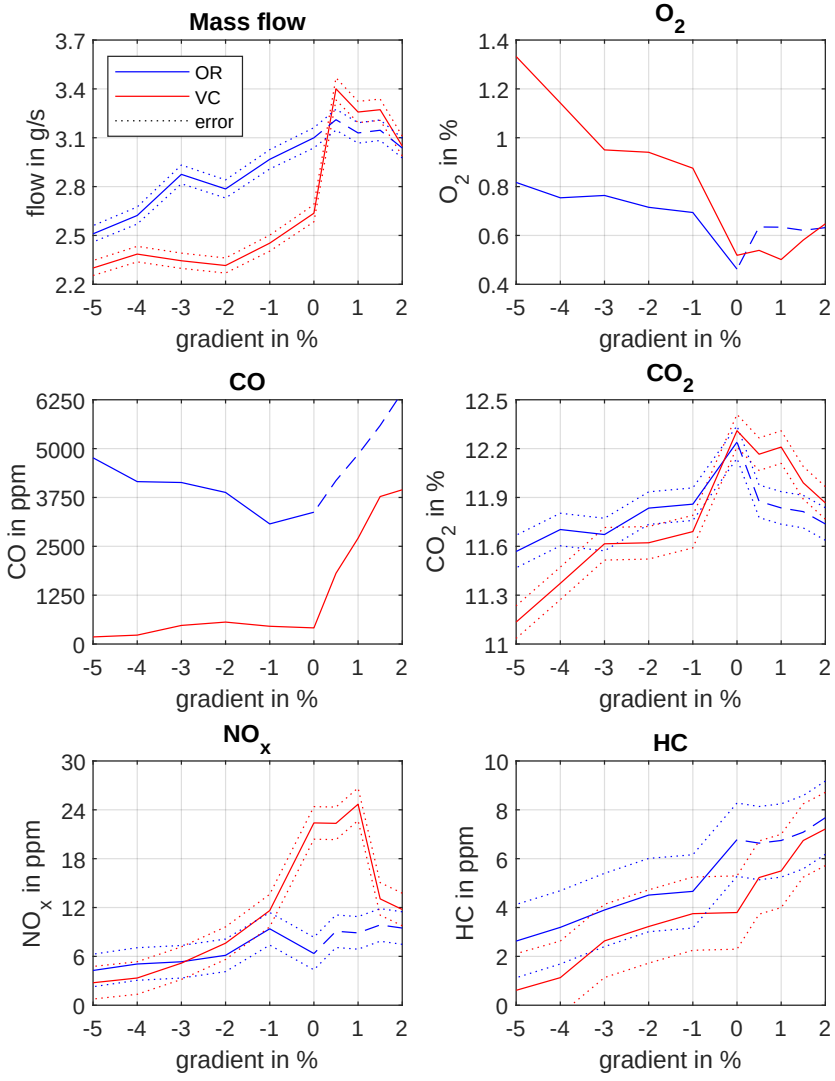

Figure 8.13 – Exhaust measurement

Relative results are directly related to the **Mass flow** and mass flow improvements reduce the emitted emissions accordingly. Despite identical conditions for the measurement of both

restriction methods, the results are only partially comparable. When evaluating the recorded vehicle velocity (see Fig. 8.10), a deviation was noticed when driving uphill. This is due to a reduced injection quantity with OR, although the engine would be able to maintain higher vehicle velocities. As a result, the mass flow is reduced, leading to different operating points (dashed line) that are not qualitatively comparable. No changes were made to the injection control as part of the VC implementation. The given behavior can already be seen in the original state. The mass flow composes of the aspirated air and the injected fuel. When using the VC, the throttle valve is not permanently open, less air is drawn in and less fuel is injected. Consequently, the exhaust mass flow is reduced. The optimized combustion within the cylinder (see Fig. 8.12) reduces the combustion in the exhaust, which is caused by the overlapping of the already opened exhaust valve. Only minor changes can be seen in the $\mathbf{CO_2}$ concentration.

The stoichiometric ratio and the combustion temperature have a major influence on the exhaust gas composition. Since only small variations of the oxygen concentration ($\Delta\lambda 0.007$) were detected during operation of both systems (see Fig. 8.10), it can be assumed that stoichiometric changes will only have minor influence on the engine's raw exhaust gases. The catalytic converter, by contrast, reacts more sensitively to changes of the oxygen concentration (optimum: $0.99 < \lambda < 1.0$). For lean mixture, the catalyst's conversion rate of nitrogen oxides decreases in particular. Due to the faster combustion (see Fig. 8.12), the combustion temperature increases significantly, as the same amount of energy is converted in a shorter time. As a result, decreasing CO/HC and increasing NO_x emissions are to be expected. The measurement actually shows extreme relative improvements in **CO** emissions by a max. factor of 26. The **HC** concentration also falls by a max. factor of 1.8. However, the increased temperatures favor the formation of NO_x emissions. $\mathbf{NO_x}$ emissions increase under load by a max. factor of 3.5. The slight increase in $\mathbf{O_2}$ concentration can be attributed to the minimally increased lambda value and the catalytic reduction of NO_x.

If the OR would exploit the powertrain's performance potential as the load increases, the exhaust gas emissions would equal those of the VC when driving uphill. At an incline of 2%, both operating points would be identical, as no restriction would limit the vehicle's velocity. The mass flow would grow due to the higher injection quantity. CO and HC emissions would decrease with rising temperature and the NO_x emission would increase accordingly. When driving downhill, all emissions fall drastically below those of OR operation. This would demonstrate emission improvements over all investigated load points. 50 cc scooters are mainly used in urban areas/on flat terrain. Table 8.2 shows the relative improvements of the exhaust gas composition when driving on level ground.

	Property	OR	VC	Improvement
1	Mass flow in g/s	3.1	2.64	1.17
2	CO in ppm	3373	412.7	8.17
3	CO_2 in %	12.24	12.3	1.00
4	NO_x in ppm	6.35	22.4	-3.53
6	HC in ppm	6.8	3.8	1.79

Table 8.2 – List of exhaust improvements

9 Discussion

The VC system developed can be discussed on several scientific levels. On the one hand, individual components or systems (e.g. TbWS) can be benchmarked against existing approaches based on their performance. Response behavior, accuracy and stability of TPS and TVA serve as assessment criteria. On the other hand, the VC system as a whole can be considered in the context of the current mobility issue of sustainability. Are two-wheelers with modern combustion engines still up to date and suitable for climate protection solutions? A comparative analysis between the test vehicle and e-scooters is carried out using CO_2 equivalents covering battery production and operation. Even if exhaust emissions demonstrably improve, the question arises as how this is reflected in the official exhaust emission measurements. The driving cycles for 50 cc two-wheelers must be questioned. Could the implemented system contribute to pass modern or even future emission standards? The classification of exhaust emissions is discussed based on the Euro emission standards. Further, the changes in exhaust gas composition must be evaluated in terms of human health.

9.1 Throttle-by-Wire-System

In order to relate the TbWS results to the context of other research, Table 9.1 gives a performance comparison to several Electronic Throttles (ETs). Therefore, position error, settling time (ST) and overshoot behavior are investigated. All three reference systems are based on a PID-controlled friction compensated DC motor for use in motorcycles. The evaluation of referred systems included only the TVA, which is why the direct comparison is made with the TVA presented here. Within a benchmark, the developed TVA performs best in both accuracy and overshoot performance. In terms of settling time, the system matches the performance of its counterparts. These were designed for use on racing motorcycles, while the requirement on a scooter is much lower. Considering the resulting system performance and the less complex design, the TbWS performs very well. The max. TbWS accuracy includes the non-linearity of both position measurements, in contrast to the specifications of the compared systems.

	TVA	ET1[35]	ET2 [26]	ET3 [36]	**TbWS**
Controller	PI	PID	PID	PID	**PI**
Motor	Step.	DC	DC	DC	**Step.**
Error (%)	0.1	0.15	0.15	0.69	**0.63**
ST, step (ms)	130	120	-	250*	**130**
ST, ramp (ms)	30	-	20	-	**60**
Overshoot (%)	<0.4	<1.0	<0.5	<1.0	**<0.4**

*step size = 10 % of the opening range

Table 9.1 – TbWS performance comparison

By merging both units, the integration effort could be reduced and the system architecture simplified. Assemblies would have to be significantly reduced in size and the use of a smaller stepper motor would have to be considered. The decisive factor would be the development of a central PCB and the elimination of one MCU. The system's temperature resistance was outlined in Chapter 5.3 by referring to ISO 16750-4. Further, the temperature dependence of the entire system could be evaluated in a climate chamber with regard to extreme temperatures.

9.2 Velocity Control

Modern four-stroke scooters already enable a comparatively environmentally friendly type of individual mobility. The system developed increases efficiency by an additional 14%. More and more electric scooters are available as alternatives, but they come with significantly smaller ranges, heavy batteries and higher prices. If CO_2 emissions are considered in comparison, vehicle production and electricity generation must be considered. One liter of gasoline emits about 2280 g [74] of CO_2 when burned, while the European average for the production of one kilowatt-hour of electrical energy is about 226 g of $C0_2$ [75]. The average consumption of combustion-powered scooters from several leading manufacturers in the EU (*Peugeot*, *Vespa*, *Piaggio*) equals an average of 2.22 l/100 km (5143 gCO_2/100 km) for gasoline-powered and 4.11 kWh/100 km (928 gCO_2/100 km) for electric-powered scooters. Taking into account the average battery capacity of the referred manufacturers, a capacity of 4.88 kWh results. The production emissions of both vehicle types differ mainly through battery production, which releases about 177 kg of CO_2 per kWh of capacity [74]. Consequently, the electric drive generates an additional 864 kg offset of CO_2 on average. With a life expectancy of scooters/mopeds of 20 000 km, the CO_2 emission for the gasoline-powered scooter is 1028.6 kg and 1049.6 kg for the electric-powered one. The test vehicle equipped with the velocity-controlled TbWS achieves a CO_2 footprint of 829.9 kg during its service life with an average consumption of 1.81 l/100 km, making it 20.9% more environmentally friendly than average electric scooters. After 26 800 km, the electric scooter would show a CO_2 benefit. When charging with electricity from renewable energy sources solely, the emissions caused by battery production would still overcome the test vehicle's footprint. By using eco-fuels, the CO_2 balance could even be neutral. Accordingly, consumption optimization would serve for economic efficiency and effective utilization of the eco-fuel resource [76].

Besides the eco-friendliness, the driving experience can be questioned. By VC implementation, there is no direct command line to the engine. The system reacts proportionally to the control deviation, which is similar to conventional acceleration behavior. Like CC functions, the system can accelerate independently on uphill/downhill grades to maintain speed. The rider has to get used to this behavior, as it differs from conventional scooters. Other control approaches could be considered. Furthermore, the highest energy loss of 28% (test vehicle) occurs in the variomatic transmission. This design-related problem affects all scooters with CVT belt drive [77]. In the future, the development of a more efficient torque converter could increase the fuel economy. Consumption of less than 1.5 l/100 km could become feasible. Hydrodynamic torque converters could be investigated [78].

Although the increase in cylinder pressure improves the efficiency of the engine, mechanical stress is increased simultaneously. The pressure results in the force acting on the piston, which must be absorbed by the crankshaft bearing. Although there are barely higher peak pressures, permanently higher forces can cause more stress. This must be taken into account when designing the engine. The impact on the engine of the VC system could be investigated in an endurance test. No signs of wear could be observed after approx. 2000 km of operation.

Finally, the question of system costs arises when it comes to integration in cost-effective scooters. Previously, costs for the TbWS were estimated at approx. 15 € for large-scale production. Components such as the MB and HMI are not required for VC implementation. MECU and WSS, in contrast, must be considered. Prototype costs amount to approx. 35 € for the MECU and approx. 60 € for the WSS. Taking into account discounted purchase prices, high quantities and mass production, experience has shown a fall to almost 10% of the initial costs. The system would be estimated to 25-35 €. Further, the merging of MECU, TPS and TVA electronics into a fully integrated unit offers potential for savings.

9.3 Exhaust Optimization

Classification of the absolute emission values is not directly feasible on the basis of the European emission standards. Here, the effects of the VC were compared in relation to the OR. Emission limits refer to measurements from standardized driving cycles (e.g. ECE R47, WMTC). A comparison for emissions at a certain operating point can not be made with official emission data of other scooters. In addition, the WMCT cycle includes numerous accelerations and braking maneuvers, between which the top speed of the scooter is not reached [79]. During test rides, the test vehicle predominantly reached the top speed, even in inner cities with high traffic density. Consequently, the exhaust measurements shown have a very clear effect in real-life use. The effect is maximized in non-urban use.

In order to place the measured emissions in the context of the European emission standard, the measurements were converted approximately. For the following evaluation, the measurement is assessed on level ground. To allow the measured emissions to be classified, a conversion to mass per kilometer driven (g/km) must be performed. As the measurements describe volumetric proportions, the exhaust gas volume must be approximated by use of the general gas equation. As pollutants (CO, HC, NO_x) only represent 1% of the exhaust gas, variations in relation to the total volume flow can be neglected. Its main components N_2 (71%), CO_2 (14%) and H_2O (13%) remain mainly constant [80]. Further, ambient pressure (101325 Pa) and gas temperature (see Fig. 8.13) must be taken into account. By inserting the parameters previously measured, an exhaust gas volume (V_{Exh}) of 0.321 m^3/min when using the OR and 0.248 m^3/min with VC results. Based on the volumetric pollutant proportions, the respective mass flow rate can be calculated using the general gas equation. By taking into account the top speed, the pollutant's volumes can be specified as masses in relation to a driven distance of one kilometer. Table 9.2 shows the converted emissions.

Param.	OR	VC	Euro 5
V_{Exh}	15.63 m^3/h	12.09 m^3/h	/
V_d	0.321 m^3/km	0.248 m^3/km	/
CO_2	43.1 g/km	36.81 g/km	/
CO	642.14 mg/km	76.48 mg/km	1000 mg/km
HC	8.06 mg/km	3.84 mg/km	100 mg/km
NO_x	2.33 mg/km	7.04 mg/km	60 mg/km

Table 9.2 – List of emissions

The comparison with the Euro 5 emissions standard (valid from 2020) demonstrates that although the vehicle can comply with all limit values for this operating point, the OR CO emissions in particular are relatively high. By using the VC, CO emissions can be reduced by a factor of 8.4. As CO is a dangerous respiratory toxin for humans, the improvements are crucial. HC emissions are also reduced by a factor of 2.1, although these are far below the limit. Since HCs are considered carcinogenic, the improvement is of importance for human health. Despite the 3-fold increase in NO_x emissions, they are still low compared to the Euro 5 limit. CO_2 emissions are not taken into account by the exhaust gas standards, even though they are largely responsible for the greenhouse effect. An improvement by a factor of 1.17 can be observed. For gradients from -1% to -8%, the emissions would further improve significantly. For gradients $> 0\%$, the emissions of both systems would equalize with increasing gradient.

9.4 Proof of Hypotheses

The research aim was defined at the outset by establishing four hypotheses that serve to answer the research question. After achieving the objectives stated in Chapter 3, it is essential to review their fulfillment. While the evaluation focused primarily on the comparison of the OR with the developed VC system, a more comprehensive subsumption of the results was undertaken as part of the discussion.

H1: The velocity-dependent control of the throttle valve position allows ITM to be bypassed and the top speed to be limited.
It has been demonstrated that when ITM is bypassed, throttle position control precisely restricts the scooter's top speed. The ignition timing was consistently proven to be in the optimum range. Implementing an adaptive VC algorithm leads to a better restricting behavior than with the OR. Sensing of the throttle position and actuation of the throttle valve were realized by the developed TPS and TVA. VC was achieved by developing the MECU including the redundant WSS for velocity measurement. H1 is therefore approved.

H2: In accordance with the optimum stoichiometric control, the reduced air supply leads to an optimized fuel economy.
By measuring the oxygen concentration on the roller dynamometer, the retention of the optimum air-fuel mixture could always be demonstrated at variable load points for VC operation. With the help of the applied VC system, fuel savings were demonstrated both on the chassis dynamometer (17%) and in real road tests (13.6%) without manipulating the

stoichiometric ratio. Thus, the load-dependent reduction of the air supply does not interfere with the injection control, but leads to an optimized fuel economy. H2 is approved.

H3: Regulating the air supply and bypassing ITM enables optimized combustion and significantly improves exhaust emissions.
Investigations of the engine operation have demonstrated the positive influence of optimum ignition timing to the combustion. In contrast to ITM, the internal cylinder pressure increases and the engine's efficiency is optimized. As a result, increased combustion temperatures could be detected, which lead to the significant reduction of HC and CO in the exhaust gas. At the same time, an increase in NO_x levels can be observed. As a consequence of reduced injection quantities, CO_2 emissions decrease. A substantial reduction in toxic exhaust gases has been verified and the optimization of pollutant emissions at top speed contributes considerably to compliance with the Euro 5 emissions standard. H3 is thus confirmed.

H4: The implementation of VC improves the vehicle's driving characteristics.
In addition to the more precise restriction of the top speed, the VC implementation also improved the driving characteristics in terms of performance. On the one hand, the overshoot behavior was improved, especially on declines. On the other hand, the full power spectrum of the powertrain is exploited on inclines in contrast to the OR, resulting in higher top speeds when driving uphill. Therefore, H4 is approved.

10 Conclusion

In this doctoral thesis, the development and performance of a velocity-controlled Throttle-by-Wire-System was treated. The Throttle-by-Wire-System consists of a sensor unit determining the throttle grip position and an actuator manipulating the throttle valve position. The throttle grip position is measured redundantly and contactless by means of an anisotropic magnetoresistance sensor. With the help of plausibility algorithms, the proper function of the throttle position sensor is verified. For easy vehicle integration/retrofit, the existing throttle cable is directly attached to the unit. The digital measured value is shared via CAN bus with the main ECU, operating the throttle valve actuator, which sets the required position at the throttle valve. The actuator consists of a stepper motor-based drivetrain and the position is controlled closed-loop using position measurement as feedback. By using a high performance motor driver, very accurate positions can be approached while vibrations and acoustic noise are kept to a minimum. A PI-controller is able to control precisely without taking friction compensation into account or working model-based. When an error occurs, the subsystems are able to differentiate between different faults. Problems with CAN communication, position measurement or faulty throttle positions can be detected. Both units are able to request calibration or perform them independently. In case of major errors, the ignition can be interrupted to guarantee a safe condition. The accuracy of the Throttle-by-Wire-System is 99.37% of the throttle grip position and is reached within approx. 60 ms, which corresponds to a much faster reaction than the response of a small-volume single-cylinder four-stroke engine. For the prototype production, costs of about 140 € have been incurred. These can be significantly reduced through improvements in size and mass production, lowering the cost of manufacturing.

Once the interfaces for sensing the throttle position and actuating the throttle valve position were established, the velocity control was developed on the second level. Instead of shifting the ignition timing to comply with the legal top speed for scooters, the system regulates the air supply to the engine. For this purpose, a redundant wheel speed sensor was designed to sense the reference variable. Power supply, data processing, motor control emulation, fail-safe functions and actual control were implemented on a main ECU. By simulating the vehicle's longitudinal dynamics, an adaptive PI-controller could be designed to control the velocity stable, with stationary accuracy and without overshoot. Control of the vehicle's top speed has been improved in terms of accuracy and overshoot. The driveability/operability of the vehicle was prioritized. A virtual dashboard was used to interface between the system and the rider, clarifying the functionality and promoting eco-friendly driving with an eco-score. Additionally, it enables the activation and adjustment of the cruise control. In order to be able to evaluate the system behavior, a measurement box was developed and integrated, logging all system parameters. Ultimately, a fuel saving of 13.6% was achieved and proven in the road test, while improving the vehicle's performance. These savings are caused by the prevention

of ignition timing manipulation for restriction. As a result, the economical and ecological competitiveness against electrically powered scooters was underlined. As long as large amounts of CO_2 are emitted during battery production, the optimized four-stroke powertrain presented here represents an excellent transitional solution. Mechanical optimizations could further reduce consumption.

In order to evaluate the influence on the mixture preparation, the combustion process and exhaust gas formation, the vehicle was equipped with measurement technology. A measurement box logged all system-relevant CAN data. The engine was fitted with a crankshaft encoder, an indicating spark plug for pressure indication and an ignition clamp. Cylinder and exhaust gas temperature were measured by attaching two temperature probes. The exhaust gas composition was examined with regard to mass flow, CO, CO_2, NO_x, O_2 and HC concentration. A coast down test was performed to determine the vehicle's resistance parameters. These were used to approach load points by varying the road gradient on a roller dynamometer at top speed. A considerable improvement in exhaust gas emissions was demonstrated caused by the velocity-controlled Throttle-by-Wire-System. The exhaust mass flow was reduced across all operating points (17% on the level). Toxic CO emissions were also reduced by a factor of 8.4. Clear reductions (max. 54%) in carcinogenic HC emissions were detected over the entire measurement range. NO_x emissions increased for gradients between -1% and 1% by a max. factor of 3. CO_2 emissions, which are largely responsible for the greenhouse effect were minimized by 17%. These improvements were achieved, as demonstrated by measuring the engine parameters, through suppressing the ignition timing shift and regulating the air supply. The measurements show a max. ignition offset of 29.5 degrees between original restriction and velocity control. The internal cylinder pressures increase with velocity control and combustion is more efficient and faster. As a result, the combustion temperatures increase, which leads to the observed optimization of CO and HC emissions.

Since fuel injected four-stroke engines and controlled three-way catalytic converters represent the current state of the art for Euro 5 scooters, the presented research could be widely applied. As a result, the vehicle owner is relieved by lower operating costs through better fuel economy and the impact on climate change is reduced primarily through minimized CO_2 emissions. In addition, the pollutant load on fellow human beings is drastically lowered. Finally, based on the studies presented, the research question posed in Chapter 3 can be answered as follows: **The development and application of a velocity-controlled Throttle-by-Wire-System on a modern combustion-powered 50 cc scooter (Euro 5) leads to significant ecological, economical and driving dynamical improvements.**

As a supplement, two videos were produced to demonstrate the vehicle integration/evaluation of the Throttle-by-Wire-System and the velocity control system, including all developed features. The corresponding links are included in Chapter A.1 of the appendix.

Acknowledgments

Dear supervisors, collaboration partners and supporters,

I would like to thank you for your continuous support during my doctoral studies. Your professional experience and supervision have been essential to the successful completion of this thesis. Special thanks are due to my supervisors Prof. Dr. Arturo Morgado-Estévez (UCA) and Prof. Dr. Hektor Hebert (Fra UAS). Their scientific discussions, professional enthusiasm and especially their encouragement strengthened me in my research. I would also like to thank Prof. Dr. Fernando Perez-Peña (research group leader at the UCA) for his motivated manner and high level of scientific expertise, which has helped me immensely. In the context of applied research, I would like to thank Jens Rau (student research assistant), whose thematic enthusiasm, expertise and investment greatly contributed to the research.

Furthermore, I would like to express my appreciation to *Peugeot Motocycles Germany*, with which I was able to exchange ideas and hold discussions in an industrial context. In particular, I would like to thank Jan Breckwoldt (Managing Director) and Detlef Wursthorn (General Manager Aftersales Europe) for their valuable contributions and for providing the test vehicle.

My thanks also go to the *University of Cadiz* and *Frankfurt University of Applied Sciences*, especially for their financial support during my PhD and access to the valuable resources of the library and laboratory facilities. In particular, I would like to acknowledge Ingo Behr (laboratory engineer at Fra UAS) of the Internal Combustion Engine Laboratory, who provided me with valuable insights and was heavily involved in the engine and exhaust testing.

Special thanks go to my parents Monika and Rainer Kreß, who supported me from the very beginning. Heartfelt thanks to my partner Mai Le, who gave me emotional support and listening for hours and days during this challenging time.

With heartfelt thanks,

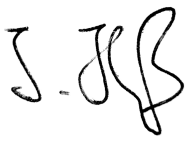

Jannis Kreß

Bibliography

[1] Bing Image Creator (DallE3), "Cover Emblem." https://www.bing.com/images/create?FORM=GENILP [Accessed: 8th March 2024].

[2] European Parliament, "Establishing the framework for achieving climate neutrality and amending regulations ('european climate law')," *Official Journal of the European Union*, vol. (EC) No 401/2009 and (EU) 2018/1999, 2021.

[3] Statistical office of the European Union, "Passenger mobility statistics." Eurostat, 2022.

[4] European Parliament, "Regulation on type approval of motor vehicles with respect to emissions from light passenger and commercial vehicles (euro 5 and euro 6) and on access to vehicle repair and maintenance information," *Official Journal of the European Union*, vol. No 715/2007, 2007.

[5] A. König, L. Nicoletti, D. Schröder, S. Wolf, A. Waclaw, and M. Lienkamp, "An overview of parameter and cost for battery electric vehicles," *World Electric Vehicle Journal*, vol. 12, pp. 1–29, 2021. DOI: https://doi.org/10.3390/wevj12010021.

[6] Peugeot Motocycle, *Range 50ccm*, 2023. https://www.peugeot-motocycles.de [Accessed: 6th February 2024].

[7] Kymco, *Kymco Prospekt 2022*, 2022. https://www.kymco.de [Accessed: 6th February 2024].

[8] M. Görgen, A. Balazs, M. Böhmer, M. Nijs, H. Lehn, J. Scharf, M. Thewes, A. Müller, N. Alt, J. Claßen, and S. Sterlepper, "All lambda 1 gasoline powertrains," in *Internationaler Motorenkongress*, pp. 93–111, 2018. DOI: https://doi.org/10.1007/978-3-658-21015-1_7.

[9] European Parliament, "Directive 2002/24/ec relating to the type-approval of two or three-wheel motor vehicles and repealing council directive 92/61/eec," *Official Journal of the European Communities*, vol. 2002/24/EC, 2002.

[10] J. Stoffregen, *Motorradtechnik (Motorcycle Technology)*, p. 43. Olching, Germany: Springer Vieweg, 9 ed., 2018. DOI: https://doi.org/10.1007/978-3-658-07446-3.

[11] K. Schreiner, *Basiswissen Verbrennungsmotor (Basics of the combustion engine)*, p. 44. Konstanz, Germany: Springer Vieweg, 3 ed., 2020. DOI: https://doi.org/10.1007/978-3-658-29226-3.

[12] G. Kumar, S. Badulla, J. Nagaraju, O. Venkatesh, G. Narasimhulu, and V. Rao, "Design and analysis of 3-way catalytic converter using cfd," *Materials Today: Proceedings*, 2023. DOI: https://doi.org/10.1016/j.matpr.2023.07.215.

[13] S. Pischinger and U. Seiffert, *Handbuch Kraftfahrzeugtechnik (Automotive engineering handbook)*, pp. 529–543. Wiesbaden, Germany: Springer Vieweg, 9 ed., 2021. DOI: https://doi.org/10.1007/978-3-658-25557-2.

[14] A. Agarwal, D. Kumar, N. Sharma, and U. Sonawane, *Engine Modeling and Simulation*, p. 10. Singapore: Springer Singapore, 1 ed., 2021. DOI: https://doi.org/10.1007/978-981-16-8618-4.

[15] K. Leyda and P. Wos, *Internal Combustion Engines*, pp. 71–72. Croatia: IntechOpen, 1 ed., 2012. DOI: https://doi.org/10.5772/2806.

[16] A. Faiz, C. Weaver, and M. Walsh, *Air Pollution from Motor Vehicles: Standards and Technologies for Controlling Emissions*, p. 115. Washington, USA: Environmental Science, 1 ed., 1997. DOI: https://doi.org/10.1596/0-8213-3444-1.

[17] P. Eckert and S. Radowski, *Combustion Engines Development*, pp. 193–223. Heidelberg, Germany: Springer Berlin, 1 ed., 2011. DOI: https://doi.org/10.1007/978-3-642-14094-5.

[18] R. Basshuysen and F. Schäfer, *Handbuch Verbrennungsmotor (Combustion Engine Manual)*, pp. 1638–643. Wiesbaden, Germany: Springer Vieweg, 7 ed., 2015. DOI: https://doi.org/10.1007/978-3-658-04678-1.

[19] Y. Zhang and H. Zhao, "Investigation of combustion, performance and emission characteristics of 2-stroke and 4-stroke spark ignition and cai/hcci operations in a di gasoline," *Elsevier Applied Energy*, vol. 130, pp. 244–255, 2014. DOI: https://doi.org/10.1016/j.apenergy.2014.05.036.

[20] G. Koltsakis and A. Stamatelos, "Catalytic automotive exhaust aftertreatment," *Elsevier Science*, vol. 23, pp. 1–39, 1997. DOI: https://doi.org/10.1016/S0360-1285(97)00003-8.

[21] G. Merker and R. Teichmann, *Grundlagen Verbrennungsmotor (Basics of the Combustion Engine)*, p. 989. Wiesbaden, Germany: Springer Vieweg, 9 ed., 2019. DOI: https://doi.org/10.1007/978-3-658-19212-9.

[22] C. Favre, J. May, D. Bosteels, J. Tromayer, G. Neumann, R. Kirchberger, and H. Eichsleder, "A demonstration of the emission behaviour of 50cm^3 mopeds in europe including unregulated components and particulate matter," *SAE International*, 2011. DOI: https://doi.org/10.4271/2011-32-0572.

[23] J. Stoffregen, *Motorradtechnik (Motorcycle Technology)*, p. 82. Olching, Germany: Springer Vieweg, 9 ed., 2018. DOI: https://doi.org/10.1007/978-3-658-07446-3.

[24] M. Micik, G. Jadnel, G. Kerzendorf, O. Pukl, and H. Voegele, "The high performance-engine for bmw m 5," *Motortechnische Zeitschrift*, vol. 51:4, pp. 142–146, 1990.

[25] J. Stoffregen, *Motorradtechnik (Motorcycle Technology)*, p. 190. Wiesbaden, Germany: Vieweg + Teubner, 8 ed., 2012. DOI: https://doi.org/10.1007/978-3-8348-2180-5.

[26] M. Corno, M. Ranelli, S. M. Savaresi, L. Fabbri, and L. Nardo, "Electronic throttle control for ride-by-wire in sport motorcycles," in *Proc. 17th IEEE International Conference on Control Applications*, pp. 223–238, 2008. DOI: https://doi.org/10.1109/CCA.2008.4629640.

[27] J. Miritsch, H. Graf, K. Böck, and R. Deuschle, "Big boxer - the engine in the new bmw r18," *MTZ worldwide*, vol. 82, pp. 48–54, 2021. DOI: https://doi.org/10.1007/s38313-021-0688-1.

[28] M. Poschner, J. Vogt, G. Wösle, and H. Wagner, "The new bmw s 1000 rr," *ATZ worldwide*, vol. 112, pp. 4–10, 2010. DOI: https://doi.org/10.1007/BF03225247.

[29] B. Smither, I. McFarlane, T. Drake, P. Ravenhill, J. Allen, and J. Boak, "Engine management system for fuel injection system specifically designed for small engines," *SAE International*, 2008. DOI: https://doi.org/10.4271/2008-32-0052.

[30] K. Reif, *Sensoren im Kraftfahrzeug (Sensors in the Motor Vehicle)*, p. 27. Wiesbaden, Germany: Springer Vieweg, 3 ed., 2016. DOI: https://doi.org/10.1007/978-3-8348-2208-6.

[31] K. Reif, *Bosch Autoelektrik und Autoelektronik (Automotive Electrics and Electronics)*, p. 257. Wiesbaden, Germany: Vieweg + Teubner, 6 ed., 2011. DOI: https://doi.org/10.1007/978-3-8348-9902-6.

[32] Treutler, "Magnetic sensors for automotive applications," *Elsevier Science B.V.*, vol. 91, pp. 2–6, 2001. DOI: https://doi.org/10.1016/S0924-4247(01)00621-5.

[33] Sensitec GmbH, *AA747 MagnetoResistive Angle Sensor*, 2017. https://www.sensitec.com/fileadmin/sensitec/Service_and_Support/Downloads/Data_Sheets/AA700/SENSITEC_AA747_DSE_07.pdf [Accessed: 6th February 2024].

[34] D. J. Adelerhof and W. Geven, "New position detectors based on amr sensors," *Elsevier Science S.A.*, vol. 85, pp. 48–53, 2000. DOI: https://doi.org/10.1016/S0924-4247(00)00341-1.

[35] G. Panzani, M. Corno, and S. M. Savaresi, "Design of an adaptive throttle-by-wire control system for a sport motorbike," in *Proc. 18th IFAC World Congress*, pp. 4785–4790, 2011. DOI: https://doi.org/10.3182/20110828-6-IT-1002.02115.

[36] C. Chen, H. Tsai, and Y. Lin, "Servo control design for electronic throttle valve with nonlinear spring effect," in *11th IEEE International Workshop on Advanced Motion Control*, pp. 88–93, 2010. DOI: https://doi.org/10.1109/AMC.2010.5464020.

[37] J. Park, J. Ryu, M. Oark, and S. Lim, "Electronic throttle valve modeling considering nonlinearity of electrical and mechanical parameters based on experiments," *IEEE/ASME Trans. on Mechatronics*, vol. 27, pp. 3309–3314, 2022. DOI: https://doi.org/10.1109/TMECH.2021.3123137.

[38] S. A. Al-Sammarraie and Y. K. Abbas, "Design of electronic throttle valve position control system using nonlinear pid controller," *Intern. Journal of Computer Applications*, vol. 59, pp. 27–34, 2012. DOI: https://doi.org/10.5120/9625-4273.

[39] X. Yuan, Y. Wang, L. Wu, X. Zhang, and W. Sun, "Neural network based self-learning control strategy for electronic throttle valve," *IEEE Trans. on Vehicular Technology*, vol. 59, pp. 3757–3765, 2010. DOI: https://doi.org/10.1109/TVT.2010.2044521.

[40] A. J. Humaidi and A. H. Hameed, "Design and comparative study of advanced adaptive control schemes for position control of electronic throttle valve," *MDPI*, vol. 10, pp. 1–14, 2019. DOI: https://doi.org/10.3390/info10020065.

[41] H. Wang, Z. Li, X. Jin, Y. Huang, H. Kong, M. Yu, Z. Ping, and Z. Sun, "Adaptive integral terminal sliding mode control for automobile electronic throttle via an uncertainty observer and experimental validation," *IEEE Trans. on Vehicular Technology*, vol. 67, pp. 8129–8143, 2018. DOI: https://doi.org/10.1109/TVT.2018.2850923.

[42] Y. Hu, H. Wang, S. He, J. Zheng, Z. Ping, K. Shao, Z. Cao, and Z. Man, "Adaptive tracking control of an electronic throttle valve based on recursive terminal sliding mode," *IEEE Trans. on Vehicular Technology*, vol. 70, pp. 251–262, 2021. DOI: https://doi.org/10.1109/TVT.2020.3045778.

[43] S. Zhang, J. Yang, and G. Zhu, "Lpv modeling and mixed constrained h_2/h_∞ control of an electronic throttle," *IEEE/ASME Trans. on Mechatronics*, vol. 20, pp. 2120–2132, 2015. DOI: https://doi.org/10.1109/TMECH.2014.2364538.

[44] U. Montanaro, A. Gaeta, and V. Giglio, "Robust discrete-time mrac with minimal controller synthesis of an electronic throttle body," *IEEE/ASME Trans. on Mechatronics*, vol. 19, pp. 524–537, 2014. DOI: https://doi.org/10.1109/TMECH.2013.2247614.

[45] H. Winner, S. Hakuli, F. Lotz, and C. Singer, *Handbuch Fahrerassistenzsysteme (Driver Assistance Systems Manual)*, p. 229. Wiesbaden, Germany: Springer Vieweg, 3 ed., 2015. DOI: https://doi.org/10.1007/978-3-658-05734-3.

[46] M. Ersoy and S. Gies, *Fahrwerkhandbuch (Chassis Manual)*, p. 254. Wiesbaden, Germany: Springer Vieweg, 5 ed., 2017. DOI: https://doi.org/10.1007/978-3-658-15468-4.

[47] K. Reif, *Bosch Autoelektrik und Autoelektronik (Automotive Electrics and Electronics)*, pp. 338–341. Wiesbaden, Germany: Vieweg + Teubner, 6 ed., 2011. DOI: https://doi.org/10.1007/978-3-8348-9902-6.

[48] P. Shakouri, A. Ordys, D. Laila, and M. Askari, "Adaptive cruise control system: Comparing gain-scheduling pi and lq controllers," *IFAC Proceedings Volumes*, vol. 44, pp. 12964–12969, 2011. DOI: https://doi.org/10.3182/20110828-6-IT-1002.02250.

[49] H. Winner, S. Hakuli, F. Lotz, and C. Singer, *Handbuch Fahrerassistenzsysteme (Driver assistance systems handbook)*, pp. 1878–882. Wiesbaden: Springer Vieweg Wiesbaden, 3 ed., 2015. DOI: https://doi.org/10.1007/978-3-658-05734-3.

[50] S. Moon and K. Yi, "Human driving data-based design of a vehicle adaptive cruise control algorithm," *International Journal of Vehicle Mechanics and Mobility*, vol. 48, pp. 661–690, 2008. DOI: https://doi.org/10.1080/00423110701576130.

[51] S. Moon, I. Moon, and K. Yi, "Design, tuning, and evaluation of full-range adaptive cruise control system with collision avoidance," *Control Engineering Practice*, vol. 17, pp. 442–455, 2009. DOI: https://doi.org/10.1016/j.conengprac.2008.09.006.

[52] N. Vedam, I. Diaz-Rodriguez, and S. Bhattacharyya, "A novel approach to the design of controllers in an automotive cruise-control system," in *Proc. 40th Annual Conference of the IEEE Industrial Electronics Society*, pp. 2927–2932, 2014. DOI: https://doi.org/10.1109/IECON.2014.7048925.

[53] B. Smither, J. Allen, P. Ravenhill, G. Farmer, P. Grosch, and E. Demesse, "Development of electronic throttle actuation for a 50cc 2-stroke scooter application," *SAE International*, 2011. DOI: https://doi.org/10.4271/2011-32-0581.

[54] M. Hirz, M. Korman, H. Eichlseder, and R. Kirchberger, "Potential of the 50cc two wheeler motor vehicle class in respect of future exhaust emission targets," in *2004 Small Engine Technology Conference*, no. SAE 2004-32-0050, 2004. DOI: https://doi.org/10.4271/2004-32-0050.

[55] J. Kreß, J. Rau, H. Hebert, F. Perez-Peña, K. Schmidt, and A. Morgado-Estévez, "Low-cost throttle-by-wire-system architecture for two-wheeler vehicles," *SAE International Journal of Engines*, vol. 17, 2024. DOI: https://doi.org/10.4271/03-17-05-0035.

[56] Infineon Technologies AG, *LE5x09A16(D) Analog AMR/GMR Angle Sensors*, 2023. https://www.infineon.com/dgdl/Infineon-TLE5x09A16_DDataSheet-v02_00-EN.pdf?fileId=5546d462696dbf12016977889fe858c9 [Accessed: 6th February 2024].

[57] STMicroelectronics, *STM32G431x6 STM32G431x8 STM32G431xB*, 2021. https://www.st.com/resource/en/datasheet/stm32g431rb.pdf [Accessed: 6th February 2024].

[58] Stepperonline, *Stepper Motor 11HS20-0674S*, 2020. https://www.omc-stepperonline.com/download/11HS20-0674S.pdf [Accessed: 6th February 2024].

[59] TRINAMIC Motion Control GmbH & Co. KG, *TMC2209 DATASHEET*, 2020. https://www.trinamic.com/products/integrated-circuits/details/tmc2209-la/ [Accessed: 6th February 2024].

[60] TT Electronics, *Non-Contacting Hall Effect Single Turn Position Sensor 6120 Series*, 2019. https://www.ttelectronics.com/TTElectronics/media/ProductFiles/Datasheet/6120.pdf [Accessed: 6th February 2024].

[61] J. Kreß, J. Rau, H. Hebert, F. Perez-Peña, K. Schmidt, and A. Morgado-Estévez, "Fuel saving effect and performance of velocity control for modern combustion-powered scooters," *Control Engineering Practice*, vol. 145, 2024. DOI: https://doi.org/10.1016/j.conengprac.2024.105849.

[62] European Parliament, "Regulation on the approval and market surveillance of two- or three-wheel vehicles and quadricycles," *Official Journal of the European Union*, vol. No 168/2013, 2013.

[63] J. Kreß, A. Morgado-Estévez, F. Perez-Peña, K. Schmidt, and H. Hebert, "Development of single-axis wheel speed sensor hil test bench for vehicle velocity control," in *Proc. 3rd International Congress on Human-Computer Interaction, Optimization and Robotic Applications (HORA)*, pp. 1–5, 2021. DOI: https://doi.org/10.1109/HORA52670.2021.9461305.

[64] STMicroelectronics, *Data brief STM32H7B3I-DK, DB3894 Rev 1*, 2019. https://www.st.com/resource/en/data_brief/stm32h7b3i-dk.pdf [Accessed: 6th February 2024].

[65] SparkFun, "OpenLog DEV-13712." https://www.sparkfun.com/products/13712 [Accessed: 6th January 2024].

[66] STMicroelectronics, *STM32F446xC/E*, 2021. https://www.st.com/resource/en/datasheet/stm32f446re.pdf [Accessed: 6th February 2024].

[67] J. Kreß, J. Rau, I. Behr, B. Mohn, H. Hebert, and A. Morgado-Estévez, "Exhaust gas optimization of modern scooters by velocity control," *arXiv*, vol. 2402.05010, 2024. DOI: https://doi.org/10.48550/arXiv.2402.05010 submitted to *Control Engineering Practice*.

[68] Kübler, *Kübler, Incremental encoders, Miniature optical*, 2023. https://www.kuebler.com/pdf?2400-2420_en.pdf [Accessed: 6th February 2024].

[69] JUMO GmbH & Co. KG, *Mineral-insulated thermocouples to DIN 43 710 and EN 60 584, Data Sheet 90.1210 (90.1221)*, 2023. https://docs.rs-online.com/64f8/0900766b812a1203.pdf [Accessed: 6th February 2024].

[70] AVL List GmbH, *AVL Pressure Sensors for Combustion Analysis*, 2016. https://www.avl.com/documents/10138/885965/AVL+Pressure+Sensors+for+Combustion+Analysis/6c844a54-7a84-429d-8e57-4f34e948f95d [Accessed: 6th February 2024].

[71] AVL List GmbH, *AVL M.O.V.E EFM Exhaust Flow Meter*, 2023. https://www.avl.com/documents/10138/3902841/AVL+M.O.V.E+EFM+Fact+Sheet.pdf [Accessed: 6th February 2024].

[72] AVL List GmbH, *AVL M.O.V.E Gas Pems 493*, 2010. https://www.avl.com/documents/10138/885965/AVL+MOVE+GAS+PEMS+ENG [Accessed: 6th February 2024].

[73] ZSE Electronic GmbH, *Sirius Technical Reference Manual, Version 1.5.5*, 2010. https://downloads.dewesoft.com/manuals/dewesoft-sirius-manual-en.pdf [Accessed: 6th February 2024].

[74] R. Kawamoto, H. Mochizuki, Y. Moriguchi, T. Nakano, M. Motohashi, Y. Sakai, and A. Inaba, "Estimation of co_2 emissions of internal combustion engine vehicle and battery electric vechicle using lca," *MPDI Sustainability*, vol. 11, 2019. DOI: https://doi.org/10.3390/su11092690.

[75] World Energy Council, "Energie für deutschland," *World Energy Council*, 2021.

[76] A. K. Agarwal and H. Valera, *Greener and Scalable E-fuels for Decarbonization of Transport*, p. 3. Singapore: Springer Singapore, 1 ed., 2022. DOI: https://doi.org/10.1007/978-981-16-8344-2.

[77] C. Zhu, H. Liu, J. Tian, Q. Xiao, and X. Du, "Experimental investigation on efficiency of the pulley-drive cvt," *International Journal of Automotive Technology*, vol. 11, pp. 257–261, 2010. DOI: https://doi.org/10.1007/s12239-010-0032-2.

[78] P. Lindemann, M. Steinberger, and T. Krause, "itc - innovative solutions for torque converters pave the way into the future," *Schaeffer Technologies AG & Co. KG*, vol. 20, pp. 280–301, 2014. DOI: https://doi.org/10.1007/978-3-658-06430-3_20.

[79] United Nations, "Worldwide harmonised motorcycle emissions certification procedure (wmtc)," *Economical and Social Council*, vol. TRANS/WP.29/GRPE/2004/10, 2004.

[80] K. Reif, *Ottomotor-Management (Gasoline Engine Management)*, p. 175. Wiesbaden, Germany: Springer Vieweg, 4 ed., 2014. DOI: https://doi.org/10.1007/978-3-8348-2102-7.

A Appendix

A.1 Demonstration Videos

The following link leads to the demonstration video of the TbWS. The video shows the vehicle integration of both TbWS components and its stand-alone/overall performance.
https://youtu.be/J3QRnSNJYAA

The following link leads to the demonstration video of the VC. All subsystems are shown in terms of vehicle integration and stand-alone function. The VC performance is evaluated by real-time measurements of the overall system.
https://youtu.be/bTjy___zY-kc

A.2 Throttle-by-Wire-System

Table A.1 summarizes all TVA parameters covering stepper motor, Hall sensor and controller.

Component	Parameter	Value
Drive	$\text{Torque}_{Stepper}$	12 Ncm
	$\text{Inertia}_{Stepper}$	18 g/cm^2
	$\text{Speed}_{Stepper}$	360°/s
	$\text{Speed}_{Throttle}$	540°/s
	Gear ratio	1.5
	Inductance/Phase	5.7 mH
	Resistance/Phase	9.2 Ω
	Amps/Phase	0.67 A
	Supply voltage	6.5 V
Sensor	Resolution	0.022°
	Lin. deviation	± 0.25 %
	Range of travel	90°
	Supply voltage	5 V
Control	K_P	0.11
	K_I	0.001
	Max. speed	360°/s

Table A.1 – TVA parameters

A.3 Virtual Dashboard

Figure A.1 shows the HMI's menu, offering mode selection, feature activation and system editing. The menu can be entered in standstill to ensure safe vehicle operation.

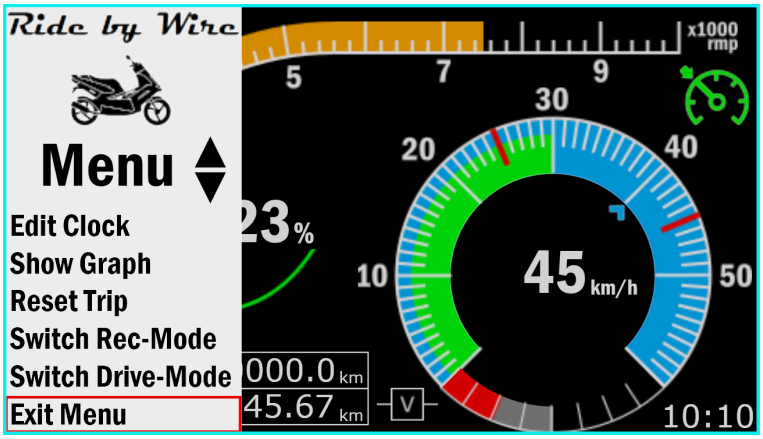

Figure A.1 – Virtual dashboard - Menu

A.4 Additional Engine Measurements

The Figures A.2-A.11 show the engine measurements of each investigated operating point (OP). These were the basis for data extraction of the overall evaluation shown in Figure 8.11.

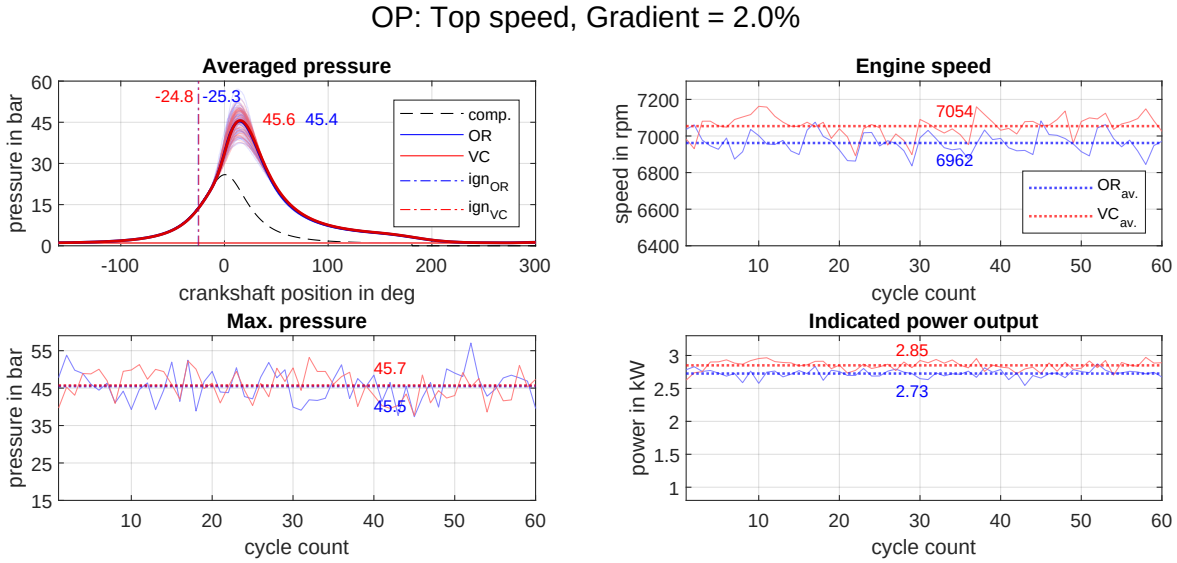

Figure A.2 – Engine measurement (2%)

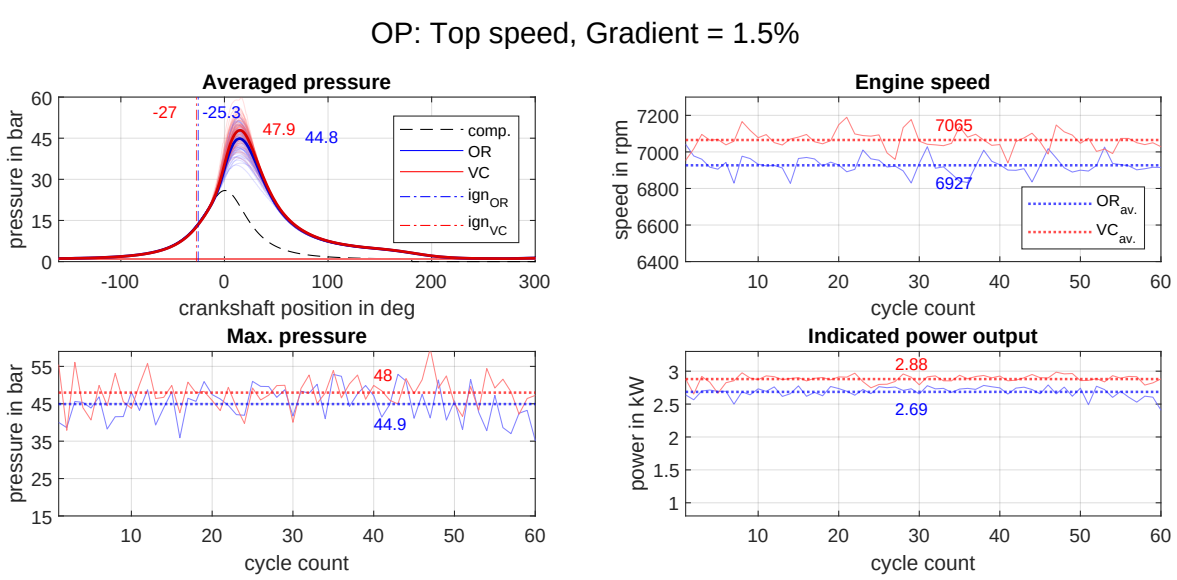

Figure A.3 – Engine measurement (1.5%)

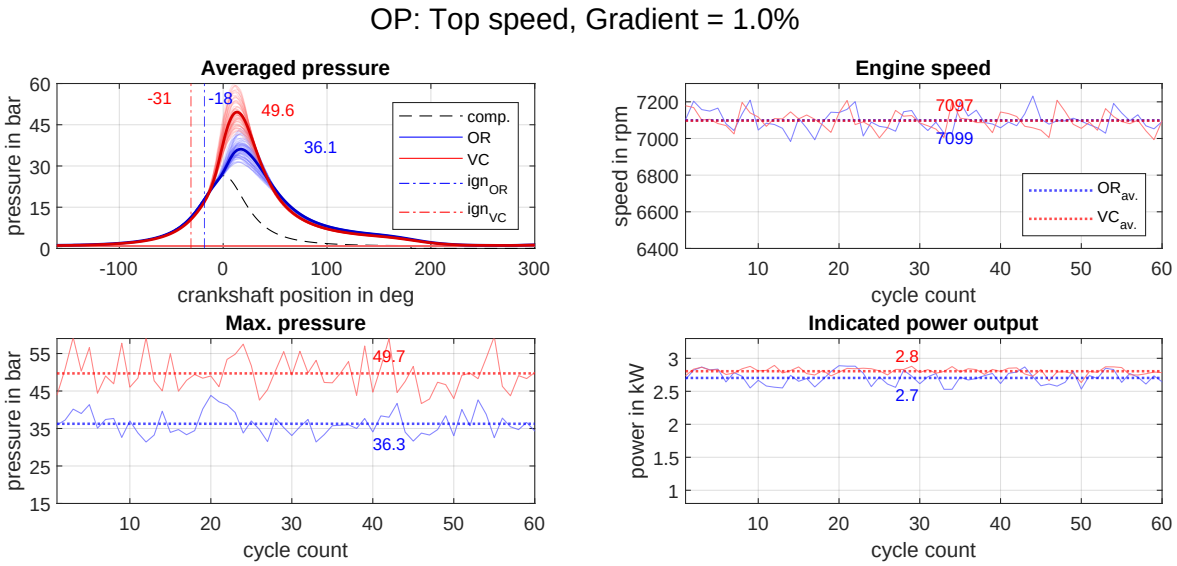

Figure A.4 – Engine measurement (1%)

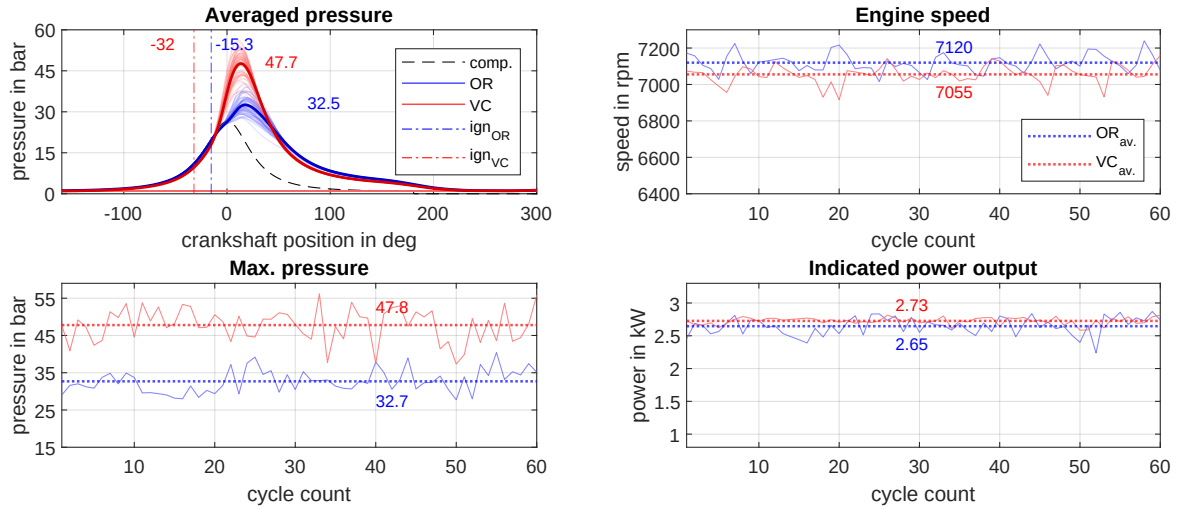

Figure A.5 – Engine measurement (0.5%)

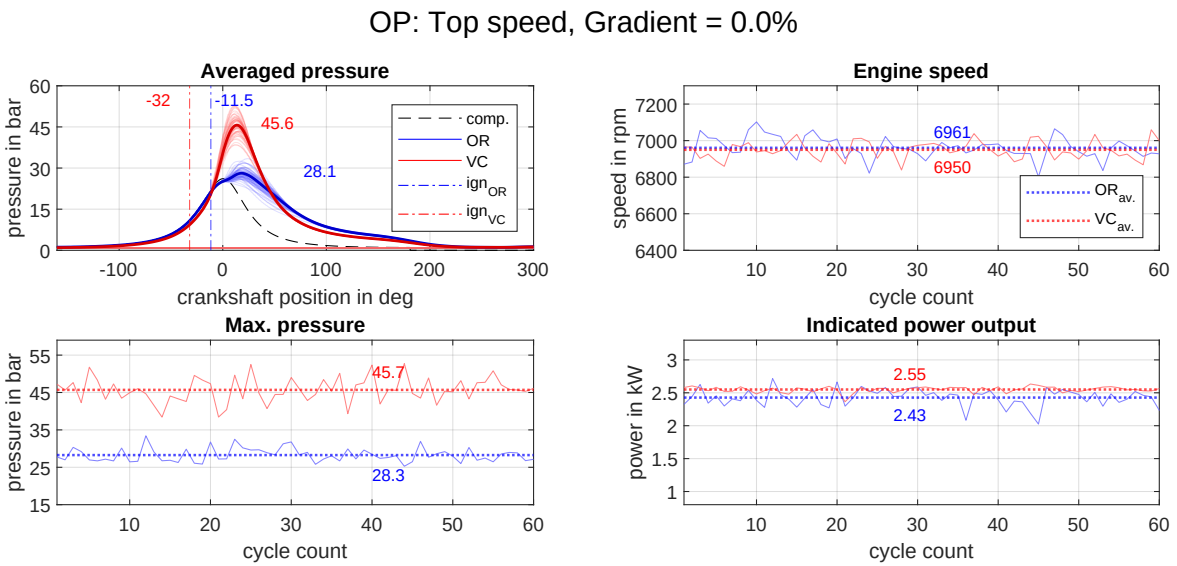

Figure A.6 – Engine measurement (0%)

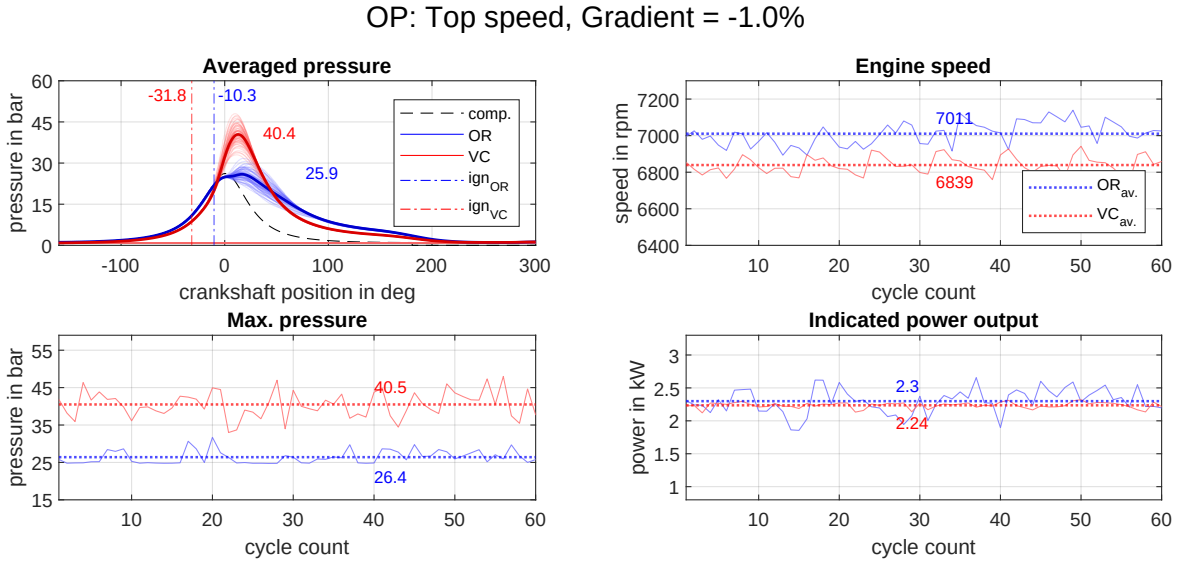

Figure A.7 – Engine measurement (-1%)

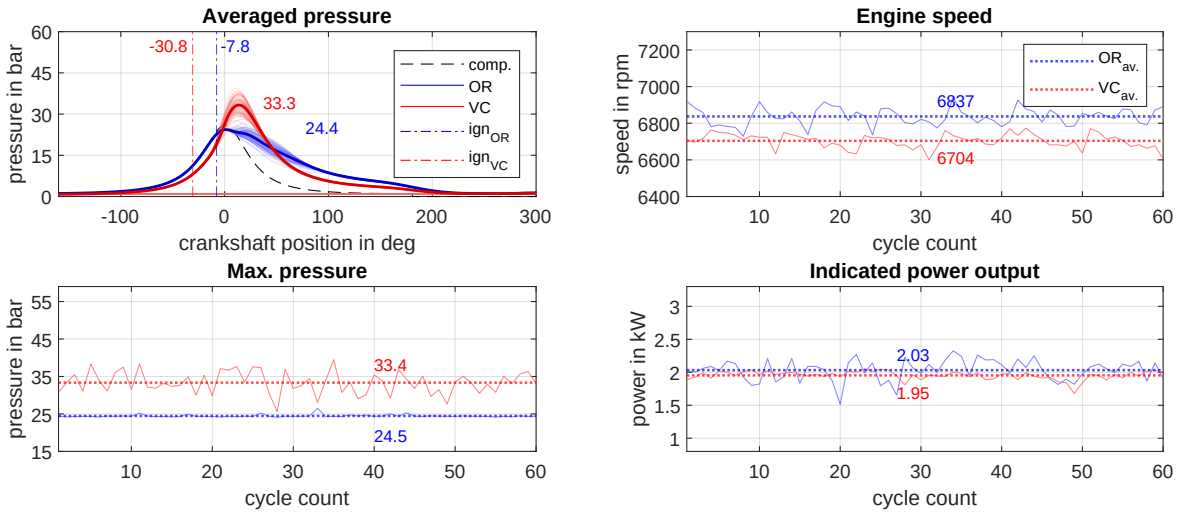

Figure A.8 – Engine measurement (-2%)

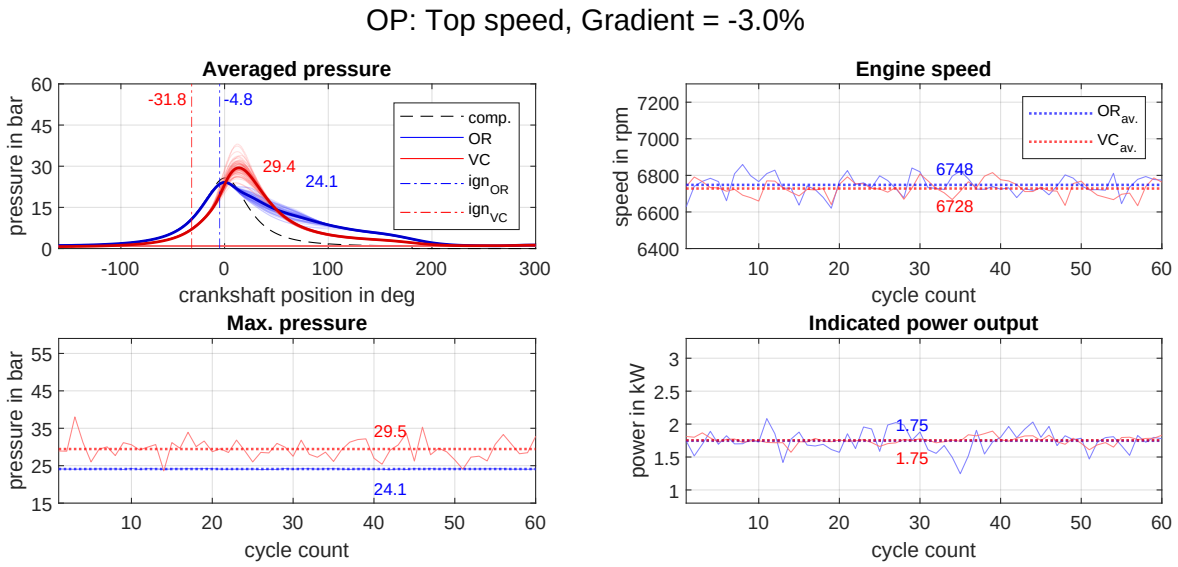

Figure A.9 – Engine measurement (-3%)

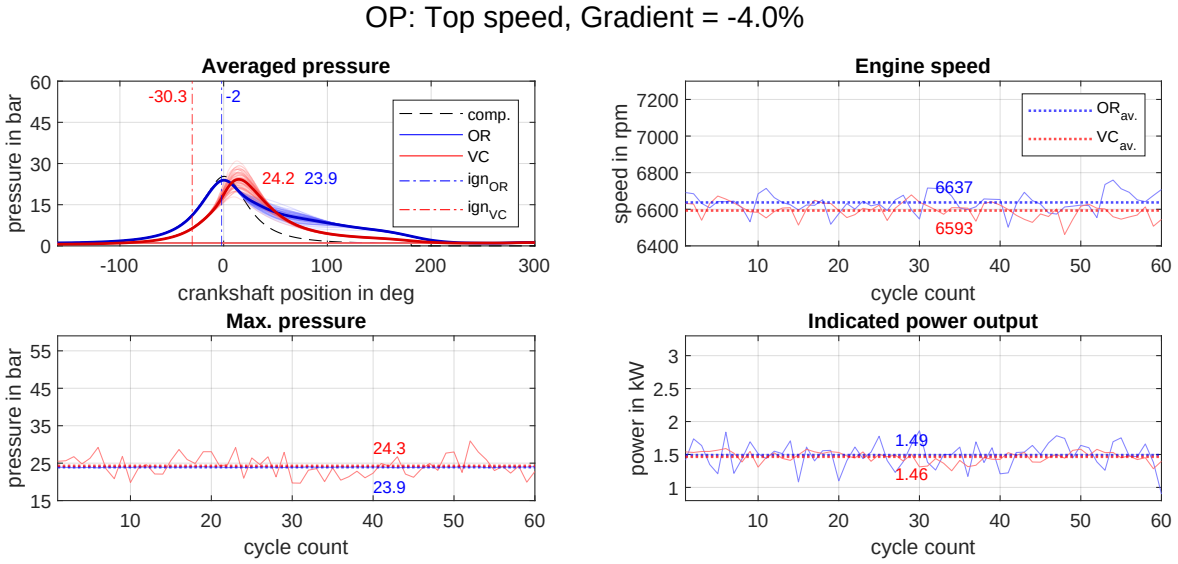

Figure A.10 – Engine measurement (-4%)

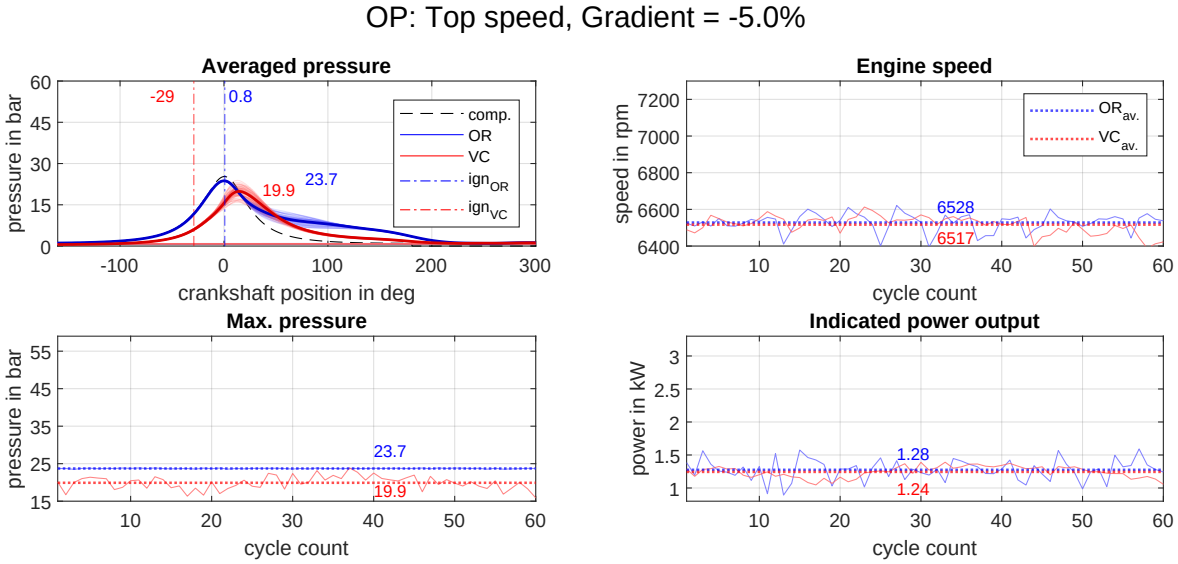

Figure A.11 – Engine measurement (-5%)